Naa12 compensates for *Naa10* in mice in the amino-terminal acetylation pathway

Hyae Yon Kweon[1¶], Mi-Ni Lee[1,#a¶*], Max Dörfel[2], Seungwoon Seo[1], Leah Gottlieb[3,4], Thomas Papazyan[2], Nina McTiernan[5], Rasmus Ree[5], David Bolton[6], Andrew Garcia[7], Michael Flory[8], Jonathan Crain[2], Alison Sebold[2], Scott Lyons[2], Ahmed Ismail[2], Elaine Marchi[7], Seong-keun Sonn[1], Se-Jin Jeong[9], Sejin Jeon[1], Shinyeong Ju[10], Simon J. Conway[11], TaeSoo Kim[1], Hyun-Seok Kim[1], Cheolju Lee[10,12], Tae-Young Roh[13], Thomas Arnesen[5,14,15], Ronen Marmorstein[3,4,16], Goo Taeg Oh[1*], Gholson J. Lyon[2,7,17,18*]

[1]Department of Life Science and College of Natural Sciences, Ewha Womans University, Seoul, Republic of Korea
[2]Stanley Institute for Cognitive Genomics, Cold Spring Harbor Laboratory, Woodbury, New York, United States of America
[3]Department of Chemistry, University of Pennsylvania, Philadelphia, United States of America
[4]Abramson Family Cancer Research Institute, Perelman School of Medicine, University of Pennsylvania, Philadelphia, United States of America
[5]Department of Biomedicine, University of Bergen, Bergen, Norway
[6]Department of Molecular Biology, New York State Institute for Basic Research in Developmental Disabilities, Staten Island, New York, United States of America
[7]Department of Human Genetics, New York State Institute for Basic Research in Developmental Disabilities, Staten Island, New York, United States of America
[8]Research Design and Analysis Service, New York State Institute for Basic Research in Developmental Disabilities, Staten Island, New York, United States of America
[9]Center for Cardiovascular Research, Washington University School of Medicine, Saint Louis, Missouri, United States of America
[10]Center for Theragnosis, Korea Institute of Science and Technology, Seoul, Republic of Korea
[11]Herman B. Wells Center for Pediatric Research, Indiana University School of Medicine, Indianapolis, United States of America
[12]Department of Converging Science and Technology, KHU-KIST, Kyung Hee University, Seoul, Republic of Korea
[13]Department of Life Sciences, Pohang University of Science and Technology, Pohang, Republic of Korea
[14]Department of Biological Sciences, University of Bergen, Bergen, Norway
[15]Department of Surgery, Haukeland University Hospital, Bergen, Norway
[16]Department of Biochemistry and Biophysics, Perelman School of Medicine, University of Pennsylvania, Philadelphia, United States of America
[17]George A. Jervis Clinic, New York State Institute for Basic Research in Developmental Disabilities, Staten Island, New York, United States of America
[18]Biology PhD Program, The Graduate Center, The City University of New York, New York, United States of America
[#a]Current Address: Laboratory Animal Resource Center, Korea Research Institute of Bioscience and Biotechnology, Chungbuk, Republic of Korea

* Corresponding author

E-mail: minilee@kribb.re.kr / tinymini@ewhain.net (MNL)

gholsonjlyon@gmail.com / gholson.j.lyon@opwdd.ny.gov (GJL)

gootaeg@ewha.ac.kr (GTO)

[¶]These authors contributed equally to this work.

Abstract

Amino-terminal acetylation is catalyzed by a set of N-terminal acetyltransferases (NATs). The NatA complex (including X-linked Naa10 and Naa15) is the major acetyltransferase, with 40-50% of all mammalian proteins being potential substrates. However, the overall role of amino-terminal acetylation on a whole-organism level is poorly understood, particularly in mammals. Male mice lacking *Naa10* show no globally apparent *in vivo* amino-terminal acetylation impairment and do not exhibit complete embryonic lethality. Rather *Naa10* nulls display increased neonatal lethality, and the majority of surviving undersized mutants exhibit a combination of hydrocephaly, cardiac defects, homeotic anterior transformation, piebaldism and urogenital anomalies. *Naa12* is a previously unannotated *Naa10*-like paralogue with NAT activity that genetically compensates for *Naa10*. Mice deficient for *Naa12* have no apparent phenotype, whereas mice deficient for *Naa10* and *Naa12* display embryonic lethality. The discovery of *Naa12* adds to the currently known machinery involved in amino-terminal acetylation in mice.

Introduction

Amino-terminal acetylation is one of the most common protein modifications, occurring co- and post-translationally. Approximately 80% of cytosolic proteins are amino-terminally acetylated in humans and ~50% in yeast [1], while amino-terminal acetylation is less common in prokaryotes and archaea [2]. Amino-terminal acetylation is catalyzed by a set of enzymes, the N-terminal acetyltransferases (NATs), which transfer an acetyl group from acetyl-coenzyme A (Ac-CoA) to the free α-amino group of a protein's N-terminus. To date, eight distinct NATs (NatA – NatH) have been identified in eukaryotes that are classified based on different subunit compositions and substrate specificities [3-5]. Amino-terminal acetylation has been implicated in steering protein folding, stability or degradation, subcellular targeting, and complex formation [6-10]. The vital role of NATs and amino-terminal acetylation in development has also emerged [11].

NatA, the major NAT complex, targets ~40% of the human proteome, acetylating Ser-, Ala-, Gly-, Thr-, Val- and Cys N-termini after removal of the initiator methionine [1, 5]. Human NatA consists of two main subunits, the catalytic subunit N-α-acetyltransferase 10 (NAA10) (Ard1) and the auxiliary subunit NAA15 (Nat1), and a regulatory subunit HYPK [12-14]. NAA15 function has been linked to cell survival, tumor progression, and retinal development [15, 16]. In addition, Naa10-catalyzed N-terminal acetylation has been reported to be essential for development in many species [11, 17-22], and although NatA is not essential in *S. cerevisiae*, depletion of *Naa10* or *Naa15* has strong effects, including slow growth and decreased survival when exposed to various stresses [23, 24].

NAA10 mutations were found to be associated with several human diseases characterized by severe phenotypes, including global developmental defects [11]. Among these, the X-linked Ogden syndrome (OS) [25, 26] shows the most severe pathological features such as infant lethality and has reduced NatA catalytic activity. In a *Saccharomyces cerevisiae* model for the Naa10 Ser37Pro mutant, the mutation impairs NatA complex

formation and leads to a reduction in NatA catalytic activity and functionality [27, 28]. Further, OS patient-derived cells have impaired amino-terminal acetylation *in vivo* of some NatA substrates [25]. Over the years, many additional pathogenic *NAA10* variants have been identified in *NAA10* or NAA15 [29-37] and the collection of presenting symptoms for families with *NAA10* mutations is currently referred to as Ogden syndrome or *NAA10*-related syndrome [38].

The autosomal *NAA10* homolog, *NAA11* (ARD2), has been reported to be present in mice and humans, and is co-expressed with *NAA10* in human cell lines [39]. Therefore, *NAA11* could conceivably compensate when *NAA10* is reduced or lacking [11]. However, *NAA11* was only found in testis and placenta in human and gonadal tissues in mouse, while *NAA10* showed widespread expression in various tissues in embryos and adults [40]. Thus, any functional redundancy or compensation might be limited to certain tissues only.

To elucidate the functional role of *Naa10* during development in mice, we used two different *Naa10*-deficient mouse lines: one, referred to as *Naa10* knockout (KO), which was previously reported specifically related to bone density in postnatal day 3 (P3) mice [41], and another denoted as $Naa10^{tm1a(EUCOMM)Hmgu}$ ($Naa10^{tm1a}$), generated in this study. These *Naa10*-deficient mice exhibit pleiotropic developmental abnormalities at a range of different ages, overlapping with some of the phenotypes seen in human disease involving NAA10 impairment. Because we did not discover major changes in the overall Nt-acetylome in *Naa10* KO mice, we hypothesized that there might be a compensating gene in mice, which led us to the identification of a new paralog of *Naa10,* which we name *Naa12*. *Naa12* is expressed in several organs (liver, kidney, heart and testis) and, like Naa10, binds to Naa15 to mediate NatA activity. Furthermore, lethality was observed in *Naa10 Naa12* double-KO mice, which supports the compensatory role of *Naa12 in vivo*. Thus, we demonstrate that *Naa10* is essential for proper development and *Naa12*, a newly-identified paralog of *Naa10*, can play a compensatory role in mice.

Results

Naa10 knockout mice can be born, but display pleiotropic developmental defects

To explore the role of *Naa10* in development, most analyses were carried out using our *Naa10* KO model mice that had been generated previously [41] using a targeting vector deleting Exon1, including the start codon, and Exon2 to Exon4 containing the GNAT domain including the Acetyl-CoA binding motif, which is crucial for *Naa10* function. We also generated another *Naa10*-deficient mouse which we called $Naa10^{tm1a}$, expressing β-galactosidase rather than the *Naa10* gene (**Supplement Fig. 1**A). *Naa10* expression was deficient in $Naa10^{tm1a}$ mice (**Supplement Fig. 1**B and **Supplement Fig. 1**C). Especially strong β-gal staining was observed during embryonic stages in the brain, heart and spinal cord (**Supplement Fig. 1**D). Male *Naa10* KO ($Naa10^{-/Y}$) embryos displayed mild to severe developmental defects compared to wild-type (WT) ($Naa10^{+/Y}$) embryos. Some $Naa10^{-/Y}$ mice had lower levels of somites and developmental delay. Additionally, some $Naa10^{-/Y}$ embryos had a normal number of somites but were retarded in growth (**Fig. 1**A). Some of the

embryos underwent lysis or remained arrested at an earlier stage than embryonic day 10.5 (E10.5), with no turning, an abnormal trunk, and underdeveloped facial features. These phenotypes also reproduced in *Naa10*$^{tm1a/Y}$ embryos. Next, we assessed whether *Naa10* is essential for viability and counted the Mendelian ratios. Both *Naa10*$^{-/Y}$ and *Naa10*$^{tm1a/Y}$ mice were under-represented after birth, while there was no significant reduction in the embryonic stage in both mouse lines (**Supplement Table 1** and **Supplement Table 2**). We monitored the pups daily at postnatal day 0 (P0) to postnatal day 3 (P3) and beyond, and the survival rate of *Naa10*$^{-/Y}$ mice dramatically decreased relative to either WT (*Naa10*$^{+/Y}$ and *Naa10*$^{+/+}$) or heterozygous female (*Naa10*$^{+/-}$) mice after the first few days of life (**Fig. 1**B), and a few *Naa10*$^{-/Y}$ mice with postnatal lethality exhibited severe developmental defects such as craniofacial anomaly, an undeveloped lower body, whole-body edema, and ocular malformations (**Fig. 1**C).

Congenital heart defects are one of the main causes of infant lethality, and cardiac diseases are a common developmental anomaly in OS patients [31], with some OS males dying in infancy with cardiac arrhythmias [26]. Therefore, we investigated whether *Naa10* KO affects cardiac development. Development of a four-chambered septated heart is normally complete at E14.5, therefore we examined the cardiovascular system at E14.5. We identified ventricular septal defects (VSD) in several *Naa10*$^{-/Y}$ embryos, as well as concomitant double outlet right ventricle (DORV) at E14.5 (Fig 1D, upper). Ventricular septal defects (VSD) and atrial septal defects (ASD) were also observed at E18.5 (**Fig. 1**D, bottom), and persistent truncus arteriosus (PTA) or DORV, along with concomitant membranous and muscular VSDs, were found in several of the mice that died in the first day of life (n= 6/28 examined). Given the presence of outflow tract defects and VSDs, we examined whether the ductus arteriosus had closed appropriately or not at birth. Significantly, both *Naa10*$^{-/Y}$ and *Naa10*$^{-/-}$ females (n=3/28 examined) exhibited a patent ductus arteriosus, meaning there is a failure of the mutant *in utero* cardiovascular system to adapt to adult life (birth) and close the interatrial and aorta-pulmonary trunk shunts that are required for normal fetal life [42]. As murine outflow tract and VSD defects are not compatible with postnatal survival [42], these data suggest that congenital heart defects in *Naa10*$^{-/Y}$ mice may explain some of their neonatal lethality (**Supplement Fig. 2**). We also examined surviving adult mice for any possible situs inversus, but we did not observe this in any adult (>4 weeks) *Naa10*$^{-/Y}$ mice examined (n=19). Combined, these data suggest that *Naa10* mutant CHDs are mainly confined to aberrant remodeling of the great vessels of the heart, leading to pulmonary overload at birth resulting in lethality.

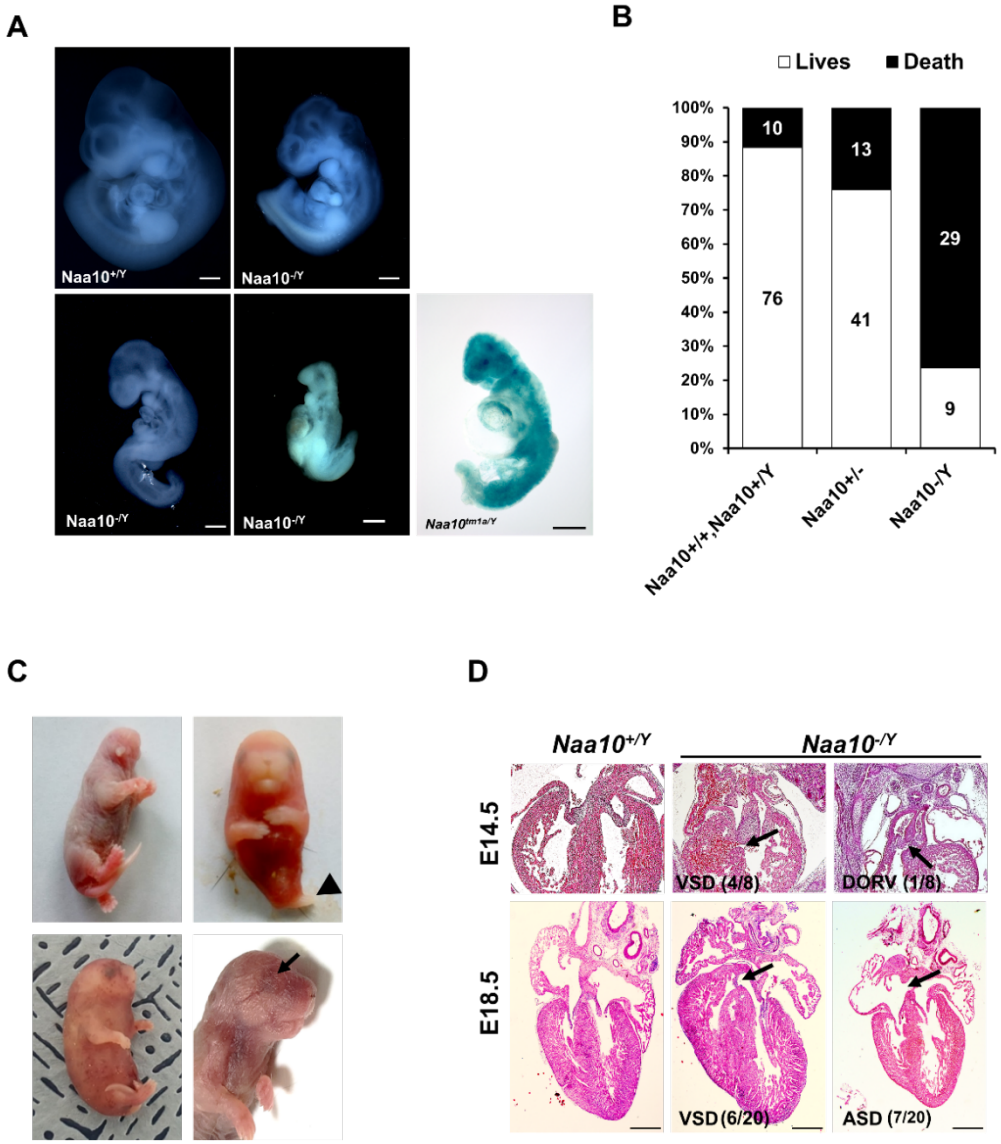

Fig. 1. Deficiency of *Naa10* leads to abnormal development and postnatal lethality. (A) *Naa10*$^{+/Y}$, *Naa10*$^{-/Y}$ and *Naa10*$^{tm1a/Y}$ embryos at E10.5. Growth retardation (5/33, more than 5 somites lower or undersized compared to littermate controls), kinky trunk and developmental arrest are shown in *Naa10*$^{-/Y}$ (4/33) and *Naa10*$^{tm1a/Y}$ (1/5). Scale bars: 500µm. (B) The percentage lethality in newborns, comparing *Naa10* wild-type (*Naa10*$^{+/Y}$ and *Naa10*$^{+/+}$), *Naa10*$^{-/+}$ and *Naa10*$^{-/Y}$ pups until P3, derived from matings between heterozygous females and wild-type (WT) males. Approximately 11.6% (10/86) of WT, 24% (13/54) of *Naa10*$^{+/-}$ and 76.3% (29/38) *Naa10*$^{-/Y}$ mice were found dead before P3. (C) Representative images of *Naa10*$^{-/Y}$ pups during early postnatal days compared with *Naa10*$^{+/Y}$. Severe developmental defects such as malformations of head and lower body (one leg; black arrowheads), whole-body edema and anophthalmia (black arrows) are shown (N=1 each). (D) Hematoxylin and Eosin (H&E)-stained heart transverse section at E14.5 and vertical section at E18.5, comparing *Naa10*$^{+/Y}$ and *Naa10*$^{-/Y}$ embryos. *Naa10*$^{-/Y}$ embryo shows a VSD at E14.5 and E18.5. Also, at E18.5, *Naa10*$^{-/Y}$ embryo shows ASD. Arrow indicates VSD, ASD and DORV. Scale bars: 20 µm. VSD, ventricular septal defect; ASD, atrial septal defect; DORV, double outlet right ventricle.

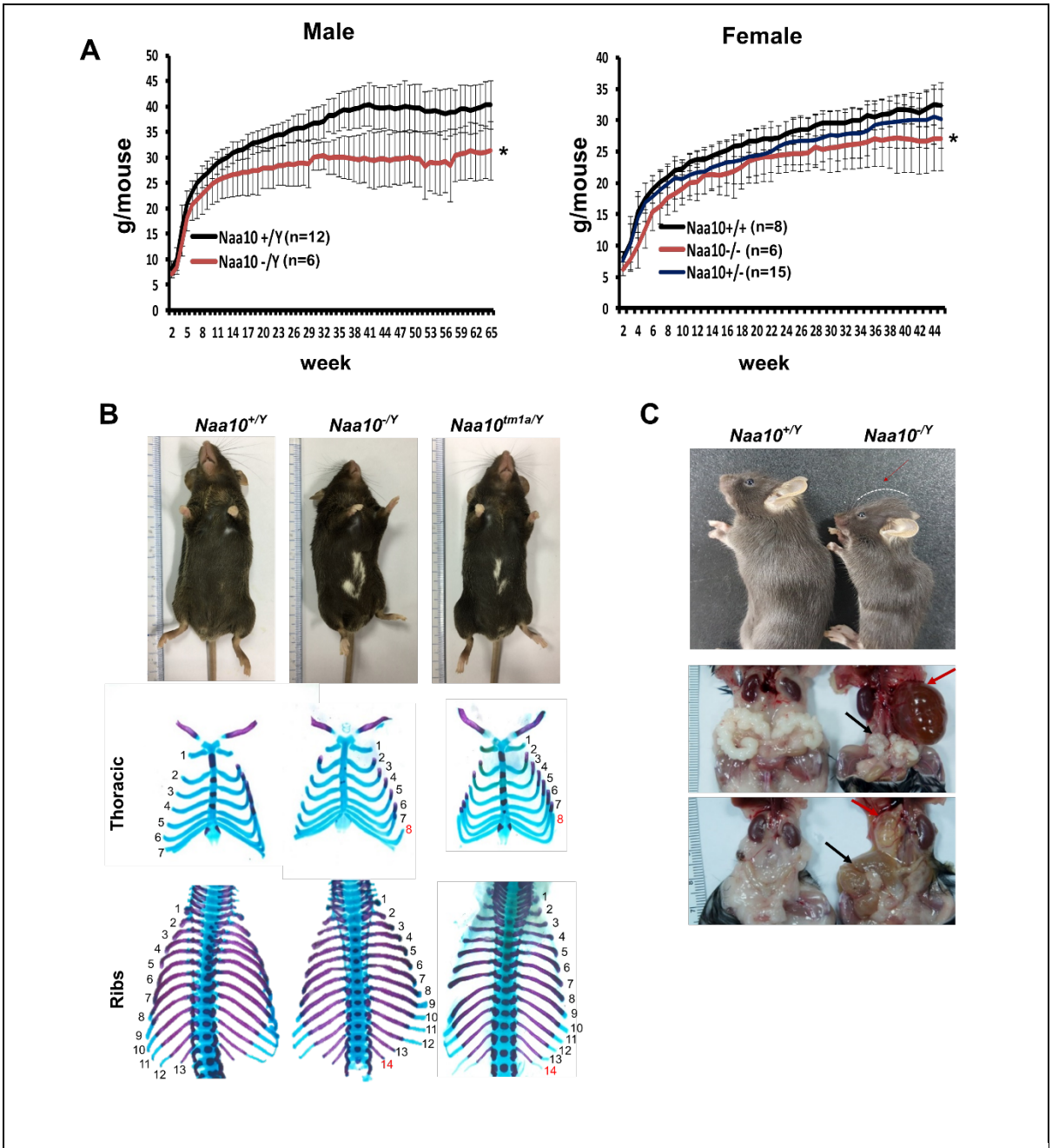

Fig. 2. Pleiotropic phenotypes of *Naa10* KO mice. (A-C) Representative images of abnormalities in *Naa10*$^{-/Y}$ compared with *Naa10*$^{+/Y}$. (A) Body weight of male (left) and female (right) verses ages was monitored from 2 weeks. The weight of *Naa10*$^{-/Y}$ and *Naa10*$^{-/-}$ mice is markedly reduced compared with that of the WT mice. Asterisks indicate a statistical difference calculated by Student's *t*-test: *p < 0.05. (B) Representative images of completely penetrant phenotypes. Hypopigmentation (*Naa10*$^{+/Y}$, n=243; *Naa10*$^{-/Y}$, n=121; *Naa10*$^{tm1a/Y}$, n=17) and supernumerary ribs (*Naa10*$^{+/Y}$, n=3; *Naa10*$^{-/Y}$, n=6; *Naa10*$^{tm1a/Y}$, n=2; E18.5) were found 100% in *Naa10* deficient mice. (C) *Naa10*$^{-/Y}$ is smaller in size and has round-shaped head (*Naa10*$^{+/Y}$ 0/59, *Naa10*$^{-/Y}$ 7/33). Over time, hydrocephaly became apparent. (N=14/29 (~48%) for >P7 male *Naa10*$^{-Y}$; N=7/19 (~36%) for >P7 female *Naa10*$^{-/-}$). Hydronephrosis (red arrow, *Naa10*$^{+/Y}$ 0/23, *Naa10*$^{-/Y}$ 14/29, *Naa10*$^{+/+}$ 0/5, *Naa10*$^{-/-}$ 7/19) and abnormal genitalia (black arrow) of male (middle, *Naa10*$^{+/Y}$ 0/23, *Naa10*$^{-/Y}$ 16/29) and female (bottom, hydrometrocolpos, *Naa10*$^{+/+}$ 0/5, *Naa10*$^{-/-}$ 7/19) are shown.

Some of the surviving homozygous mice (*Naa10*$^{-/Y}$ and *Naa10*$^{-/-}$) had reduced body weight (**Fig. 2**A). This reduced body weight continued through weaning, and some mice lost more weight as they developed progressive hydrocephaly. We observed that the smallest weight animal between the *Naa10*$^{+/Y}$ and one *Naa10*$^{-/Y}$ genotypes was almost always the *Naa10*$^{-/Y}$ genotype when the analysis was restricted to only include litters in which there was at least one of each of those genotypes living beyond four days of life. For example, 13 litters met this criteria from the mating (*Naa10*$^{+/-}$ x *Naa10*$^{+/Y}$), and 12/13 of the litters had the *Naa10*$^{-/Y}$ as the lower weight (Fisher's exact test, two-tailed, P value <0.0001). 5 litters met this criteria from the mating (*Naa10*$^{+/-}$ x *Naa10*$^{-/Y}$), and of these, all of them had the *Naa10*$^{-/Y}$ as the lower weight (Fisher's exact test, two-tailed, P value = 0.0079). Therefore, despite the known variability in weight data as a function of genetic background, environment, and stochastic variation [43], it does appear at least for "within-litter" analysis that *Naa10*$^{-/Y}$ males are born at a smaller weight than *Naa10*$^{+/Y}$ males and on average remained the smallest male in the litter throughout their life.

Although piebaldism has never been reported in humans with OS, all (100%) of *Naa10*$^{-/Y}$ and *Naa10*$^{tm1a/Y}$ mice exhibited hypopigmentation on their belly (**Fig. 2**B, upper), with this piebaldism quite varied in its extent but not appearing to correlate in any way with other phenotypes, such as hydrocephaly. Another phenotype with complete penetrance was bilateral supernumerary ribs (14 pairs of rib instead of 13) in all *Naa10*$^{-/Y}$ and *Naa10*$^{tm1a/Y}$ mice (**Fig. 2**B, middle and bottom, **Table 1**). This extra pair of ribs linking to the sternum transforms the T8 vertebrae into an anterior T7-like phenotype (**Supplement Fig. 3**A-**Supplement Fig. 3**D Fig, **Table 1**).

Table 1. Skeletal analyses for ribs, sternebrae, and vertebrae

	Naa10$^{+/Y}$ (n=50)	Naa10$^{+/+}$ (n=10)	Naa10$^{+/-}$ (n=17)	Naa10$^{-/Y}$ (n=17)	Naa10$^{-/-}$ (n=1)
4 sternebrae	7 (14.0%)	1 (10%)	3(17.6%)	9 (52.9%)	1 (100%)
3 sternebrae	27 (54.0%)	8 (80%)	11(64.7%)	5 (29.4%)	0 (0%)
4 sternebrae but with 3/4 fusion	16 (32%)	1 (10%)	3 (17.6%)	3 (17.6%)	0 (0%)
14 ribs total bilaterally	0 (0%)	0 (0%)	0 (0%)	17 (100%)	1 (100%)
13 ribs total bilaterally	50 (100%)	10 (100%)	17 (100%)	0 (0%)	0 (0%)
8 ribs attached to sternum bilaterally	0 (0%)	0 (0%)	0 (0%)	17 (100%)	1 (100%)
7 ribs attached to sternum bilaterally	50 (100%)	10 (100%)	17 (100%)	0 (0%)	0 (0%)
14 Thoracic vertebrae	0 (0%)	0 (0%)	0 (0%)	17 (100%)	1 (100%)
13 Thoracic vertebrae	50 (100%)	10 (100%)	17 (100%)	0 (0%)	0 (0%)

Tabulation regarding the number of sternebrae found in skeletons, including ones in which there was partial fusions between the 3rd and 4th sternebrae.

A majority of the *Naa10*$^{-/Y}$ and *Naa10*$^{-/-}$ mice also had four instead of the usual three sternebrae, which were sometimes fused (**Table 1**). Cervical vertebrae fusion was also

demonstrated in *Naa10*$^{-/Y}$ mice, particularly involving C1 and C2, suggesting possible anteriorization of C2 into a C1-like phenotype (**Supplement Fig. 3**E and **Supplement Fig. 3**F, and **Supplement Table 3**). The number of lumbar vertebrae remained the same, thus suggesting an anterior transformation of the first sacral vertebra to a lumbar-like phenotype. These combined observations suggest possible anterior transformations in the *Naa10* mutant skeletal phenotype, with an anteriorization of C2, a T8 transformation to a T7-like phenotype with ribs connecting to the sternum, an extra pair of ribs on L1 likely due to an L1 transformation to a T13-like phenotype, and an anterior transformation of the first sacral vertebra to a lumbar-like phenotype with loss of fusion to the sacral wings.

Out of 32 *Naa10*$^{-/Y}$ that survived past the third day of life and which were then examined longitudinally, about 60% survived past 200 days of life (~7 months) (**Supplement Fig. 4C**) , with some of these then developing hydronephrosis (**Fig. 2**C, middle). They had some hollowed space in the kidney, which had been filled with fluid and their ureter was thickened already at P3 stage of prenatal development in some *Naa10*$^{-/Y}$ mice (**Supplement Fig. 4**A). Commonly, hydronephrosis is caused by a blockage or obstruction in the urinary tract. We speculate that this swelling in *Naa10* KO (*Naa10*$^{-/Y}$ and *Naa10*$^{-/-}$) mice is likely caused by ureteral defects rather than the kidney itself. Moreover, some *Naa10* KO mice displayed genital defects, such as seminal vesicle malformation and hydrometrocolpos, respectively (**Fig. 2**C, bottom). Many *Naa10*$^{-/-}$ female mice appeared to have decreased fecundity, although they were fertile upon the first mating, and this decrease in fecundity is possibly due to the development of hydrometrocolpos (**Fig. 2**C, bottom), which might result from structural issues, like vaginal atresia or a retained vaginal septum, although this requires further investigation. Additionally, hydrocephaly became clinically apparent with a round-shaped head (**Fig. 2**C, upper) in ~40% of the *Naa10*$^{-/Y}$ mice that had survived past 3 days of life (**Supplement Fig. 4C**). CT scanning of some of these mice confirmed hydrocephaly as the primary cause of their rapid deteriorating condition, usually within the first 3 months of life (**Supplement Fig. 4B** and **4C**). CT scanning did not reveal any obstructive lesions (such as a tumor) in any of the ventricles that could account for the hydrocephaly. Taken together, these results indicate that *Naa10* contributes to overall development and is particularly important for viability.

Litter sizes and offspring from other matings were also investigated, as shown in **Supplement Table 4**. Matings were set up between *Naa10*$^{-/-}$ females and C57bl6J WT (*Naa10*$^{+/Y}$) males, involving eleven mating pairs with 7 unique females and 7 unique males. Of a total of 127 pups that were born, 37 died in the first day of life and were degraded and/or cannibalized prior to any tail sample being retrieved, thus not being genotyped. This was a relatively high death rate in the first 24 hours of life (29%), more so than with the other matings, except for the one between *Naa10*$^{-/-}$ females and *Naa10*$^{-/Y}$ males (**Supplement Table 4**). However, this is substantially less than the death rate of 90% (46/51) reported for the same mating in the Lee *et al.* paper [44], and we currently do not have an explanation for this discrepancy. Of the remaining 90 pups that could be genotyped, 59 of these were *Naa10*$^{+/-}$ females and 31 were *Naa10*$^{-/Y}$ males. Seven of the 59 *Naa10*$^{+/-}$ females and two of the 31 *Naa10*$^{-/Y}$ males died in the first 3 days of life (for a total death rate in the first three days for

all born pups of 46/127, or 36%), and after this time, none of the remaining *Naa10*$^{+/-}$ females died in the first ten weeks of life (52/59, or 88% overall survival), whereas ten of the remaining 29 *Naa10*$^{-/Y}$ males developed hydrocephaly and died in the first ten weeks of life, for an overall survival of 19/31, or 61%). The death rate for all pups of 36% in the first three days of life is similar to the rate of 42.4% seen with the mating of *Naa10*$^{-/-}$ females with *Naa10*$^{-/Y}$ males (**Supplement Table 4**), whereas this rate is higher than that seen for *Naa10*$^{+/-}$ females mated with *Naa10*$^{+/Y}$ males (15.8%) or with *Naa10*$^{-/Y}$ males (13.6%).

Naa10-deficient mice have a functionally active NatA complex

Prior experiments showed reduced *in vivo* protein amino-terminal acetylation of a few putative targets in patient cells [25]. Reduced Nt-acetylomes were also observed in the *Naa10* mutant yeast models [27]. Given these prior reports, we hypothesized that pleiotropic phenotypes in *Naa10*-deficient mice are due to a decrease in global N-terminal acetylation. To test our hypothesis, integrated N-terminal peptide enrichment method (iNrich) [45] was used to analyze the level of protein amino-terminal acetylation in mouse embryonic fibroblast (MEF) lysates of *Naa10*$^{+/Y}$ and *Naa10*$^{-/Y}$. Since the samples are treated with deuterated acetic anhydride prior to MS, unacetylated N-terminal site appears with +3 Da mass shift in the MS spectrum of the corresponding acetylated N-terminal site [46]. The peak intensity ratios of acetyl/heavy acetyl pairs represent degree of acetylation of the N-terminal site. We found 765 acetyl/heavy acetyl pairs of N-termini throughout five replicates of *Naa10*$^{+/Y}$ and five replicates of *Naa10*$^{-/Y}$ MEFs . Except for the sites detected only in either WT or mutant, 533 N-terminal sites could be compared (see tab called "N-term" in **Supplement Table 5)**. Approximately 98% (n=522) of N-termini sites showed less than 10% variation in the degree of terminal acetylation, indicating that there is no major difference in amino-terminal acetylation between *Naa10*$^{-/Y}$ and *Naa10*$^{+/Y}$ MEFs (**Fig. 3**A). A more stringent analysis was also conducted in which peptides had to be detected in all ten samples (i.e. tab marked "N-term detected in all samples" in **Supplement Table 5**), and this resulted in 152 N-termini sites, of which only 3 (Rpl27, PPia, and Histone H1.0) had only a slightly greater than 10% difference in the degree of acetylation between *Naa10*$^{+/Y}$ and *Naa10*$^{-/Y}$. Although this was not a significant result statistically (p=0.09), it is worth noting that peptidyl-prolyl cis–trans isomerase A (PPIA), having a 10.3% decrease in amino-terminal acetylation, was previously identified with decreased amino-terminal acetylation in patient-derived B cells and fibroblasts in boys with the S37P mutation in NAA10 [25], along with being decreased in siNatA knockdown HeLa cells [1]. PPIA also had decreased amino-terminal acetylation in one sample from homozygous null *NAA15*$^{L314*/L314*}$ induced pluripotent stem cells [47].

Overall, given the very minor differences with amino-terminal acetylation, we measured the *in vitro* amino-terminal acetylation activity of NatA via immunoprecipitation of the large auxiliary subunit Naa15 from mouse tissues. This analysis showed normal expression of Naa15 in *Naa10* KO liver tissue as in WT tissues (**Fig. 3**B), and we isolated a physical complex composed of Naa15 and undefined partners that retains NatA activity from *Naa10* KO tissues (**Fig. 3**C). These data suggest that despite the loss of *Naa10* in mice, the

NatA complex remains active, thus explaining the lack of major differences with amino-terminal acetylation.

A *Naa10* paralog exists in mice

Naa10 disruption is lethal in a variety of organisms, including *D. melanogaster* [17], *C. elegans* [18] *and T. brucei* [48]. Given the relatively mild phenotype and no reduction of the Nt-acetylome in *Naa10* KO mice, we hypothesized that there might be a yet unidentified paralog of *Naa10,* which can compensate for loss of function in mice. A Blast search for genomic sequences with homology to *Naa10* exposed several *Naa10* pseudogenes on chromosome 2, 3, 7, 12, 15 and 18. Additionally, southern blot analysis from C57BL/6J DNA with *Naa10* cDNA probe detected bands of the expected sizes on the X chromosome (**Supplement Fig. 5**A and **Supplement Fig. 5**B), while other bands of unexpected sizes appeared on other chromosomes 2, 5, 15 and 18. The previously identified *Naa10* paralog *Naa11* is located on chromosome 5, however, this paralog is only expressed in testes [40]. We found a predicted gene (Gm16286, UniProt: Q9CQX6) on chromosome 18, with high similarity to *Naa10*, which we name *Naa12*, and RiboSeq and mRNA traces of this region suggest possible transcription and translation of this gene (**Supplement Fig. 5**C). The protein sequence of *Naa12* is >80% identical to *Naa10* and almost 90% identical with *Naa11* (**Supplement Fig. 6**).

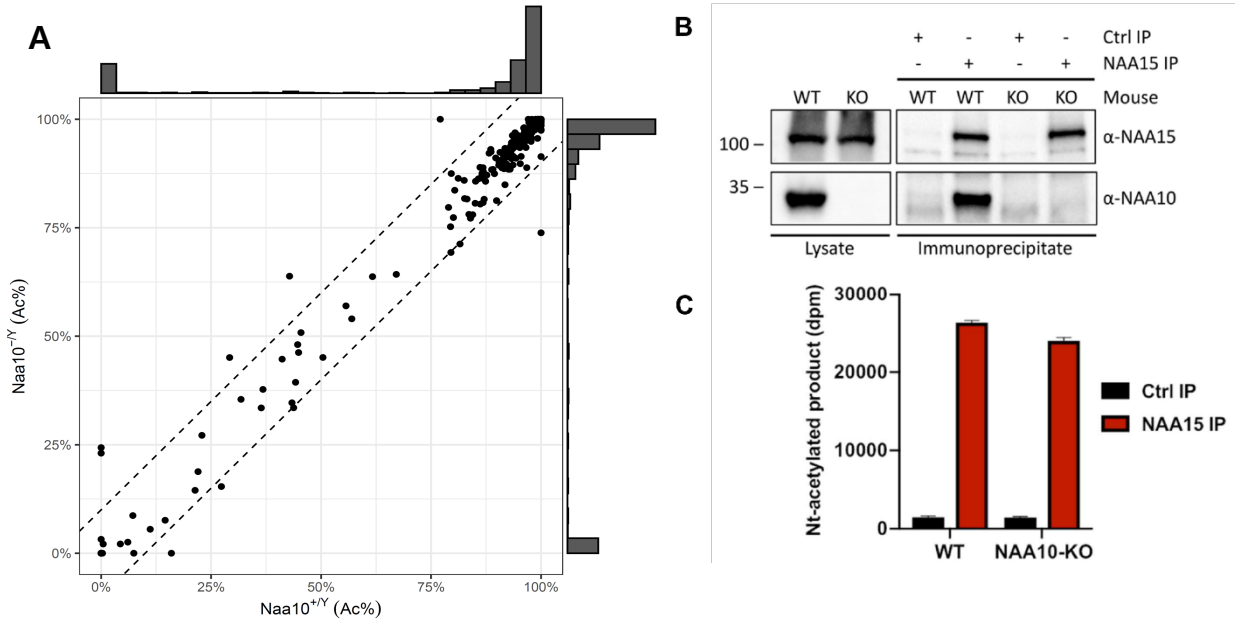

Fig. 3. Activity measurement of NatA from WT and *Naa10* KO mice. (A) Correlation of Naa10 alteration state on amino-terminal acetylation in mouse embryonic fibroblasts (MEFs). Each dot (n=533) represents the average amino-terminal acetylation percentage of 5 replicates of *Naa10*$^{+/Y}$ and *Naa10*$^{-/Y}$, respectively. Dashed lines are the borders of ±10% difference. Except for the ten dots, 522 of the 533 dots are within the borders. The marginal histograms show the distribution of amino-terminal acetylation data points. (B) Immunoprecipitation of Naa15. Liver tissue from WT and *Naa10* KO mouse was lysed and incubated with anti-Naa15 antibody to retrieve NatA complexes. Proteins were separated by SDS-PAGE and immunoblots probed with anti-Naa15 antibody and anti-NAA10 antibody. (C) Catalytic activity of immunoprecipitated NatA. The catalytic activity of NatA precipitated from WT and *Naa10* KO mouse liver tissue by anti-Naa15 was measured towards the NatA substrate peptide $SESS_{24}$ in an *in vitro* [^{14}C]-Ac-CoA–Based Acetylation Assay. Control reactions were performed with no enzyme or no peptide to account for background signal. The immunoprecipitation (IP) and activity measurements were performed in three independent setups, each with three technical replicates per assay. One representative setup is shown.

Quantitative PCR (q-PCR) analysis also confirmed the expression of this transcript in all tested tissues (**Supplement Fig. 6**A), with the expression of Naa12 unchanged in the corresponding *Naa10* KO tissues. We attempted to test for Naa12 expression in mouse tissues by developing an antibody specific for Naa12, by performing a sequence alignment of the two known mNaa10 isoforms, mNaa11 and mNaa12 and selecting a unique Naa12 peptide for immunization and antibody generation (**Supplement Fig. 6**B). After generation and affinity-purification, we validated the specificity and sensitivity of this Naa12 antibody with recombinant proteins purified from bacterial hosts (**Supplement Fig. 6**C and **Supplement Fig. 6**D). However, multiple attempts to use this antibody to detect Naa12 in mouse tissues met with conflicting results, so that we were unable to consistently detect Naa12 even in WT liver, kidney, or brain tissue lysates, which could be due to a poor antibody and/or very low expression or post-translational modification of Naa12 in these tissues thus making it difficult to detect. Furthermore, given that this antibody was raised against a peptide at the C-terminus of Naa12, such data could not be used anyway to completely exclude the possibility of truncated non-functional mini-protein expression, although the lack of any signal with RT-PCR (**Supplement Fig. 7**A) likely means that nonsense-mediated decay occurred. Presently,

the rabbit polyclonal antibody is no longer recognizing any consistent protein bands in Western blotting, so we have abandoned any further attempts to use this antibody.

To test whether Naa12 has a similar enzymatic activity as Naa10, we performed a radioactive-based acetyltransferase assay using synthetic peptides (**Fig. 4**A). Since monomeric Naa10 preferentially acetylates N-termini with acidic side chains [49-51], we used peptides representing the N-termini of γ -actin (starting DDDIA-) and γ-actin (starting EEEIA-), which are two known Naa10 *in vitro* substrates. Additionally, we used a peptide starting with SESSSKS-, representing an in vitro NatA complex substrate High mobility group protein A1. As expected for the monomeric proteins, we could not detect any activity towards the SESSSKS-substrate. Importantly, both Naa10 and Naa12 significantly Nt-acetylated the acidic N-terminal peptides demonstrating the intrinsic capacity of Naa12 to catalyze amino-terminal acetylation (**Fig. 4**A).

Across species, Naa10 is bound to its auxiliary subunit, Naa15, which links the catalytic subunit to the ribosome to facilitate co-translational amino-terminal acetylation of proteins as they emerge from the exit tunnel [23, 52-56]. Due to its high sequence similarity (see also **Supplement Fig. 4**B), we suspected that Naa12 may also interact with Naa15. To test this hypothesis, we performed co-immunoprecipitation assays in HEK 293 cells. Apart from Naa10 (isoform 1, $Naa10^{235}$) and Naa12, we also included the second isoform of mNaa10, $mNaa10^{225}$ that has been described earlier [12, 53, 57] as well as Naa11. Both Naa10 isoforms as well as Naa11 and Naa12 co-precipitated with V5-Naa15 but not V5 alone, suggesting that all tested proteins could form a stable complex with Naa15 in mouse (**Fig. 4**B). As we have previously purified the human NatA complex composed of truncated human Naa10 (residues 1-160) and full-length human Naa15 complexes that had been expressed in insect cells [14], we attempted to co-express a chimeric truncated mouse Naa12 (residues 1-160) with full-length human Naa15 complex in insect cells (human and mouse Naa15 are highly conserved with a sequence conservation of 98.2%). The complex was purified by a combination of affinity, ion exchange and size-exclusion chromatography and size exclusion fractions harboring a clearly detectable band of Naa15 and a lighter band for Naa12, as determined by silver staining, was analyzed for activity towards a SESSSKS-peptide (**Fig. 4C and Supplemental Figs. 6E and 6F**). This analysis revealed that peak fractions containing the Naa12-Naa15 complex harbored detectable amino-terminal acetylation activity toward the SESSSKS- peptide (**Fig. 4C and Supplemental Fig. 6F**), thus demonstrating catalytic activity of a NatA complex with mouse Naa12.

In a mass spectrometry analysis of a similar setup to that shown in **Fig. 3**B, NAA15 immunoprecipitates from WT or *Naa10*-KO mouse livers were analyzed by mass spectrometry. We found five distinct peptides derived from Naa12 (**Table 2** and **Supplementary Excel File 1**). Three of these derive from the same part of the peptide sequence, RDLSQMADELRR, and all of these three peptides had one or two missed trypsin cleavages (DLSQMADELRR, RDLSQMADELR, and RDLSQMADELRR). The other two peptides, AMIENFSAK and ENQGSTLPGSEEASQQENLAGGDSGSDGK, are not the results of missed cleavages. None of these peptides are found in other sequences in the mouse genome and thus unambiguously identify Naa12 in our experiments. They have higher

intensities in Naa15 IPs compared to Ctrl IPs, indicating that Naa12 is selectively enriched by Naa15 IP. Some peptides are additionally assigned to the Naa10/Naa11/Naa12 protein group, as a large part of their sequences are identical. As expected, no unique Naa10 peptides are identified in the IPs from *Naa10*-KO mice. 12 peptides were ambiguously assigned to Naa12 or to Major urinary proteins (Mup9, Mup8, Mup1, Mup17, Mup5, or Mup2), but these are as likely to be derived from Mups as from Naa12, as they have comparable intensities between Ctrl and Naa15 IPs.

Table 2. Naa10, Naa11 and Naa12 peptides identified by LC-MS/MS analysis in Naa15 IP samples from WT and *Naa10*-KO mouse.

Gene name	Peptide sequence	Log2 LFQ intensity Naa15-IP	
		WT mouse	*Naa10*-KO mouse
Naa12	AMIENFSAK	23.8144	27.5563
Naa12	DLSQMADELRR	25.2637	28.38
Naa12	ENQGSTLPGSEEASQQENLAGGDSGSDGK	21.299	22.09
Naa12	RDLSQMADELR	-	22.20
Naa12	RDLSQMADELRR	-	27.77
Naa10	AALHLYSNTLNFQISEVEPK	26.7672	-
Naa10	AMIENFNAK	27.3981	-
Naa10	DLTQMADELRR	25.5107	-
Naa10	GNVLLSSGEACREEK	25.0717	-
Naa10	HMVLAALENK	25.5293	-
Naa10	NARPEDLMNMQHCNLLCLPENYQMK	25.8928	-
Naa10	YYFYHGLSWPQLSYIAEDENGK	26.5915	-
Naa12;Naa11	AALHLYSNTLNFQVSEVEPK	-	27.3833
Naa12;Naa11	YYFYHGLSWPQLSYIAEDEDGKIVGYVLAK	-	25.2517
Naa12;Naa11;Naa10	IVGYVLAK	28.0873	25.7753
Naa12;Naa11;Naa10	MEEDPDDVPHGHITSLAVK	29.1069	29.265
Naa12;Naa11;Naa10	MEEDPDDVPHGHITSLAVKR	24.7605	21.7784
Naa12;Naa11;Naa10	YVSLHVR	22.8611	23.7383
Naa12;Naa11;Naa10	YYADGEDAYAMK	-	27.2083
Naa12;Naa11;Naa10	YYADGEDAYAMKR	27.2319	27.1689

Samples were run in technical duplicates and the average log2 LFQ intensity of the peptides are presented.

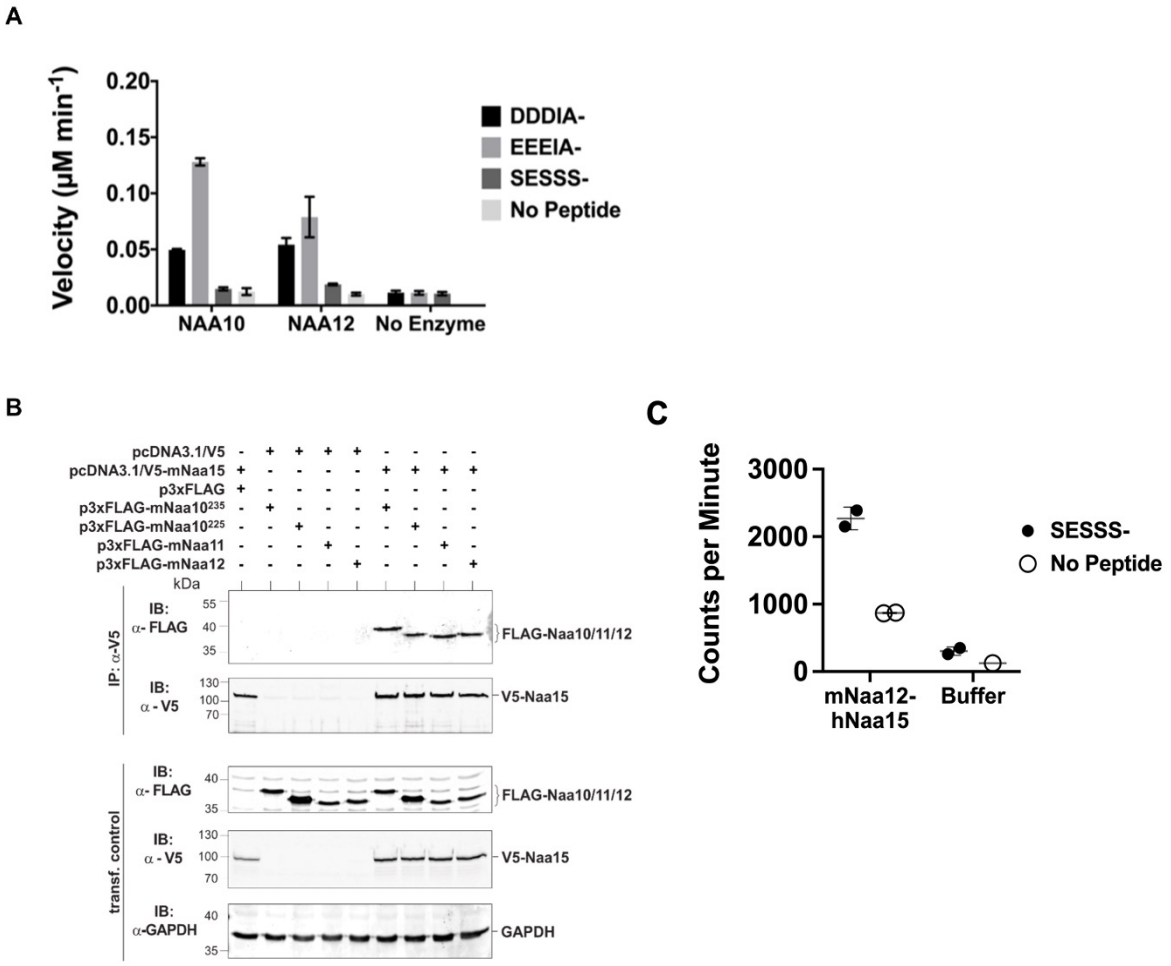

Fig. 4. Characterization of *Naa12*. (A) In vitro N-terminal acetyltransferase radioactive-based assay. Comparison of mouse Naa10 and Naa12 towards Naa10 peptide substrates, beta-actin (DDDIA-) and gamma-actin (EEEIA-), and the optimal NatA complex peptide substrate, SESSS-. Background control reactions were performed in the absence of either peptide or enzyme. Assays were performed in triplicate; error bars represent S.E.M. (B) Co-immunoprecipitation assay. HEK293 cells were transfected as indicated and lysed after 48 h. Cell lysates were incubated with 1 μg anti-V5 antibody to precipitate V5-tagged Naa15. The isolated complexes were separated on SDS-PAGE and probed with the indicated antibodies. (C) Recombinant mouse Naa12/human Naa15 chimera complex activity. Radioactive acetyltransferase activity assay evaluating the activity of mNaa12-hNaa15 towards peptide (closed circles, "mNaa12-hNaa15") and peptide chemical acetylation in the absence of enzyme (closed circles, "Buffer") as well as chemical acetylation of the the enzyme in the absence of peptide (open circles) assay and background (open circles). Error bars represent SD of two technical replicates. These are the same results from fraction #14 (both SESSS- and No Peptide) and both Buffer and Background used to illustrate the size-exclusion-purified mNaa12-hNaa15 complex activity in Supplement Fig. 6F.

Naa12 rescues loss of *Naa10* in mice

To investigate whether *Naa12* can rescue the loss of the function of Naa10 *in vivo*, *Naa12* KO mice were generated using CRISPR technology [58]. One 95-base pair deletion Δ131-225 in *Naa12* was characterized in depth (**Fig. 5**A). This mutation introduces a frameshift, leading to a termination codon at amino acid 67, which should either result in complete knockout of the protein or, at best, the expression of a truncated mini-protein that

would be far shorter than the usual 220 amino acid Naa12. We confirmed the deletion by PCR with genomic DNA (**Fig. 5**B). QPCR further showed deletion of *Naa12* in the tested tissues of *Naa12* KO mice (**Fig. 5**C), however, it seemed that *Naa12* might be slightly expressed in testis. Due to the high similarity between *Naa11* and *Naa12*, the expression shown in *Naa12* KO testis could actually be *Naa11* rather than *Naa12*, and this was confirmed by RT-PCR showing definite deletion (**Supplement Fig. 7**A).

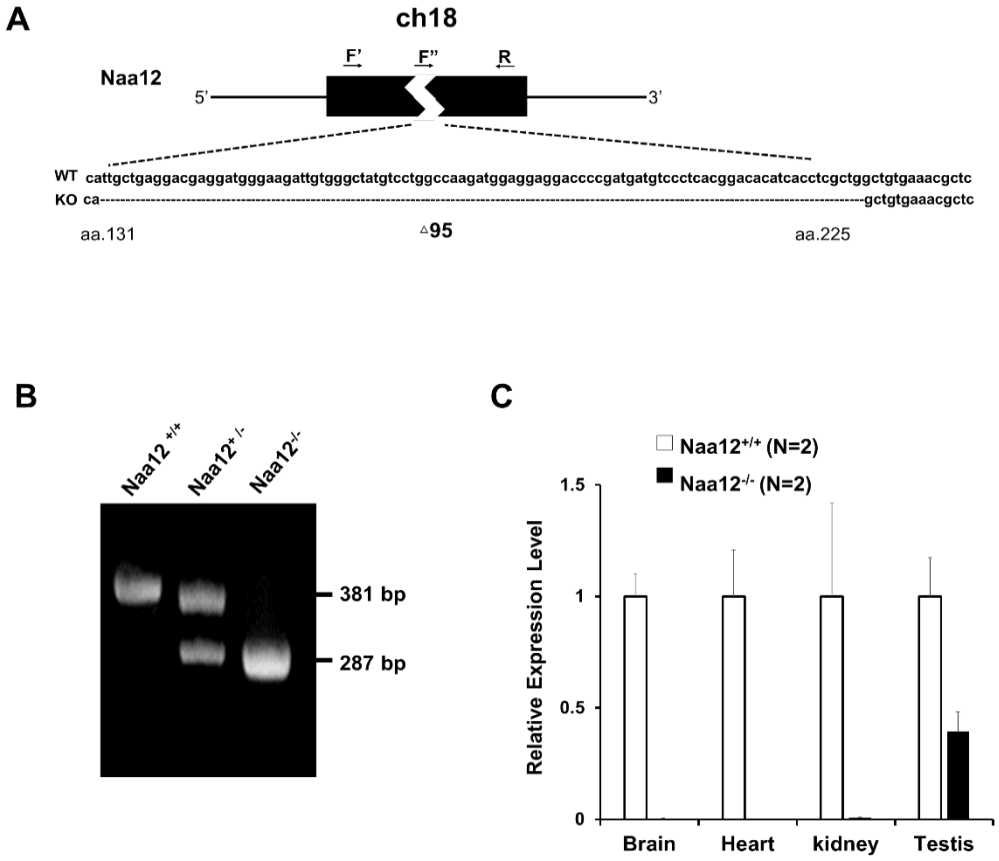

Fig. 5. Generation of *Naa12* KO mice. (A) Scheme of *Naa12 (*Gm16286, UniProt: Q9CQX6) deletion used to generate *Naa12* KO mouse. 95 base pairs (131-225) were deleted. F'; genomic DNA forward primer, F"; cDNA forward primer, R; reverse primer. (B) Genotyping of *Naa12* KO mice by PCR. WT allele size was 381bp and targeted allele size was 287bp. (C) mRNA level of *Naa12* were analyzed in selected tissues by qPCR. Relative expression level of WT (white bars) and *Naa12* KO (black bars) after normalizing to that of GAPDH.

Paralogs are homologous genes that originate from the intragenomic duplication of an ancestral gene. Homologs that play a compensatory role can sometimes show similar phenotypes to each other when one of them is deficient [59], whereas other homologs might only offer partial compensation when the primary gene is more widely expressed or has higher activity levels. We analyzed *Naa12* KO mice to see if they produced similar developmental defects to those in *Naa10* KO mice. Knockout mice for this gene were viable

(**Supplement Table 6).** Although there was initially a question of decreased fertility for the male mice, larger numbers of matings and litters did not bear this out (**Supplement Table 4**), and necropsy and inspection of testes and seminal vesicles under a stereomicroscope did not reveal any macroscopic differences. Furthermore, the phenotypes (piebaldism and bilateral supernumerary ribs, **Fig. 2**B) observed in *Naa10* KO mice with complete penetrance were not present in *Naa12* KO mice (**Supplement Fig. 7**C). Overall, there were not any obvious phenotypes in these mice.

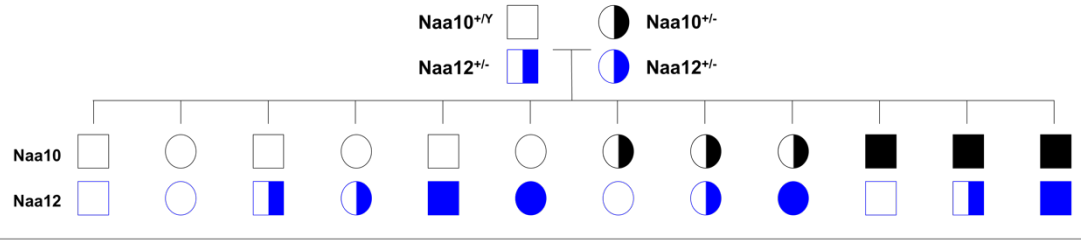

Genotype	Naa10+/Y Naa12+/+	Naa10+/+ Naa12+/+	Naa10+/Y Naa12+/-	Naa10+/+ Naa12+/-	Naa10+/Y Naa12-/-	Naa10+/+ Naa12-/-	Naa10+/- Naa12+/+	Naa10+/- Naa12+/-	Naa10+/- Naa12-/-	Naa10-/Y Naa12+/+	Naa10-/Y Naa12+/-	Naa10-/Y Naa12-/-	Unable t genotyp
E10.5 (n=29)	1	2	1	4	3	3	3	6	2†	0	4*†	0	3
E18.5 (n=33)	4	5	5	7	3	1	1	5	0	1	1	0	23
Postnatal (n=157)	17	16	31	28	17	16	14	5	0	13	0	0	0

* delayed embryonic days
† lysed embryo

Fig. 6. Lethality in *Naa10 Naa12* DKO mice. *Naa10 Naa12* DKO exhibit embryonic lethality. Pedigree and genotypes of pups and embryos at E10.5 and E18.5 from *Naa10*$^{+/-}$ *Naa12*$^{+/-}$ female mice crossed to the *Naa10*$^{+/Y}$ *Naa12*$^{+/-}$ male mice.

Matings between *Naa10*$^{+/-}$ *Naa12*$^{+/+}$ female mice and either *Naa10*$^{+/y}$ *Naa12*$^{+/-}$ or *Naa10*$^{+/y}$ *Naa12*$^{-/-}$ males produced zero male *Naa10*$^{-/y}$ *Naa12*$^{+/-}$ progeny, while also suggesting that compound heterozygous (*Naa10*$^{+/-}$ *Naa12)* female mice are produced at a rate much less than predicted by Mendelian ratios (**Supplement Table 7** and **Supplement Table 8**). Matings between surviving compound heterozygous (*Naa10*$^{+/-}$ *Naa12*$^{+/-}$) females and *Naa10*$^{+/Y}$ *Naa12*$^{+/-}$ males demonstrate that no live births occurred for *Naa10 Naa12* double-knockout (DKO) males (*Naa10*$^{-/Y}$ *Naa12*$^{-/-}$) (**Fig. 6**). In addition, the average litter size was small when compared to the control (WT x WT) matings, suggesting embryonic lethality (**Table 2**). In order to determine whether lethality occurs during the embryonic stage, we genotyped E18.5 litters – just before birth. Consistent with our previous observations, we could not obtain any *Naa10*$^{-/Y}$ *Naa12*$^{-/-}$ embryos, and many embryos could not be genotyped because they were already in the midst of resorption (n=23) (**Fig. 6**). We checked an even earlier stage at E10.5 and also found zero *Naa10*$^{-/Y}$ *Naa12*$^{-/-}$ embryos, and also with far fewer resorptions at this stage (N=3). Interestingly, we did observe *Naa10*$^{-/Y}$ *Naa12*$^{+/-}$ embryos where two of them displayed delayed developmental stage (appearing younger than E10.5) and another two embryos were lysed and had already begun degenerating (but despite this,

we could at least genotype these embryos). This helps explain why only one *Naa10*$^{-/Y}$ *Naa12*$^{+/-}$ embryo was observed at E18.5. Furthermore, *Naa10*$^{+/-}$ *Naa12*$^{-/-}$ female embryos were also lysed/degenerating at E10.5 and were not observed from that day onward. Matings between compound heterozygous females and *Naa10*$^{+/Y}$ *Naa12*$^{-/-}$ males also did not yield any *Naa10*$^{-/Y}$ *Naa12*$^{-/-}$ male mice at any embryonic stage examined, and only a couple of *Naa10*$^{+/-}$ *Naa12*$^{-/-}$ female mice at early stages of development (**Supplement Fig. 8**), and the litter sizes were even smaller, suggesting increased embryonic lethality (**Table 2**). Consistent with this, we noted many resorptions at E12.5 and E18.5 that could not be genotyped. The number of living postnatal compound heterozygous female mice was also considerably lower than the predicted Mendelian ratios (**Fig. 6** and **Supplement Fig. 8**), and the surviving *Naa10*$^{+/-}$ *Naa12*$^{+/-}$ females were smaller in size than littermate controls (**Fig. 7**D).

Table 2. Litter size of Naa10 Naa12 DKO matings

Genotypes of Naa10; Naa12 breeders (♀ x ♂)	Total number of pups	Total number of litters	Average litter size (pups/litters)	SD of litter size
Naa10$^{+/+}$ *Naa12*$^{+/+}$ X *Naa10*$^{+/Y}$ *Naa12*$^{+/+}$	206	24	8.6	1.6
Naa10$^{+/-}$ *Naa12*$^{+/-}$ X *Naa10*$^{+/Y}$ *Naa12*$^{+/-}$	157	32	4.9	1.5
Naa10$^{+/-}$ *Naa12*$^{+/-}$ X *Naa10*$^{+/Y}$ *Naa12*$^{-/-}$ ***	225	63	3.6	1.7

SD : Standard Deviation
***This mating was performed at IBR in Staten Island, New York, whereas the other two matings were performed at Ewha Womans University, Seoul, Republic of Korea.

Due to the severe embryonic lethality observed in the *Naa10 Naa12* DKO male mice and the *Naa10*$^{+/-}$ *Naa12*$^{-/-}$ female mice, which was not seen in each single KO (*Naa10* KO or *Naa12* KO), it seems likely that, without compensation by Naa12, amino-terminal acetylation is disrupted in *Naa10 Naa12* DKO mice. Together, these data support the compensatory role of Naa12 *in vivo*.

Genotype distribution modeling of *Naa10*- and *Naa12*-deficient offspring

The discrepancies we noted between the observed offspring genotype distributions and the expected Mendelian frequencies prompted us to examine the results from four matings (**Supplement Table 9** – **Supplement Table 14**) with the goal of understanding the effects of combined *Naa10* and *Naa12* mutations on embryonic and postnatal mortality. We created mathematical models to predict the observed genotype distribution at each age based on successive incorporation of assumptions of the lethality of specific offspring genotypes. Embryonic genotype data was obtained from two matings for which embryonic genotype data were obtained (**Supplement Table 9** and **Supplement Table 10**). Those matings were (1) *Naa10*$^{+/Y}$*; Naa12*$^{+/-}$ males crossed with *Naa10*$^{+/-}$*; Naa12*$^{+/-}$ females (**Fig. 6**; **Supplement Table 9**) and (2) *Naa10*$^{+/Y}$*; Naa12*$^{-/-}$ males crossed with *Naa10*$^{+/-}$*; Naa12*$^{+/-}$ females (**Supplement Fig. 8**; **Supplement Table 10**). The genotype numbering shown in

Supplement Table 9 was used throughout this analysis and the corresponding genotypes for all other crosses are aligned to have the same numbers. Each model described below adjusted the expected observed genotype frequencies at each age to account for loss of embryos or pups due to the predicted lethal effects of one or more genotypes by the method described in Materials and Methods. Three stages of models (B – D) were compared with the expected Mendelian distribution (model A).

Model B assumed that the double KO male genotype 12 (*Naa10*$^{-/Y}$*; Naa12*$^{-/-}$ is lethal from very early in development based on the observation that this genotype was not found in any embryos or pups out of 483 obtained genotypes from all litters. Specifically, 0 out of an expected 7.9 were detected at E10.5 or earlier, 0 out of an expected 14.5 were detected at E18.5 or earlier and 0 out of an expected 46.7 were detected by postnatal day 3. Thus, the survival for genotype 12 was 0% for all ages examined.

Model C was developed from model B in two stages by incorporating separately observations that the male genotype 11 (*Naa10*$^{-/Y}$*; Naa12*$^{+/-}$) and the female genotype 6 (*Naa10*$^{+/-}$*; Naa12*$^{-/-}$) were lethal during mid to late fetal development. Based on the Mendelian model, 5 of 9.8 (51%) expected genotype 11 were detected by E10.5 but only 1 of expected 8.6 (11.6%) were identified on E12.5 or E18.5 and none were detected at postnatal day 3. The five embryos that were present at E10.5 were noted to be lysed and/or developmentally delayed; the single E18.5 genotype 11 embryo was not observed to be abnormal. Based on the Mendelian model for genotype 6, 1 of 2.6 expected E8.5 embryos and 3 of 5.3 expected E10.5 embryos were identified. All three E10.5 embryos were identified as lysed. Genotype 6 was not identified after age E10.5. Cumulatively, 4 of 7.9 expected embryos detected by E10.5 and 0 of 38.8 expected embryos/pups thereafter.

Model D incorporated the assumptions of models B and C and added adjustments to the survival rates of genotype 5 (*Naa10*$^{+/-}$*; Naa12*$^{+/-}$) and genotype 10 (*Naa10*$^{-/Y}$*; Naa12*$^{+/+}$) based on the observations that these genotypes were underrepresented at late fetal ages or early postpartum. Genotype 5 was overrepresented during embryogenesis (31 identified but only 18.4 expected for all embryonic ages) but was underrepresented at P3 (17 of 42 expected) based on the expected Mendelian frequencies. A better analysis was achieved by comparing the observed genotype frequencies with those predicted by model C because the expected distributions are significantly affected by the lethal effects of the three genotypes considered in that model. In that case, the genotype overrepresentation during embryogenesis is somewhat less (31 identified but only 22.1 expected) but the underrepresentation at P3 is significantly increased (17 identified of 62 expected, or 27%). Using a model (D_3) that incorporated adjusted survival rates for genotypes 12, 11, 6 and 5, we found that genotype 10 remained underrepresented in the observed postnatal offspring counts. The subsequent model (D_4) incorporated adjustments to genotype 10 survival rates at E18.5 and P3 to account for this and then was slightly refined by adjusting other genotype survival rates to maximize the fit of all genotypes at all ages. The survival values for model D_4 are shown in **Table 3**. A comparison of the observed offspring numbers with those predicted by the Mendelian distribution and model D_4 are shown in **Supplement Fig. 9** – **Supplement Fig. 12**.

476 **Table 3. Model D_4 Genotype Survival by Age**

#*	Genotype	E8.5	E10.5	E12.5	E18.5	Postnatal
12	*Naa10*$^{-/Y}$; *Naa12*$^{-/-}$	0%	0%	0%	0%	0%
11	*Naa10*$^{-/Y}$; *Naa12*$^{+/-}$	40%	35%	10%	10%	0%
6	*Naa10*$^{+/-}$; *Naa12*$^{-/-}$	40%	33%	0%	0%	0%
5	*Naa10*$^{+/-}$; *Naa12*$^{+/-}$	100%	100%	100%	100%	35%
10	*Naa10*$^{-/Y}$; *Naa12*$^{+/+}$	100%	100%	100%	55%	55%
	All Others	100%	100%	100%	100%	100%

477 *Genotype number according to **Supplement Table 9**.

478 The observations of reduced survival for selected *Naa10*/*Naa12* mutants suggests that
479 *Naa10* is the more dominant function (e.g., is able to provide *Naa12* functions more
480 successfully than *Naa12* can provide *Naa10* functions) but that two copies of *Naa10* are
481 required to replace complete loss of *Naa12* in females, possibly due to X-linked inactivation
482 of *Naa10* during development. The stochastic nature of X-linked inactivation in time and
483 space may make *Naa10* functionality somewhat unpredictable during development in a
484 background having a mixture of *Naa10* and *Naa12* mutations.

485 **Statistical examination of weight data in *Naa10*- and *Naa12*-deficient mice**

486 To determine whether Naa10 and Naa12 are essential for viability and development,
487 we examined the survival, weights, and growth rates of 688 *Naa10* and *Naa12* knockout and
488 wild type mice. The genotypes of mice examined are listed in **Supplement Table 15**. To
489 avoid potential survival biases, only weights taken during the first 180 days were included.
490 Growth curves are shown in **Fig. 7**. Age and age-squared (the quadratic term) are both
491 entered in the analyses; the quadratic term shows the degree to which the effect of age itself
492 changes with age.

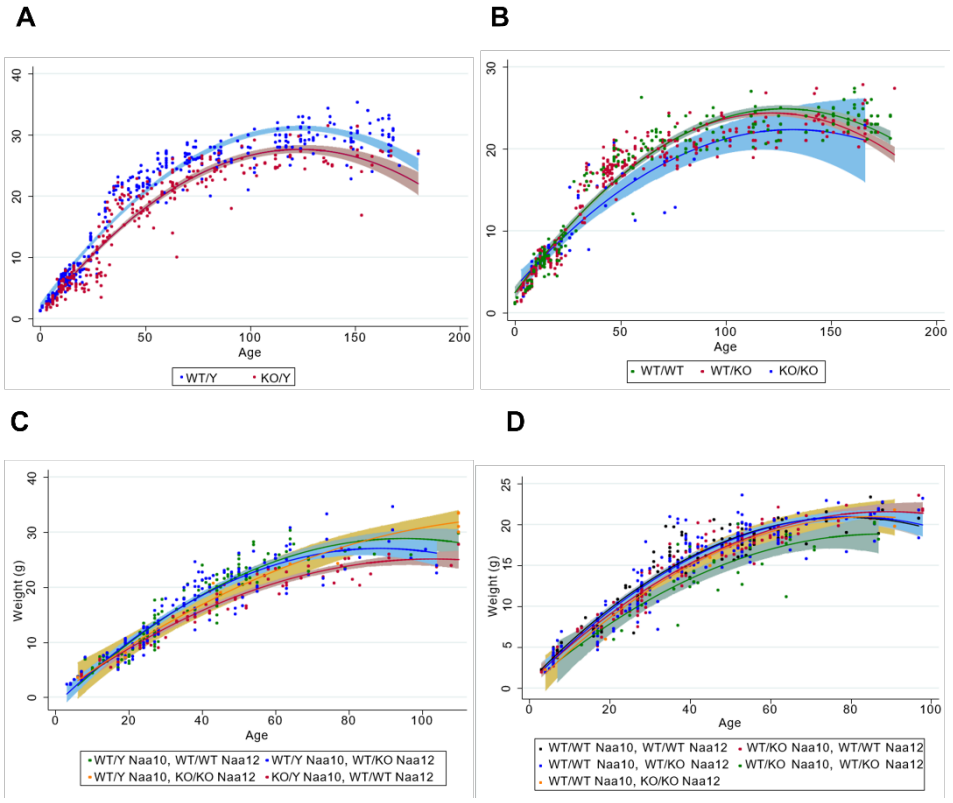

Fig. 7. Decreased body weight in compound heterozygous females. (A) Male body weight for the *Naa10* mice on inbred genetic background (8 backcrosses to C57bl6/J). (B) Female body weight for the *Naa10* mice on inbred genetic background (8 backcrosses to C57bl6/J). (C) Male body weight for the *Naa10* and *Naa12* mice on mixed genetic background. (D) Female body weight for the *Naa10* and *Naa12* mice on mixed genetic background.

Supplement Table 16 shows the results in which weight of *Naa10* mice in grams is regressed upon age, Naa10 knockout status, and their interaction. Unsurprisingly, age predicts weight for males and females strongly, with growth slowing with age (first column). Though a strong negative effect of the knockout is seen in for both males and females (second column), when both age and knockout status are modeled together (third column) this effect all but disappears in females. Moreover, in females there is no interaction of knockout status with age (fourth column), suggesting that the *Naa10* knockout status itself has no significant effect on the growth rate in females. For males, however, the main effect of the knockout remains when age is included in the model (third column) and the interaction is significant (fourth column), indicating that the *Naa10* knockout both reduces weight of males overall and lowers the rate of growth.

Results of analyses of mixed-genetic background Naa10/Naa12 mice are shown in **Supplement Table 17**. Effects of age and knockouts on weight comprise the upper portion of the table, while the lower portion shows their effect on the rate of weight gain. Among females a significant reduction of weight (above, second column) and in the rate of growth (below, first column) is seen among mice heterozygous for the Naa10 KO. There were no homozygous Naa10 KO female mixed-breed mice available to analyze, as the matings were not set up to yield any such mice (so breeding patterns, not mortality in utero, are the reason

for this absence). No significant effect on growth rate is seen for heterozygous or homozygous Naa12 KO (above, third column) or for their interactions with age (below, second column), and only the effects of the heterozygous Naa10 KO and its interaction with age are seen in the full model (below, third column). Thus, the Naa12 KO, whether heterozygous or homozygous, does not appear to reduce the weight or growth rate of females, while a heterozygous Naa10 KO is sufficient to reduce both weight and growth rate. Interestingly, when modeled together, both the Naa10 and the *Naa12* KOs significantly reduced weight (above, fourth column) and the interaction of the Naa10 and the *Naa12* heterozygous KOs significantly reduced weight (above, fifth column). As no female mice were both KO for *Naa10* and homozygous KO for *Naa12*, the effect of the interaction of those two factors could not be determined. The triple interaction of heterozygous *Naa10* KO, *Naa12* KO and age was weakly significant, suggesting that the presence of both knockouts affects growth rate above and beyond the effects of each knockout independently (below, fourth column). No males with knockouts of both *Naa10* and *Naa12* were born, so no test of their interaction was possible. An effect was seen for the Naa10 knockout on weight when modeled with age and age^2 (second column), and the significant interaction of the *Naa10* knockout with age and age^2 (third column) shows that the *Naa10* KO in males reduces the growth rate. As with females, no significant effect of a *Naa12 KO*, whether heterozygous or homozygous, was seen in males, nor is there a significant interaction with age (fourth column). When the interactions of age with both *Naa10* and *Naa12* knockout status are entered in one model, *Naa10* alone is seen to reduce growth rates (fifth column).

Discussion

We have shown that Naa10 deficiency results in pleotropic developmental defects in two different Naa10-deficient mouse models. Similar to infant mortality in some OS males, the lethality of *Naa10* KO mice increased dramatically in pups in the first 3 days of life (**Fig. 1**B). Defects in kidney, brain, pigmentation (piebaldism), and ribs were observed during embryonic or early postnatal stages in some mice (**Fig. 2**B and **Fig. 2**C). These observed phenotypes overlap with some of the phenotypes found in surviving humans with OS, including supernumerary vertebrae and hydrocephaly, although piebaldism has not been reported to date in any humans. However, the puzzling lack of embryonic lethality in the *Naa10* KO mice prompted us to discover *Naa12* as a possible compensatory NAT, with Naa10-like amino-terminal acetylation activity (**Fig. 4A**), with an interaction between Naa15 and Naa12 (**Fig. 4B**), and with enzymatic activity in a chimeric complex with human NAA15 (**Fig. 4C**). In addition, co-immunoprecipitation of endogenous Naa15 from Naa10 KO mouse tissues followed by mass spectrometry analysis (Error! Reference source not found.) and amino-terminal acetylation assays (**Fig. 3**C) fully support that the endogenous Naa12-Naa15 complexes produces NatA activity. Finally, we found genetic proof of the compensatory activity of Naa12 in mice when we observed embryonic lethality in in *Naa10 Naa12* DKO male and *Naa10*$^{+/-}$ *Naa12*$^{-/-}$ female mice (**Fig. 6** and **Supplement Fig. 7**). This compensation by Naa12 explains the mouse proteomics data indicating normal amino-terminal acetylation

in Naa10 KO mice (**Fig. 3**A). We have confirmed the expression of Naa12 in various tissues using qPCR and Western blot analyses (**Supplement Fig. 5**A-**Supplement Fig. 5**E). The band for Naa12 runs a little higher in the Western blot than the calculated molecular weight would suggest, which is consistent with previous observations of NAA10 gel migration. Future characterization of Naa12 may define possible post-translational modifications specific for Naa12 that might account for the variability of detection by the antibody.

Gene duplication has long been believed to be a major driving force in evolution that provides genetic novelty in organisms. Paralogous genes, originating by small-scale or whole-genome duplication, overlap functional roles for each other and can completely or partially compensate for the loss of the duplicate gene [59, 60]. There is not yet any human reported with complete knockout for *NAA10*. There is one published truncating variant in the C-terminal portion of NAA10 in a male patient with microphthalmia [35], but unfortunately there are no cell lines available from this family to confirm whether any truncated NAA10 protein is expressed, as was shown with a splice-site mutation in a Lenz microphthalmia family [29]. NAA10 was also identified in screens for essential genes in human cell lines [61, 62], so it seems unlikely that an unknown NAA10-like paralogous gene exists in humans, other than the already known NAA11.

The pleiotropic phenotypes shown in *Naa10* KO mice, including hypopigmentation and supernumerary ribs with a penetrance of 100%, were not observed in the *Naa12* KO mice. Naa10 itself has been described to have N-ε-acetyl-activity towards internal lysine residues of proteins involved in various disease- and development-related signaling pathways [11], although its acetylation of some substrates is controversial [63, 64]. Since the Nt-acetylome appears to be globally intact in MEFs from *Naa10* KO mice, it is possible that the presented phenotypes could be due to the loss of Naa10-specific N-ε-acetyl-activity or non-catalytic roles of Naa10 [4]. Alternatively, the quantitative expression of Naa10 and Naa12 might be different within or between tissues, which might then explain why there is clearly a phenotype for $Naa10^{+/-}$ $Naa12^{+/-}$ female mice (not born at Mendelian ratios and the few that are born are usually much smaller) but no apparent phenotype in $Naa10^{+/+}$ $Naa12^{-/-}$ female mice. It seems likely that the mechanism cannot be simply additive between two equally expressed proteins, because if the expression of each protein is theoretically set at an arbitrary unit of 10, then $Naa10^{+/-}$ $Naa12^{+/-}$ female mice might possibly have half as much of each protein, so that the total dose of both proteins together would be 10, instead of 20. Likewise, the total dose of both proteins together would also be predicted to be 10 in a $Naa10^{+/+}$ $Naa12^{-/-}$ female. Yet, the $Naa10^{+/-}$ $Naa12^{+/-}$ female mice have a phenotype, whereas the $Naa10^{+/+}$ $Naa12^{-/-}$ female mice do not (**Fig 6**). Therefore, other explanations could include different tissue-specific dosages of each protein, different expression between different tissues, possible X-chromosome skewing for the X-linked *Naa10* in different tissues, or different functions of the two enzymes, including Naa10-specific N-ε-acetyl-activity or non-catalytic roles of Naa10 [4]. These questions remain unanswered and are worth exploring in future studies. It is worth highlighting that X-chromosome inactivation could certainly be one explanation, given that males that are $Naa10^{+/Y}$ with $Naa12^{+/-}$ or $Naa12^{-/-}$ show expected

survival rates, whereas females that are *Naa10*$^{+/-}$ with *Naa12*$^{+/-}$ show ~35% survival but with *Naa12*$^{-/-}$ show 0% survival.

There are several clinical features that were presented in the original description of OS [26] which can now be better understood in light of the phenotypes found in the knockout mouse model. For example, all of the affected children in the first families with OS were noted to have large and, in some cases, persistently open fontanels [25, 26]. For one child (Family 1, Individual II-1), CT scanning revealed cerebral atrophy with enlarged ventricles, and in another child (Family 1, Individual III-4), there was evidence on magnetic resonance imaging (MRI) of "moderate lateral and third ventricular dilatation without identified cause". Lastly, all of the children had respiratory depression and apneic episodes, along with varying course of hypotonia and/or hypertonia (including documented hyperreflexia in at least one case (Family 2, Individual III-2)). In retrospect, it seems that these clinical features could be consistent with mild hydrocephaly in these probands with Ogden syndrome, which resolved over time. This is also consistent with the ventriculomegaly reported in several female OS probands with missense mutations in *NAA10*, along with ventriculomegaly in one other male proband who died in the first week of life, with generalized hypotonia and lack of spontaneous respirations [65]. One of the female patients with an Arg83Cys mutation in Naa10 (#9 in table 1 of that paper) was reported as having intraventricular hemorrhage in the occipital horn, hypoxic-ischemic encephalopathy, and a ventriculo-peritoneal shunt. It is possible that this sequence of events is compatible with hydrocephaly with clinical signs and symptoms that required the placement of the shunt.

There are additional cardiac and skeletal features that are also worth re-examining in light of these new findings. In some of the original cases of OS, there were varying levels of pulmonary valve stenosis detected on echocardiography, along with some documentation of pulmonary hypoplasia [26]. For example, individual III-7 in Family 1 was found on echocardiography to have small persistent ductus arteriosus, a mildly decreased left ventricular systolic function, an abnormal appearing aortic valve, an enlargement of the right ventricle, decreased right ventricular systolic function, and persistence of the foramen ovale. Individual III-6 from this same extended family was found on echocardiography to have a thickened bicuspid aortic valve and mild pulmonary hypertension. One of the OS female patients with an Arg83Cys mutation in *NAA10* was reported to have “supernumerary vertebrae” [65]. Prompted by our findings of supernumerary ribs in the mice, we obtained an MRI report for this patient, in which the radiologist concluded that there appeared to be 25 distinct vertebrae, as opposed to the usual 24, with a suggestion of a 13th rib, at least on the right. The report went on to state that "the vertebrae represent 7 cervical vertebrae, 13 rib-bearing thoracic vertebrae, and 5 lumbar vertebrae, and the L1 vertebra is mildly dysmorphic, with a suggestion of anterior breaking". In addition, chest and abdominal X-rays from two of the brothers in generation VI of a family with microphthalmia demonstrated the presence of 13 rib-bearing thoracic vertebrae, alongside the dramatic scoliosis in both individuals. Four other females carrying mutations in Naa10 were reported as having either pectus carinatum or excavatum [65], one of the boys with OS (Family 1, Individual III-4) was noted to have pectus excavatum, and retrospective review of some of the clinical photographs appears to

show mild pectus excavatum in individual III-6 of the same family. Studies of human populations have shown that the levels of transition may be shifted cephalad, resulting in 23 mobile vertebrae, or shifted caudad, resulting in 25 presacral vertebrae. Such variations may occur in 2-11% of the population [66]. In addition, the number of ribs can also vary in mice, as a result of teratogenic and genetic influences [67, 68]. However, the complete penetrance for supernumerary ribs in the *Naa10*-deficient mice, along with the presence of extras ribs in some of the patients, suggest that there is a pathway common to humans and mice that is altered by mutations involving *NAA10*.

Several mouse mutants show similar cardiac or skeletal phenotypes to the *Naa10*-deficient mice. *Pax3* mutants phenocopy our *Naa10*$^{-/-}$ mutants, as *Pax3*$^{+/-}$ adults exhibit 100% piebaldism, and exhibit neural crest (NC)-related PTA/DORV with concomitant VSDs [69-72]. *Pax3* systemic nulls also have skeletal defects due to abnormal somite morphogenesis [73, 74]. Moreover, *Pax3* cKOs demonstrated that NC-specific deletion is sufficient to cause DORV/VSDs and death at birth [72, 75], and that restricted deletion within the neuroepithelium causes congenital hydrocephalus [76]. While *Pax7* systemic deletion does not cause NC-associated defects, it does exhibit overlapping expression, and Pax3-Pax7 compound heterozygous mice develop hydrocephalus [76], suggesting combinatorial function. *Hox C8*$^{-/-}$ mice exhibit an extra rib and an extra rib articulating with the sternum [77, 78], and an unfused sacral vertebra which lead to 27 presacral vertebrae [79], as seen in our model. *Hox A4*$^{-/-}$ mice described in Horan et al. [80] shows cervical fusions of C2/C3, a rib on C7 not fully penetrant and sternal defects with bone ossification anomalies. *Hox A5*$^{-/-}$ mice display numerous cervico-thoracic defects such as a rib process coming from the 7th cervical vertebra, an increased in the number of sternebrae and total number of ribs [81]. Both *Hox A4*$^{-/-}$ and *A5*$^{-/-}$ mice exhibit an extra rib articulating with the sternum. *Hox D3*$^{-/-}$ mice are the only Hox gene mutation leading to cervical fusion of both the atlas and axis [82]. *Hox A9*$^{-/-}$ mice have anteriorization of both sacral and lumbar parts, with an extra pair of ribs at the lumbar level. *Hox A9*$^{-/-}$ mice do not have any relevant sternal defect [83]. *Hox B9*$^{-/-}$ mice have an extra rib articulating with the sternum and 14 pairs of rib [84]. These phenotypes, especially *Hox C8*, share common features with the *Naa10*-deficient mice. This phenotype is also close to the *Rpl38*$^{-/-}$ phenotype [85], except for the sacral fusion described in *Rpl38*$^{-/-}$ mice. Interestingly, it was shown that *Hox* genes were dysregulated in this genotype. The skeletal findings and comparison to other mutant mice suggest a pattern consistent with a homeotic anterior transformation hypothesis.

The developmental role of Naa10 in mice has been previously described [44]. Lee *et al.* reported embryonic lethality at E12.5-14.5 and beyond (due to placental defects), hydrocephaly, postnatal growth retardation, and maternal effect lethality in *Naa10* KO mice and suggested that genomic imprinting dysregulation is associated with those developmental phenotypes. In the present study, hydrocephaly and postnatal growth retardation were also apparent, but embryonic lethality was not observed, which prompted the search for and discovery of Naa12. The previous paper [44] did not report the piebaldism, homeotic anterior transformation, hydronephrosis, and genital defects (such as seminal vesicle malformation and hydrometrocolpos), nor did they explain the cause of death in the first day of life, which

is at least partly due to congenital heart defects, as reported herein. A more recent paper from the same group reported that conventional and adipose-specific Naa10p deletions in mice resulted in increased energy expenditure, thermogenesis, and beige adipocyte differentiation in the surviving mice [86], although the authors do not comment on whether any of the male mice used in that study starting at age 5 weeks ended up developing hydrocephaly and/or hydronephrosis, which we have observed in older mice. Although the Lee *et al.* paper [44] reported a very high maternal effect lethality rate of 90% (46/51) (otherwise stated as a survival rate of 10% (5/51)) for newborns in matings following *Naa10*$^{-/-}$ female and C57BL/6J wild type male intercrossing, this rate was only 29% (37/127) in this same mating herein in the first 24 hours of life and with a total death rate in the first three days for all newborns of 46/127, or 36% (**Supplement Table 4**), with this result deriving from a larger number of mating pairs, litters and pups. Although this rate of 36% is higher than that seen with matings involving *Naa10*$^{+/-}$ females (15.8% and 13.6%) (**Supplement Table 4**), the explanation for this ~20% difference in survival in the first 3 days of life could involve differences in maternal care provided by the *Naa10*$^{+/-}$ and *Naa10*$^{-/-}$ females, but this would have to be investigated in future studies, involving detailed behavioral and cognitive assessment of the dams.

The reasons for the differences between the studies in regards to maternal effect lethality and *in utero* lethality are unknown at present. Whilst Lee *et al.* deleted *Naa10* exons 2-6 [44], the current study deleted *Naa10* exons 1-4 or used an allele *Naa10*^{tm1a} expressing β-galactosidase instead of the *Naa10* gene (**Supplement Fig. 1**), and there was not any significant embryonic lethality in either line (**Supplement Table 1** and **Supplement Table 2**). All three of these mouse models were made using 129Sv/Ev ES cells, and all three are nulls lacking Naa10 protein. It is the case that the previous study used the Cre/loxP system to generate the *Naa10* KO mice, where a floxed Naa10 female mouse was crossed with the Ella-Cre transgenic male mouse expressing Cre recombinase for germ line deletion of loxP-flanked *Naa10*, whereas our mice were made using standard gene-targeting methods without the use of Cre recombinase, but it is not clear how this would have resulted in embryonic lethality, particularly as these mice were only used after "at least six generations of backcross with C57BL/6 mice", which are noted by the authors to be the substrain C57BL/6JNarl, first established at the Animal Center of National Research Institute from the Jackson Laboratory (JAX) in 1995. The explanation for differences in embryonic lethality might be more likely due to different combinations of modifying alleles that are present in the different C57BL/6J substrain genetic backgrounds, rather than differences in our model systems, and future plans will address this after back-crossing more than 20 generations to C57BL/6J (imported annually from JAX) to achieve an entirely inbred line. The impact of genetic background is supported by the observation that additional null alleles on mixed genetic backgrounds, made during the process of generating missense mouse models for OS, have far less penetrance for a range of the various phenotypes, including much less perinatal lethality (unpublished observations).

In conclusion, our study provides strong evidence that Naa10, the catalytic subunit of N-acetyltransferase A (NatA), is critical for normal development in mice. Furthermore, this

study explains the puzzle regarding the lack of complete embryonic lethality in the *Naa10* knockout mice due to the discovery of a second mouse *Naa10* paralog, which, unlike *Naa11*, is expressed in the heart as well as other tissues. Taken together, our findings suggest that the newly identified Naa12 can functionally rescue Naa10 loss and act as a catalytic subunit in mouse NatA complexes.

Materials and Methods

Mice. All experiments were performed in accordance with guidelines of International Animal Care and Use Committee (IACUC) of Ewha Womans University, Cold Spring Harbor Laboratory (CSHL), and Institute for Basic Research in Developmental Disabilities (IBR). At CSHL and IBR, any matings that required genotyping were screened on a daily basis by animal husbandry staff, with notation of how many newborn pups were present each morning, but with paw tattoo and tail genotyping not being performed until day 3 of life, so as to not disturb the litters and thus to not increase the risk for maternal rejection of the litter. The stock of C57BL/6J was replenished annually from Jackson Laboratory, so as to avoid genetic drift from the JAX inbred line.

Generation of *Naa10* deficient mice. The *Naa10* knockout (KO) mice were generated as previously described [41]. *Naa10*^{tm1a} [B6;129P2-Ard1$^{tm1a(Eucomm)Gto}$/J] (*Naa10*^{tm1a}) mice, used for *Naa10* reporter mouse, were generated using standard method based on a standard gene-targeting in E14 embryonic stem (ES) cells (129/Sv) by using a targeting vector from EUCOMM. Correctly targeted ES clones were used for blastocyst microinjection and generation of chimeric mice. Chimeric mice were crossed to C57BL/6J mice, and then the progeny were backcrossed to C57BL/6J for more than ten generations. The *Naa10*-deficient mice used in the weight analyses were derived from mice backcrossed 8 times to a C57BL/6J inbred genetic background, and this was confirmed with genome scanning at the Jackson Laboratory, showing heterozygosity for only one marker for 129S1/SvImJ out of 290 autosomal markers tested, thus giving a percentage of C57BL/6J of 99.66%.

Generation of *Naa12* (Gm16286, UniProt: Q9CQX6) knockout mice. The mice were made using standard methods by microinjection of CRISPR reagent mix into zygotes obtained from the mating of B6D2F1 females (i.e. 50% C57BL/6J, 50% DBA/2J (D2)) females to inbred C57BL/6J males. The guide RNA was produced and validated from Sigma using a Cel1-nuclease assay, and the most active guide was selected, which was Naa12_0_125 (C9587), with a target sequence of: GAGCGTTTCACAGCCAGCG and including the targeting cr-RNA sequence and the tracrRNA portion. The indels were transmitted by breeding again to inbred C57BL/6J males, and the resulting progeny were interbred on a mixed genetic background of approximately 12.5% DBA/2J (D2) / 87.5% C57BL/6J, for use in the reported experiments, including the weight analyses. Progeny from these mice have been backcrossed to C57BL/6J for more than ten generations, with no discernible new phenotypes emerging. Genomic DNA was isolated from paw and tail. DNA was screened for mutations using PCR and Surveyor assay [87], followed by Sanger sequencing of selected clones and the use of CRISP-ID [88] to identify putative deletions.

Primers for mice genotyping. The primers used for *Naa10 KO* and *Naa10*^{tm1a} genotyping were Naa10-F: 5'-cctcacgtaatgctctgcaa-3', Naa10-neo-F: 5'-acgcgtcaccttaat-atgcg-3', Naa10-R: 5'- tgaaagttgagggtgttgga-3', Naa10^{tm1a}-F: 5'-gcacactctctgaattggac-3', Naa10^{tm1a}-neo-F: 5'-ggccgcttttctggattcat-3' and Naa10^{tm1a}-R: 5'-gcaggggaataaggcattgg-3'. The primers used for

Naa12 KO were Naa12 Surveyor F: 5'-gctccacctcgctaacctgg-3', Naa12 Surveyor R: 5'-gccagatgacctgatgaacatgc-3' and HEX-Naa12 Surveyor F: 5'-gctccacctcgctaacctgg-3'.

Antibodies. The following antibodies were used: Rabbit anti-Naa10 (Abcam #ab155687), rabbit anti-Naa10 (Protein Tech #14803-1-AP), rabbit monoclonal anti-NAA10 (CellSignaling, #13357), goat anti-Naa10 (Santa Cruz, #sc-33256), rabbit anti-Naa10 (Santa Cruz, #sc-33820), rabbit anti-Naa11 (Novus Biologicals ; #NBP1-90853), mouse anti-Naa15/NARG1 (Abcam ; #ab60065), rabbit polyclonal anti-NAA15 [12], rabbit anti-Naa50 (LifeSpan BioSciences ; #LS-C81324-100), rabbit anti-FLAG (Sigma; #F7425), mouse anti-GAPDH (Abcam ; #ab9484), goat anti-Actin (Santa Cruz, #1615), mouse anti-GST (GenScript ; #A00865) and mouse anti-V5 (Life Technologies ; #R960-25). The antibody against the potential mNaa10 paralog mNaa12 (Gm16286, UniProt: Q9CQX6) was raised in rabbits after immunization with a synthetic peptide of the Naa12 C-terminus (aa191-205: QENLAGGDSGSDGKD-C) conjugated to OVA by PrimmBiotech.

Alcian blue and Alizarin red co-staining of skeletons. After the skin and internal organs were removed, embryos were fixed in 95% ethanol (EtOH) for 4h, then in 100% acetone for overnight. Embryos were stained with 0.03% Alcian Blue 8GX in ethanol/ acetic acid (4:1 v/v) for overnight and kept in 1% KOH for 2 days until they became clearly visible, followed by staining with 0.05% Alizarin Red in 1% KOH for 4h. After washing with 100% Glycerol/ 1% KOH (1:1 v/v), skeletons were kept in 100% Glycerol.

Isolation and imaging of mouse embryos. Timed matings were performed either by using the presence of a vaginal plug to assess fertilization. The morning vaginal plug was designated E0.5. Pregnant mice were sacrificed at several time points after conception. The embryos were isolated in ice-cold PBS with 1% FBS and washed three times in ice-cold PBS. Embryos were imaged using a Zeiss Axiozoom V16 with Zen software and merged 50 slides between Z-stack intervals.

β-galactosidase staining. Isolated E10.5 embryos were incubated in fixation solution (4% paraformaldehyde) at 4°C for 25min. Samples were washed in ice-cold PBS and then incubated in permeabilization solution (PBS containing 0.01% Na deoxycholate, 0.02% Nonidet-P40, 2 mM MgCl2) for 20 min at 4°C. Subsequently, samples were incubated in β-gal staining solution (PBS containing 1 mg/mL X-Gal, 5 mM potassium ferrocyanide, 5 mM potassium ferricyanide, 0.02% Nonidet-P40, 2 mM MgCl2) at 37°C overnight. Following β-gal staining, samples were washed with PBS and incubated in fixation solution at 4°C for storage.

Hematoxylin and Eosin Staining. Isolated kidney tissues at E18.5 and P3 were fixed with 4% paraformaldehyde at 4°C for overnight and embedded in paraffin. Samples were sectioned at 8 micron thick and stained with Hematoxylin (MHS80, Sigma) and Eosin (HT110116, Sigma) for morphology.

Cloning. Full-length mouse Naa10 and Naa12 (Gm16286, UniProt: Q9CQX6) expression vectors were separately constructed using a pMAL-c5x vector. In both cases, the catalytic subunit contained an N-terminal uncleavable MBP-tag. Bacterial expression vectors of mNATs were cloned from cDNA generated from mouse liver or testes. mRNA was isolated using the Oligotex direct mRNA kit (Qiagen) according to the manufacturer recommendations. 1µg RNA was reverse transcribed with Superscript IV reverse transcriptase (Thermo Fisher) and Oligo dT(18) primer. The PCR product was digested and

cloned into BamHI restriction sites of pGEX-4T1 (GE Healthcare), pMAL-p5X and p3xFLAG-CMV10 (Sigma-Aldrich) using standard techniques. All constructs were sequenced to validate correct insert and orientation.

Primers for cloning. cDNA was amplified using the primers CCG GGA TCC ATG AAC ATC CGC AAT and CTG GGA TCC CTA GGA GGC AGA GTC AGA for mNaa10 variants, CCG GGA TCC ATG AAC ATC CGC AAT GC and CTG GGA TCC CTA GGA GAT GGA ATC CAA GTC for mNaa11, CCG GGA TCC ATG AAC ATC CGC CGG and CTG GGA TCC CTA GGA GGC GGA CCC TAG for mNaa12.

Peptide competition assay. To determine the specificity of the mNaa12 antibody, a peptide competition assay was performed using the same peptide as used for immunization (aa 191-205: QENLAGGDSGSDGKD-C). 100 µg antibody were bound to 50 mg peptide-coupled CNBr-Sepharose (10 mg peptide/g Sepharose) in PBS + 0.2 % Triton X-100 for 1 h at 4° C on an orbital shaker. The beads were pelleted by centrifugation at 2.700 × g for 3 min at 4°C and 250 µl of the antibody-depleted supernatant diluted in 5 mL TST for detection (1:100 final antibody dilution). Western blots of mouse lysates were probed with the depleted antibody or untreated antibody as control (1:100 dilution in TST).

Cell lines. HEK293 cells were purchased from ATCC, authenticated via STR profiling, and confirmed mycoplasma free.

Co-immunoprecipitation assay. Protein-protein interaction studies were performed in HEK293 cells. Briefly, 8 x 10^5 cells were seeded per well in 6-well plates. After 24 h, cells were co-transfected with pcDNA3.1/V5-His-mNaa15 and p3xFLAG-CMV10-Naa10^{235} (isoform 1), -Naa10^{225} (isoform 2), -Naa11 or -Naa12 or the corresponding empty vectors. Cells were lysed after 48 h in 200 µl PBS-X per well and cellular debris pelleted at 20.800×g for 10 min at 4°C. 350 µl of the generated lysate was incubated with 1 µg anti-V5 antibody for 1 h at 4°C, followed by a 30 min incubation with 30 µl protein-A Sepharose (Sigma-Aldrich). Protein complexes were washed three times by centrifugation (2.700×g, 2 min) and eluted in 30 µl 2×SDS sample buffer.

Proteins were separated by SDS-PAGE and transferred onto a nitrocellulose membrane (Amersham Protran 0.2 µM NC) by immunoblotting. The membrane was blocked in 5% non-fat dry milk and incubated overnight with rabbit polyclonal anti-NAA15[12] (1:2000, BioGenes) and rabbit monoclonal anti-NAA10 (anti-ARD1A, 1:1000, CellSignaling, #13357) diluted in 1xPBS containing 1% non-fat dry milk and 0.1% Tween. The immunoblots were washed and incubated for 1 h at RT with HRP-linked secondary antibody donkey anti-rabbit IgG (GE Healthcare, NA934). The HRP-signal was detected using SuperSignalTM West Pico PLUS Chemiluminescent Substrate Kit (Thermo Scientific) and ChemiDocTM XRS+ system (Bio-Rad) and visualized by ImagelabTM Software (Bio-Rad).

Immunoprecipitation of Naa15 to form NatA complex. For immunoprecipitation of Naa15, 90-120 mg liver tissue from a WT- and Naa10 KO mouse was lysed in 500 µl IPH lysis buffer (50 mM Tris-HCl pH 8.0, 150 mM NaCl, 5 mM EDTA, 0.5% NP-40, 1× complete EDTA-free protease inhibitor cocktail (Roche) using Kontes Pellet Pestle Motor and incubated on ice for 40 min. Cell debris was pelleted by centrifugation (17000 × *g*, 4 °C, 10 min) and the supernatants transferred to new Eppendorf tubes. The protein concentration was determined by BCA Protein Assay Kit (Thermo Scientific) and the tissue lysates were subsequently diluted with IPH lysis buffer to an equal protein concentration of 25 µg/µl. The

WT- and Naa10 KO tissue lysates were then divided in two, whereof one half was mixed with 15 µg of anti-Naa15 antibody and the other half with 15 µg of anti-V5 antibody as a negative control. The mixtures were incubated at 4 °C for 3 h on a rotator. Afterwards, 180 µl of Protein A/G magnetic beads (Millipore) pre-washed in IPH lysis buffer was added to each sample and incubated overnight. Then, the magnetic beads were washed three times in IPH lysis buffer and two times in 1x acetylation buffer (100 mM Tris-HCl pH 8.5, 2 mM EDTA, 20% Glycerol) prior to being resuspended in 90 µl of 2x Acetylation buffer and used in a [^{14}C]-Ac-CoA–Based acetylation assay.

[^{14}C]-Ac-CoA–based acetylation assay of immunoprecipitated samples. Three positive replicates were prepared for each IP sample containing 10 µl IP beads, 200 µM synthetic oligopeptide $SESS_{24}$ (BioGenes), 100 µM [^{14}C]-Ac-CoA (Perkin-Elmer) and dH_2O to a final volume of 25 µl. In addition, two replicates for each IP sample were prepared without synthetic oligopeptide as negative controls. The samples were incubated at 37 °C for 45 min in a thermomixer with shaking at 1400 rpm. Finally, the magnetic beads were isolated and 23 µl of the supernatant transferred to P81 phosphocellulose filter discs (Millipore). The filter discs were washed three times for 5 min in 10 mM HEPES buffer (pH 7.4) and air dried. To determine the amount of incorporated [^{14}C]-Ac, the filter discs were added to 5 mL Ultima Gold F scintillation mixture (Perkin-Elmer) and analyzed by a Perkin-Elmer TriCarb 2900TR Liquid Scintillation Analyzer.

Proteomics sample preparation. Immunoprecipitation of Naa15 from a WT- and Naa10 KO mouse was performed as described above. Bound proteins were eluted from the magnetic beads using 60 µl of elution buffer (2% SDS, 100 mM Tris-HCl pH 7.6, 0.1 M DTT) and heated for 5 min at 95 °C. The eluates were processed for LC-MS/MS analysis using filter-aided sample preparation (FASP) method[89]. The eluted protein mixtures were mixed with UA buffer (8 M urea, 100 Mm Tris-HCl pH 8.0) and centrifuged through Microcon 30kDa MWCO filters followed by Cys-alkylation with 50 mM iodoacetamide dissolved in UA buffer. Afterwards, the buffer was exchanged with 50 mM ammonium bicarbonate through sequential centrifugation, proteins were trypsinized (Sequencing Grade Modified Trypsin, Promega) and digested peptides were collected by centrifugation. Peptides were acidified using 5% formic acid and desalted using C18-stagetips according to protocol[90]. Briefly, 40 µg peptides from each sample were loaded onto C18-stagetips pre-conditioned with buffer A (1% formic acid). The C18-stagetips were then washed with buffer A, before peptides were eluted with buffer B (80% acetonitrile/ACN, 1% formic acid). The final eluate was concentrated by Speedvac to evaporate ACN and diluted to desired volume with 5% formic acid.

Mass spectrometric analysis. 1 µg of the peptide samples were injected into an Ultimate 3000 RSLC system (Thermo Scientific) connected to a Q-Exactive HF mass spectrometer (Thermo Scientific) equipped with EASY-spray nano-electrospray ion source (Thermo Scientific). Trapping and desalting was performed with 0.1% TFA (flow rate 5 µl/min, 5 min) on a pre-column (Acclaim PepMap 100, 2cm x 75µm ID nanoViper column, 3µm C18 beads). Peptides were separated on an analytical column (PepMap RSLC, 50cm x 75 µm i.d. EASY-spray column, 2µm C18 beads) during a biphasic ACN gradient with a flow rate of 200 nl/min. Solvent A (0.1% FA (vol/vol) in water) and B (100% ACN) were used for the following gradient composition: 5% B for 5 min, 5-8% B for 0.5 min, 8–24% B for 109.5 min, 24–35% B for 25 min and 35–80% B for 15 min, 80% B for 15 min and conditioning with 5% B for 20 min. The mass spectrometer was operated in data-dependent mode to automatically switch between full scan MS and MS/MS acquisition. MS spectra (m/z 375-

1500) were acquired with a resolution of 120 000 at m/z 200, automatic gain control (AGC) target of 3 x 10^6 and maximum injection time (IT) of 100 ms. The 12 most intense peptides above an intensity threshold (50 000 counts, charge states 2-5) were sequentially isolated to an AGC target of 1 x 10^5 and maximum IT of 100 ms and isolation width maintained at 1.6 m/z, before fragmentation at a normalised collision energy of 28%. Fragments were detected in the orbitrap at a resolution of 15 000 at m/z 200, with first mass fixed at m/z 100. Dynamic exclusion was utilized with an exclusion time of 25 s and "exclude isotopes" enabled. Lock-mass internal calibration (m/z 445.12003) was used. Raw files were processed with MaxQuant v. 1.6.17.0 [91] and searched against a database of Swiss-Prot annotated mouse protein sequences (retrieved 22.06.2018) in which the NAA12 sequence was added manually, and with a reverse decoy database. MaxQuant was run with default settings. Peptide and protein identifications were filtered to a 1 % false discovery rate (FDR). Minimum peptide length was set to 7. Modifications included in protein quantification were oxidation (M), Nt-acetylation, acetylation (K), and phosphorylation (STY). Other parameters: match between runs – true, matching time window – 0.7 min, alignment time window – 20 min, find dependent peptides – true, mass bin size – 0.0065. Protein and peptide intensities were quantified by label-free quantification (LFQ) [92].

Whole body CT scanning. CT scans were acquired on a Nanoscan PET/CT scanner from Mediso using Nucline v2.01 software. All mice were kept sedated under isoflurane anesthesia for the duration of the scan. Scans were acquired with an X-ray tube energy and current of 70kVp and 280uA respectively. 720 projections were acquired per rotation, for 3 rotations, with a scan time of approximately 11 minutes, followed by reconstruction with a RamLak filter and voxel size 40x40x122µm. For *ex vivo* analyses, mouse heads were fixed in 10% formalin buffered saline, followed by scanning and reconstruction with 1440 projections per revolution. Cranial volume was measured using VivoQuant software (v2.50patch2), using the spline tool to manually and accurately draw around the circumference of the cranium on multiple stepwise 2D slices.

Integrated N-terminal peptide enrichment (iNrich) assay. iNrich assays were performed as described [45]. Mouse embryonic fibroblasts (MEFs) were made from E13.5 embryos, using standard techniques, with DMEM media supplemented with 10% fetal bovine serum (FBS), L-glutamine and penicillin/streptomycin. Cells were harvested by trypsinization, washed twice with ice-cold PBS (phosphate-buffered saline, pH 7.4; Gibco), and resuspended in ice-cold lysis buffer containing 0.2 M EPPS (pH 8.0), 6 M guanidine, 10 mM TCEP (Thermo Fisher Scientific), and 40 mM 2-chloroacetamide (Sigma-Aldrich). After 10 min of incubation on 95 °C, cells were lysed by ultrasonication by a BranSonic 400B. The proteins from the cell lysate were isolated by transferring supernatant after centrifugation at 12000g for 10 min at 4 °C. The protein concentration of the collected supernatant was determined by BCA (bicinchoninic acid) protein assay. Mass spectrometry data were uploaded to PRIDE under Project Name: Naa10 mutant mouse N-terminome LC-MS, Project accession: PXD026410. Data analysis used unpaired, equal variance algorithm for Student's t-test.

RNA and protein isolation and assays. 70-120 mg tissues were lysed in 5 µl/mg tissue RIPA buffer (Sigma) with 1x Complete protease inhibitors and 1 U/µl Superase In RNase inhibitor (Thermo Scientific) using Fisherbrand Pellet Pestle Cordless Motor. After homogenization debris was removed by centrifugation at 20.800 g for 10 min at 4°C. Protein concentration was determined using APA assay (Cytoskeleton Inc.) and 50 µg total protein were separated on SDS-PAGE followed by western blot. Membranes were stained with anti-Naa10, anti-Naa15 and anti-GAPDH antibodies (all Abcam).

For RNA purification, 30 µl clarified lysate were mixed with 70 µl RNase free water and RNA isolated using the RNeasy Mini Kit (Qiagen) according the manufacturers recommendations, including on-column Dnase digest. 1 µg RNA was reverse transcribed using the TaqMan Reverse transcription kit and gene level detection performed using SYBR Green Master Mix (all Thermo Scientific). Relative expression was normalized to GAPDH and ACTB.

For the characterization of the mNaa12 antibody, tissue was lysed in 2 µl per mg tissue PBS-X (PBS + 0.2 % (v/v) Triton X-100 + 1 × Complete protease inhibitor cocktail). 10-200 µg lysate were subjected to SDS-PAGE and western blot.

Primers for mice qPCR. The following primers pairs were used: mNaa10-Exon2/3-F: 5'-ctcttggccccagctttctt-3' and mNaa10-Exon3/4-R: 5'- tcgtctgggtcctcttccat -3', mNaa11-F: 5'-accccacaagcaaagacagtg-3' and mNaa11-R: 5'- agcgatgctcaggaaatgctct -3', mNaa12(Gm16286)-F: 5'-acgcgtatgctatgaagcga-3' and mNaa12(Gm16286)-R: 5'-ccaggaagtgtgctaccctg-3', mNaa15-F: 5'-gcagagcatggagaaaccct-3' and mNaa15-R: 5'-tctcaaacctctgcgaacca-3', mNaa50-F: 5'-taggatgccttgcaccttacc-3' and mNaa50-R: 5'-gtcaatcgctgactcattgct-3', mGAPDH-F: 5'-aggtcggtgtgaacggatttg-3' and mGAPDH-R: 5'-tgtagaccatgtagttgaggtca-3', mACTB-F: 5'-ggctgtattcccctccatcg-3' and mACTB-R: 5'-ccagttggtaacaatgccatgt-3'.

Expression and purification of WT mouse, Naa10 and Naa12. All constructs were expressed in Rosetta (DE3)pLysS competent *E. coli* cells. Cells were grown in LB-media to OD_{600} 0.6-0.7 prior to inducing protein expression with 0.5 mM isopropyl β-D-1-thiogalactopyranoside (IPTG) at 18°C for ~16 hrs. All subsequent purification steps were carried out at 4°C. Cells were isolated by centrifugation and lysed in lysis buffer containing 25 mM Tris, pH 8.0, 150 mM NaCl, 10 mM β-mercaptoethanol (β-ME), 10 µg/mL phenylmethanesulfonylfluoride (PMSF), and DNase. The lysate was clarified by centrifugation and incubated with amylose agarose resin (New England Biolabs) for 1 hour before washing the resin with ≥100 column volumes of lysis buffer and then eluted with ten column volumes of lysis buffer supplemented with 20 mM maltose. The resulting eluent was pooled and concentrated to ~10 mg/mL (30 kDa concentrator; Amicon Ultra, Millipore) such that 500 µl was loaded onto on a Superdex 200 Increase 10/300 GL gel filtration column (GE Healthcare). The gel filtration run was performed in sizing buffer containing 25 mM HEPES, pH 7.0, 200 mM NaCl, and 1 mM TCEP. After confirming the purity of the peak fractions at ~14 mL by denaturing SDS-PAGE (15% acrylamide), peak fractions were concentrated to 0.6 (6.1 µM) WT mouse Naa10 and 0.3 mg/mL (3.5 µM) WT mouse Naa12, as measured by UV_{280} (Nanodrop 2000; Thermo Fisher Scientific), and stored at 4°C.

Expression and Purification of recombinant mNaa12 (1-160)-hNaa15 constructs

Subcloning Both full-length and truncated (1-160) mouse Naa12 were amplified from the pMAL-c5x Naa12 plasmid using Q5 HF Master Mix (NEB), AAAACCCGGGTATGAACATCCGCCGGGCTCGGC as the forward primer, and either AAAAGGTACCCTAGGAGGCGGACCCTAGGGTCTG (full-length) or AAAAGGTACCTCACCGTCTCAGCTCATCGGCCATCTG (1-160) as the reverse primer. An *S. frugiperda* (*Sf*9) pFastBac dual vector containing the sequence for the N-terminally 6xHis-tagged human Naa15 and truncated human Naa10 (residues 1-160) sequences was digested using KpnI-HF (NEB) and XmaI (NEB) to remove the human Naa10 sequence. The PCR product was also digested using the same restriction enzymes and ligated into the

corresponding restriction sites using Mighty mix (Takara) using standard techniques. Both constructs were sequenced to validate the insert sequence and directionality.

Sf9 cells were grown to a density of $1x10^6$ cells/ml and infected using the amplified baculoviruses to an MOI (multiplicity of infection) of ~1-2. Because the full-length mNaa12 construct did not produce protein, cells transfected with mNaa12$_{1-160}$/hNaa15 were grown at 27°C and harvested 48 hours post-infection. All subsequent purification steps were carried out at 4°C. Following centrifugation of the cells, the pellet was resuspended and lysed in buffer containing 25 mM Tris, pH 8.0, 500 mM NaCl, 10 mM Imidazole, 10 mM β-ME, 10 µg/ml PMSF, DNase, and complete, EDTA-free protease inhibitor tablet (Roche). The lysate was clarified by centrifugation and incubated with nickel resin (Thermo Scientific) for 1 hr before washing the resin with ~125 column volumes of lysis buffer and then eluted with ten column volumes of elution buffer (25 mM Tris, pH 8.0, 500 mM NaCl, 200 mM Imidazole, 10 mM β-ME). Eluted protein was diluted to a final salt concentration of 200 mM NaCl and loaded onto a 5 mL HiTrap SP ion-exchange column (GE Healthcare).The protein was eluted in the same buffer with a salt gradient (200mM-1 M NaCl) over the course of 20 column volumes. Using the resulting peak fractions, the remainder of the purification was performed as described for the recombinant monomeric mNaa10 and mNaa12. However, resulting size exclusion fractions were analyzed by denaturing SDS-PAGE using a 12% acrylamide gel, which was then silver stained (Bio Rad) according to manufacturer instructions.

***In vitro* radioactive acetyltransferase assays with recombinant protein**. For recombinant mNaa12 and mNaa10 constructs, the assays were carried out in 40 mM HEPES, pH 7.5 200 mM NaCl, where reactions were incubated with 150 nM of the gel-filtration purified WT mouse Naa10 or Naa12 in a 30 µl reaction volume containing each 250 µM substrate peptide and radiolabeled [^{14}C]acetyl-CoA (4 mCi/mmol; PerkinElmer Life Sciences) for 12 min (Naa12) or 13 min (Naa10) at 25°C. Respective time points were selected to ensure detection of sufficient activity within the linear range as determined by a time course experiment. The substrate peptides used in the assay corresponds to the first 7 amino acids of β-actin (DDDIAAL-), γ-actin (EEEIAAL-), or the *in vivo* NatA complex substrate High mobility group protein A1 (SESSS-) , along with C-terminal positively charged residues for capture to the anion exchange paper. Background control reactions were performed in the absence of enzyme or in the absence of substrate peptide to ensure that any possible signal due to chemical acetylation was negligible. Each reaction was performed in triplicate.

To quench the reaction, 20 µl of the reaction mixture was added to negatively charged P81 phosphocellulose squares (EMD Millipore), and the paper disks were immediately placed in wash buffer (10 mM HEPES, pH 7.5). The paper disks were washed three times, at 5 min per wash, to remove unreacted acetyl-CoA. The papers were then dried with acetone and added to 4 mL of scintillation fluid, and the signal was measured with a PerkinElmer Life Sciences Tri-Carb 2810 TR liquid scintillation analyzer. The counts per minute were converted to molar units using a standard curve of known [^{14}C]acetyl-CoA concentrations in scintillation fluid.

Full peptide sequences:
β-actin: NH2-DDDIAALRWGRPVGRRRRPVRVYP-COOH
γ-actin: NH2-EEEIAALRWGRPVGRRRRPVRVYP-COOH
High mobility group protein A1: NH2-SESSSKSRWGRPVGRRRRPVRVYP-COOH

For mNaa12-hNaa15, reactions were carried out similar to the monomeric mNaa12 and mNaa10, with the following exceptions: reactions were prepared by combining 21 µL of the respective fraction or sizing buffer with 5 µL of 10X buffer (500 mM HEPES pH 7.5) to yield a buffer composed of 50 mM HEPES, pH 7.5, 140 mM NaCl, 0.7 mM TCEP and 250 µM of each substrate upon reaction initiation. The reactions were allowed to incubate overnight at ambient temperatures (~25°C) and then quenched as described above. Control reactions were conducted in parallel as described above without conversion to molar units. Two technical replicates of the reactions were performed.

Statistical analyses. Significant differences ($p<0.05$) are indicated by asterisks. Weight analyses were performed using generalized estimating equations (GEEs) [93], an extension of generalized linear models which adjusts for the effects of autocorrelation resulting from multiple measurements, and implemented within version 15.1 of Stata (Statacorp 2017).

Genotype Distribution Analyses and Modeling. Genotype distributions for several *Naa10/Naa12* knockout crosses were analyzed and models were created to estimate the number of the live (or at least intact) embryos or pups that are expected to be observed based on the assumptions and rules that follow. (1) Genotype survival rates are the fractional value, from zero to one (or 0% to 100%), of the expected Mendelian fraction for that genotype in the cross being evaluated. (2) Genotype survival rates cannot exceed 1 (or 100%). (3) Genotype survival rates can decrease with age but not increase. (4) Wild-type genotypes ($Naa10^{+/Y}$; $Naa12^{+/+}$ and $Naa10^{+/+}$; $Naa12^{+/+}$) are expected to have 100% survival at all ages because the models predict the number of embryos or pups relative to wild-type survival. Reductions in overall in litter sizes for crosses were estimated through other calculations. (5) The biological basis for a reduced survival rate assumes that loss of one or more copies of either *Naa10* or *Naa12* removes or reduces functions that are required for successful embryonic development or postnatal life. Reduced survival rates for non-wild-type genotypes were estimated based on differences (delta) between the expected number of embryos or pups based on the Mendelian proportion (or the current best model) and the observed number of embryos or pups. Separate comparisons were made using deltas for each specific age and for the cumulative numbers at each age. (6) Genotype frequencies for each model were calculated as described in the section below. (7) The fit between a model and the observed data was determined by calculating the relative standard deviation (SD) for the deltas across all genotypes, e.g. the standard deviation across genotypes divided by the number of animals observed (either age-specific or cumulative). Each model was evaluated at each age by minimizing the relative SD for all genotypes at that age and over all ages. The final model (D_4) was created by refining the assumptions for model D_3 in a sequential series of comparisons of survival rates for genotypes 12, 11, 6, 10 and 5 in that order.

Genotype Frequency Calculations. The models described adjust the expected observed genotype frequencies at each age to account for loss of embryos or pups due to the presumed lethal effects of one or more genotypes. The models account directly for the effect of genotype-specific mortality by reducing the number (or frequency) observed for that genotype in the sample and thus, increasing the expected proportion of other genotypes. This also indirectly implies a larger theoretical litter size at conception, which can be used to determine the theoretical litter sizes had there been no mortality in the affected genotypes. The predicted proportion for each genotype is calculated at each age as the genotype Mendelian frequency multiplied by the fractional genotype survival at that age divided by the expected total fractional survival (i.e., one minus the sum of all genotype fractional losses). The formula is:

For all "n" possible genotypes

$$G_x = M_x * S_x / (1 - [(1 - S_1) * M_1) + (1 - S_2) * M_2) + \ldots + (1 - S_n) * M_n)]$$

where:

G_x = Model genotype fractional value (frequency) for genotype "x" (G_x value from 0 to 1)

M_x = Mendelian fractional value (frequency) for genotype "x" for the cross

S_x = Fractional survival between 0 and 1

$(1 - S_n) * M_n$ is the fractional reduction due to survival < 100% for genotype "n", e.g., when $S_n = 1$ (e.g., 100% survival) the loss is zero

when $S_n = 0$ (e.g., 0% survival) the loss is M_n or the entire Mendelian fraction.

Note that the sum of all G_x for all genotypes at any age is always equal to 1 (or 100%).

Acknowledgments

G.T.O. thanks Huiju Jo for supporting mouse genotyping. G.J.L. would like to thank Ryan Driscoll for mouse genotyping, Fatima Inusa for embryo dissection, Jemima Kadima for mouse husbandry, Leyi Li for transgenic mouse assistance, Melissa Nashat, Jodi Coblentz, Rachel Rubino, and Lisa Bianco for veterinary advice, and Vicky Brandt for editorial assistance.

This work was supported by National Research Foundation of Korea (NRF) grants funded by the Korean Government (2020R1A3B2079811 (G.O.), 2017RIDIAB03032286 (M.L.), and 2020RICIC1007686 (M.L.)). Research reported in this publication was also supported by the National Institute of General Medical Sciences of the National Institutes of Health (NIH) under Award Numbers R35GM133408 (G.J.L) and R35GM118090 (R.M.), and NIH grant HL148165 (S.J.C.). The work was also supported by the Research Council of Norway (Project 249843), the Norwegian Health Authorities of Western Norway (Projects 912176 and F-12540-D11382), and the Norwegian Cancer Society (PR-2009-0222). The content is solely the responsibility of the authors and does not necessarily represent the official views of the National Institutes of Health. Funding was also provided by the Stanley Institute for Cognitive Genomics at Cold Spring Harbor Laboratory, the George A. Jervis Clinic and the Department of Human Genetics, Laboratory of Genomic Medicine at the New York State Institute for Basic Research in Developmental Disabilities (IBR), New York State Office for People with Developmental Disabilities. Part of the work was carried out at the Proteomics Unit at University of Bergen (PROBE).

Competing interests

The authors declare no competing interest.

References

1. Arnesen, T., et al., *Proteomics analyses reveal the evolutionary conservation and divergence of N-terminal acetyltransferases from yeast and humans.* Proc Natl Acad Sci U S A, 2009. **106**(20): p. 8157-62.
2. Dorfel, M.J. and G.J. Lyon, *The biological functions of Naa10 - From amino-terminal*

acetylation to human disease. Gene, 2015. **567**(2): p. 103-31.
3. Polevoda, B., T. Arnesen, and F. Sherman, *A synopsis of eukaryotic Nalpha-terminal acetyltransferases: nomenclature, subunits and substrates.* BMC Proc, 2009. **3 Suppl 6**: p. S2.
4. Aksnes, H., R. Ree, and T. Arnesen, *Co-translational, Post-translational, and Non-catalytic Roles of N-Terminal Acetyltransferases.* Mol Cell, 2019. **73**(6): p. 1097-1114.
5. Starheim, K.K., K. Gevaert, and T. Arnesen, *Protein N-terminal acetyltransferases: when the start matters.* Trends Biochem Sci, 2012. **37**(4): p. 152-61.
6. Ree, R., S. Varland, and T. Arnesen, *Spotlight on protein N-terminal acetylation.* Exp Mol Med, 2018. **50**(7): p. 1-13.
7. Shemorry, A., C.S. Hwang, and A. Varshavsky, *Control of protein quality and stoichiometries by N-terminal acetylation and the N-end rule pathway.* Mol Cell, 2013. **50**(4): p. 540-51.
8. Dikiy, I. and D. Eliezer, *N-terminal acetylation stabilizes N-terminal helicity in lipid- and micelle-bound alpha-synuclein and increases its affinity for physiological membranes.* J Biol Chem, 2014. **289**(6): p. 3652-65.
9. Holmes, W.M., et al., *Loss of amino-terminal acetylation suppresses a prion phenotype by modulating global protein folding.* Nat Commun, 2014. **5**: p. 4383.
10. Scott, D.C., et al., *N-terminal acetylation acts as an avidity enhancer within an interconnected multiprotein complex.* Science, 2011. **334**(6056): p. 674-8.
11. Lee, M.N., H.Y. Kweon, and G.T. Oh, *N-alpha-acetyltransferase 10 (NAA10) in development: the role of NAA10.* Exp Mol Med, 2018. **50**(7): p. 87.
12. Arnesen, T., et al., *Identification and characterization of the human ARD1-NATH protein acetyltransferase complex.* Biochem J, 2005. **386**(Pt 3): p. 433-43.
13. Arnesen, T., et al., *The chaperone-like protein HYPK acts together with NatA in cotranslational N-terminal acetylation and prevention of Huntingtin aggregation.* Mol Cell Biol, 2010. **30**(8): p. 1898-909.
14. Gottlieb, L. and R. Marmorstein, *Structure of Human NatA and Its Regulation by the Huntingtin Interacting Protein HYPK.* Structure, 2018. **26**(7): p. 925-935 e8.
15. Arnesen, T., et al., *Induction of apoptosis in human cells by RNAi-mediated knockdown of hARD1 and NATH, components of the protein N-alpha-acetyltransferase complex.* Oncogene, 2006. **25**(31): p. 4350-60.
16. Gendron, R.L., et al., *Loss of tubedown expression as a contributing factor in the development of age-related retinopathy.* Invest Ophthalmol Vis Sci, 2010. **51**(10): p. 5267-77.
17. Wang, Y., et al., *Drosophila variable nurse cells encodes arrest defective 1 (ARD1), the catalytic subunit of the major N-terminal acetyltransferase complex.* Dev Dyn, 2010. **239**(11): p. 2813-27.
18. Chen, D., et al., *daf-31 encodes the catalytic subunit of N alpha-acetyltransferase that regulates Caenorhabditis elegans development, metabolism and adult lifespan.* PLoS Genet, 2014. **10**(10): p. e1004699.
19. Linster, E., et al., *Downregulation of N-terminal acetylation triggers ABA-mediated drought responses in Arabidopsis.* Nat Commun, 2015. **6**: p. 7640.
20. Ree, R., et al., *The N-terminal acetyltransferase Naa10 is essential for zebrafish development.* Biosci Rep, 2015. **35**(5).
21. Feng, J., et al., *Protein N-terminal acetylation is required for embryogenesis in Arabidopsis.* J Exp Bot, 2016. **67**(15): p. 4779-89.
22. Chen, H., et al., *Nalpha-Acetyltransferases 10 and 15 are Required for the Correct*

Initiation of Endosperm Cellularization in Arabidopsis. Plant Cell Physiol, 2018. **59**(10): p. 2113-2128.

23. Mullen, J.R., et al., *Identification and characterization of genes and mutants for an N-terminal acetyltransferase from yeast.* EMBO J, 1989. **8**(7): p. 2067-75.
24. Polevoda, B. and F. Sherman, *Composition and function of the eukaryotic N-terminal acetyltransferase subunits.* Biochem Biophys Res Commun, 2003. **308**(1): p. 1-11.
25. Myklebust, L.M., et al., *Biochemical and cellular analysis of Ogden syndrome reveals downstream Nt-acetylation defects.* Hum Mol Genet, 2015. **24**(7): p. 1956-76.
26. Rope, A.F., et al., *Using VAAST to identify an X-linked disorder resulting in lethality in male infants due to N-terminal acetyltransferase deficiency.* Am J Hum Genet, 2011. **89**(1): p. 28-43.
27. Van Damme, P., et al., *A Saccharomyces cerevisiae model reveals in vivo functional impairment of the Ogden syndrome N-terminal acetyltransferase NAA10 Ser37Pro mutant.* Mol Cell Proteomics, 2014. **13**(8): p. 2031-41.
28. Dorfel, M.J., et al., *Proteomic and genomic characterization of a yeast model for Ogden syndrome.* Yeast, 2017. **34**(1): p. 19-37.
29. Esmailpour, T., et al., *A splice donor mutation in NAA10 results in the dysregulation of the retinoic acid signalling pathway and causes Lenz microphthalmia syndrome.* J Med Genet, 2014. **51**(3): p. 185-96.
30. Popp, B., et al., *De novo missense mutations in the NAA10 gene cause severe non-syndromic developmental delay in males and females.* Eur J Hum Genet, 2015. **23**(5): p. 602-9.
31. Casey, J.P., et al., *NAA10 mutation causing a novel intellectual disability syndrome with Long QT due to N-terminal acetyltransferase impairment.* Sci Rep, 2015. **5**: p. 16022.
32. McTiernan, N., et al., *NAA10 dysfunction with normal NatA-complex activity in a girl with non-syndromic ID and a de novo NAA10 p.(V111G) variant - a case report.* BMC Med Genet, 2018. **19**(1): p. 47.
33. Ree, R., et al., *A novel NAA10 p.(R83H) variant with impaired acetyltransferase activity identified in two boys with ID and microcephaly.* BMC Med Genet, 2019. **20**(1): p. 101.
34. Stove, S.I., et al., *A novel NAA10 variant with impaired acetyltransferase activity causes developmental delay, intellectual disability, and hypertrophic cardiomyopathy.* Eur J Hum Genet, 2018. **26**(9): p. 1294-1305.
35. Cheng, H., et al., *Phenotypic and biochemical analysis of an international cohort of individuals with variants in NAA10 and NAA15.* Hum Mol Genet, 2019. **28**(17): p. 2900-2919.
36. Cheng, H., et al., *Truncating Variants in NAA15 Are Associated with Variable Levels of Intellectual Disability, Autism Spectrum Disorder, and Congenital Anomalies.* Am J Hum Genet, 2018. **102**(5): p. 985-994.
37. Johnston, J.J., et al., *polyadenylation signal variants cause syndromic microphthalmia.* J Med Genet, 2019. **56**(7): p. 444-452.
38. Wu, Y. and G.J. Lyon, *NAA10-related syndrome.* Exp Mol Med, 2018. **50**(7): p. 1-10.
39. Arnesen, T., et al., *Characterization of hARD2, a processed hARD1 gene duplicate, encoding a human protein N-alpha-acetyltransferase.* BMC Biochem, 2006. **7**: p. 13.
40. Pang, A.L., et al., *Expression of human NAA11 (ARD1B) gene is tissue-specific and is regulated by DNA methylation.* Epigenetics, 2011. **6**(11): p. 1391-9.
41. Yoon, H., et al., *NAA10 controls osteoblast differentiation and bone formation as a feedback regulator of Runx2.* Nat Commun, 2014. **5**: p. 5176.

42. Conway, S.J., et al., *What cardiovascular defect does my prenatal mouse mutant have, and why?* Genesis, 2003. **35**(1): p. 1-21.
43. Pun, A., et al., *Genetic parameters for birthweight environmental variability in mice.* J Anim Breed Genet, 2013. **130**(5): p. 404-14.
44. Lee, C.C., et al., *The Role of N-alpha-acetyltransferase 10 Protein in DNA Methylation and Genomic Imprinting.* Mol Cell, 2017. **68**(1): p. 89-103 e7.
45. Ju, S., et al., *iNrich, Rapid and Robust Method to Enrich N-Terminal Proteome in a Highly Multiplexed Platform.* Anal Chem, 2020. **92**(9): p. 6462-6469.
46. Van Damme, P., et al., *NatF contributes to an evolutionary shift in protein N-terminal acetylation and is important for normal chromosome segregation.* PLoS Genet, 2011. **7**(7): p. e1002169.
47. Ward, T., et al., *Mechanisms of Congenital Heart Disease Caused by NAA15 Haploinsufficiency.* Circ Res, 2021. **128**(8): p. 1156-1169.
48. Ingram, A.K., G.A. Cross, and D. Horn, *Genetic manipulation indicates that ARD1 is an essential N(alpha)-acetyltransferase in Trypanosoma brucei.* Mol Biochem Parasitol, 2000. **111**(2): p. 309-17.
49. Foyn, H., et al., *Design, synthesis, and kinetic characterization of protein N-terminal acetyltransferase inhibitors.* ACS Chem Biol, 2013. **8**(6): p. 1121-7.
50. Van Damme, P., et al., *Proteome-derived peptide libraries allow detailed analysis of the substrate specificities of N(alpha)-acetyltransferases and point to hNaa10p as the post-translational actin N(alpha)-acetyltransferase.* Mol Cell Proteomics, 2011. **10**(5): p. M110 004580.
51. Liszczak, G., et al., *Molecular basis for N-terminal acetylation by the heterodimeric NatA complex.* Nat Struct Mol Biol, 2013. **20**(9): p. 1098-105.
52. Sugiura, N., S.M. Adams, and R.A. Corriveau, *An evolutionarily conserved N-terminal acetyltransferase complex associated with neuronal development.* J Biol Chem, 2003. **278**(41): p. 40113-20.
53. Park, E.C. and J.W. Szostak, *ARD1 and NAT1 proteins form a complex that has N-terminal acetyltransferase activity.* EMBO J, 1992. **11**(6): p. 2087-93.
54. Gautschi, M., et al., *The yeast N(alpha)-acetyltransferase NatA is quantitatively anchored to the ribosome and interacts with nascent polypeptides.* Mol Cell Biol, 2003. **23**(20): p. 7403-14.
55. Magin, R.S., et al., *Probing the interaction between NatA and the ribosome for co-translational protein acetylation.* PLoS One, 2017. **12**(10): p. e0186278.
56. Varland, S. and T. Arnesen, *Investigating the functionality of a ribosome-binding mutant of NAA15 using Saccharomyces cerevisiae.* BMC Res Notes, 2018. **11**(1): p. 404.
57. Kim, S.H., et al., *Characterization of ARD1 variants in mammalian cells.* Biochem Biophys Res Commun, 2006. **340**(2): p. 422-7.
58. Singh, P., J.C. Schimenti, and E. Bolcun-Filas, *A mouse geneticist's practical guide to CRISPR applications.* Genetics, 2015. **199**(1): p. 1-15.
59. Peng, J., *Gene redundancy and gene compensation: An updated view.* J Genet Genomics, 2019. **46**(7): p. 329-333.
60. Veitia, R.A., *Gene Duplicates: Agents of Robustness or Fragility?* Trends Genet, 2017. **33**(6): p. 377-379.
61. Blomen, V.A., et al., *Gene essentiality and synthetic lethality in haploid human cells.* Science, 2015. **350**(6264): p. 1092-6.
62. Wang, T., et al., *Identification and characterization of essential genes in the human genome.* Science, 2015. **350**(6264): p. 1096-101.

63. Magin, R.S., Z.M. March, and R. Marmorstein, *The N-terminal Acetyltransferase Naa10/ARD1 Does Not Acetylate Lysine Residues.* J Biol Chem, 2016. **291**(10): p. 5270-7.
64. Vo, T.T.L., et al., *Characterization of Lysine Acetyltransferase Activity of Recombinant Human ARD1/NAA10.* Molecules, 2020. **25**(3).
65. Saunier, C., et al., *Expanding the Phenotype Associated with NAA10-Related N-Terminal Acetylation Deficiency.* Hum Mutat, 2016. **37**(8): p. 755-64.
66. Bornstein, P.E. and R.R. Peterson, *Numerical variation of the presacral vertebral column in three population groups in North America.* Am J Phys Anthropol, 1966. **25**(2): p. 139-46.
67. McLAREN, A. and D. MICHIE, *Factors affecting vertebral variation in mice. 4. Experimental proof of the uterine basis of a maternal effect.* J Embryol Exp Morphol, 1958. **6**(4): p. 645-59.
68. Chernoff, N. and J.M. Rogers, *Supernumerary ribs in developmental toxicity bioassays and in human populations: incidence and biological significance.* J Toxicol Environ Health B Crit Rev, 2004. **7**(6): p. 437-49.
69. Conway, S.J., D.J. Henderson, and A.J. Copp, *Pax3 is required for cardiac neural crest migration in the mouse: evidence from the splotch (Sp2H) mutant.* Development, 1997. **124**(2): p. 505-14.
70. Conway, S.J., et al., *Development of a lethal congenital heart defect in the splotch (Pax3) mutant mouse.* Cardiovasc Res, 1997. **36**(2): p. 163-73.
71. van den Hoff, M.J. and A.F. Moorman, *Cardiac neural crest: the holy grail of cardiac abnormalities?* Cardiovasc Res, 2000. **47**(2): p. 212-6.
72. Olaopa, M., et al., *Pax3 is essential for normal cardiac neural crest morphogenesis but is not required during migration nor outflow tract septation.* Dev Biol, 2011. **356**(2): p. 308-22.
73. Henderson, D.J., S.J. Conway, and A.J. Copp, *Rib truncations and fusions in the Sp2H mouse reveal a role for Pax3 in specification of the ventro-lateral and posterior parts of the somite.* Dev Biol, 1999. **209**(1): p. 143-58.
74. Dickman, E.D., R. Rogers, and S.J. Conway, *Abnormal skeletogenesis occurs coincident with increased apoptosis in the Splotch (Sp2H) mutant: putative roles for Pax3 and PDGFRalpha in rib patterning.* Anat Rec, 1999. **255**(3): p. 353-61.
75. Koushik, S.V., et al., *Generation of a conditional loxP allele of the Pax3 transcription factor that enables selective deletion of the homeodomain.* Genesis, 2002. **32**(2): p. 114-7.
76. Zhou, H.M. and S.J. Conway, *Restricted Pax3 Deletion within the Neural Tube Results in Congenital Hydrocephalus.* J Dev Biol, 2016. **4**(1).
77. Le Mouellic, H., Y. Lallemand, and P. Brulet, *Homeosis in the mouse induced by a null mutation in the Hox-3.1 gene.* Cell, 1992. **69**(2): p. 251-64.
78. Juan, A.H. and F.H. Ruddle, *Enhancer timing of Hox gene expression: deletion of the endogenous Hoxc8 early enhancer.* Development, 2003. **130**(20): p. 4823-4834.
79. van den Akker, E., et al., *Axial skeletal patterning in mice lacking all paralogous group 8 Hox genes.* Development, 2001. **128**(10): p. 1911-21.
80. Horan, G.S., et al., *Homeotic transformation of cervical vertebrae in Hoxa-4 mutant mice.* Proc Natl Acad Sci U S A, 1994. **91**(26): p. 12644-8.
81. Jeannotte, L., et al., *Specification of axial identity in the mouse: role of the Hoxa-5 (Hox1.3) gene.* Genes Dev, 1993. **7**(11): p. 2085-96.
82. Condie, B.G. and M.R. Capecchi, *Mice homozygous for a targeted disruption of Hoxd-3 (Hox-4.1) exhibit anterior transformations of the first and second cervical*

vertebrae, the atlas and the axis. Development, 1993. **119**(3): p. 579-95.

83. Fromental-Ramain, C., et al., *Specific and redundant functions of the paralogous Hoxa-9 and Hoxd-9 genes in forelimb and axial skeleton patterning.* Development, 1996. **122**(2): p. 461-72.
84. Chen, F. and M.R. Capecchi, *Targeted mutations in hoxa-9 and hoxb-9 reveal synergistic interactions.* Dev Biol, 1997. **181**(2): p. 186-96.
85. Kondrashov, N., et al., *Ribosome-mediated specificity in Hox mRNA translation and vertebrate tissue patterning.* Cell, 2011. **145**(3): p. 383-397.
86. Lee, C.C., et al., *Naa10p Inhibits Beige Adipocyte-Mediated Thermogenesis through N-alpha-acetylation of Pgc1alpha.* Mol Cell, 2019. **76**(3): p. 500-515 e8.
87. Qiu, P., et al., *Mutation detection using Surveyor nuclease.* Biotechniques, 2004. **36**(4): p. 702-7.
88. Dehairs, J., et al., *CRISP-ID: decoding CRISPR mediated indels by Sanger sequencing.* Sci Rep, 2016. **6**: p. 28973.
89. Wisniewski, J.R., et al., *Universal sample preparation method for proteome analysis.* Nat Methods, 2009. **6**(5): p. 359-62.
90. Rappsilber, J., M. Mann, and Y. Ishihama, *Protocol for micro-purification, enrichment, pre-fractionation and storage of peptides for proteomics using StageTips.* Nat Protoc, 2007. **2**(8): p. 1896-906.
91. Cox, J. and M. Mann, *MaxQuant enables high peptide identification rates, individualized p.p.b.-range mass accuracies and proteome-wide protein quantification.* Nat Biotechnol, 2008. **26**(12): p. 1367-72.
92. Cox, J., et al., *Accurate proteome-wide label-free quantification by delayed normalization and maximal peptide ratio extraction, termed MaxLFQ.* Mol Cell Proteomics, 2014. **13**(9): p. 2513-26.
93. Zeger, S.L. and K.Y. Liang, *Longitudinal data analysis for discrete and continuous outcomes.* Biometrics, 1986. **42**(1): p. 121-30.

Supporting information

Supplement Table 1. Genotypes of offspring from *Naa10*$^{+/-}$ female mice crossed to the *Naa10*$^{+/Y}$ male mice.

Genotype (Expected Mendelian %)	Naa10$^{+/Y}$ or Naa10$^{+/+}$ (50%)	Naa10$^{+/-}$ (25%)	Naa10$^{-/Y}$ (25%)
E10.5 (n=134)	62 (46.3%)	39 (29.1%)	33 (24.6%)
E13.5 (n=98)	53 (54.1%)	22 (22.4%)	23 (23.4%)
E18.5 (n=170)	82 (48.2%)	49 (28.8%)	39 (23.0%)
Adults (n=733)	438 (59.8%)	207 (28.2%)	88 (12.0%)

Expected and observed Mendelian ratio of genotypes in offspring at E10.5, E13.5, E18.5 and adults from crosses of *Naa10*$^{+/-}$ female and *Naa10*$^{+/Y}$ male mice. The percentage of adult *Naa10*$^{-/Y}$ mice significantly decreases.

Supplement Table 2. Genotypes of offspring from *Naa10*$^{+/tm1a}$ female mice crossed to the *Naa10*$^{+/Y}$ male mice.

Genotype (Expected Mendelian %)	Naa10$^{+/Y}$ or Naa10$^{+/+}$ (50%)	Naa10$^{+/tm1a}$ (25%)	Naa10$^{tm1a/Y}$ (25%)
E10.5 (n=109)	55 (50.46%)	26 (23.85%)	28 (25.69%)
E12.5 (n=45)	20 (44.4%)	12 (26.7%)	13 (28.9%)
E18.5 (n=53)	27 (51.0%)	13 (24.5%)	13 (24.5%)
Adults (n=260)	152 (58.5%)	85 (32.7%)	23 (08.8%)

Expected and observed Mendelian ratio of genotypes in offspring at E10.5, E13.5, E18.5 and adults from crosses of *Naa10*$^{+/tm1a}$ female and *Naa10*$^{+/Y}$ male mice. The percentage of adults *Naa10*$^{tm1a/Y}$ mice significantly decreases.

Supplement Table 3. Cervical fusion skeletal analyses in *Naa10* KO mice.

genotype	sample size	one or more fusion events	two or more fusion events	consecutive fusion events	C1+2 fusion	C2+3 fusion	C3+4 fusion	C4+5 fusion	C5+6 fusion	C6+7 fusion	C7+ T1 fusion	T1+2 fusion
Naa10$^{+/Y}$	19	2/17 (12%)	1/17 (6%)	0/17 (0%)	2/17 (12%)	0/18 (0%)	0/18 (0%)	0/19 (0%)	0/19 (0%)	0/19 (0%)	1/19 (5%)	0/19 (0%)
Naa10$^{+/+}$	4	1/4 (25%)	0/4 (0%)	0/4 (0%)	1/4 (25%)	0/4 (0%)	0/4 (0%)	0/4 (0%)	0/4 (0%)	0/4 (0%)	0/4 (0%)	0/4 (0%)
Naa10$^{+/-}$	4	1/4 (25%)	0/4 (0%)	0/4 (0%)	1/4 (25%)	0/4 (0%)	0/4 (0%)	0/4 (0%)	0/4 (0%)	0/4 (0%)	0/4 (0%)	0/4 (0%)
Naa10$^{-/Y}$	9	9/10 (90%)	3/9 (33%)	1/9 (11%)	7/10 (70%)	2/9 (22%)	2/9 (22%)	1/9 (11%)	0/9 (0%)	0/9 (0%)	1/9 (11%)	0/9 (0%)
Naa10$^{-/-}$	1	1/1 (100%)	1/1 (100%)	1/1 (100%)	1/1 (100%)	1/1 (100%)	0/1 (0%)	0/1 (0%)	0/1 (0%)	0/1 (0%)	0/1 (0%)	0/1 (0%)

1359 **Supplement Table 4. Matings and litter size analyses.**

	***Naa10* KO matings, all WT/WT for Naa12, all >99.6% C57BL/6J**						**Naa10 x Naa12 matings, mixed genetic background**	
Genotypes of breeders (♀ x ♂)	***Naa10*$^{+/+}$ x *Naa10*$^{+/Y}$**	***Naa10*$^{+/+}$ x *Naa10*$^{-/Y}$**	***Naa10*$^{+/-}$ x *Naa10*$^{+/Y}$**	***Naa10*$^{+/-}$ x *Naa10*$^{-/Y}$**	***Naa10*$^{-/-}$ x *Naa10*$^{-/Y}$**	***Naa10*$^{-/-}$ x *Naa10*$^{+/Y}$**	**Naa10$^{+/-}$ Naa12$^{+/+}$ x Naa10$^{+/Y}$ Naa12$^{+/-}$**	**Naa10$^{+/-}$ Naa12$^{+/+}$ x Naa10$^{+/Y}$ Naa12$^{-/-}$**
#pups	**255**	**18**	**330**	**59**	**59**	**127**	**214**	**252**
#litters	**39**	**2**	**66**	**13**	**11**	**31**	**43**	**64**
#pups/ #litters, or litter size	**6.5**	**9.0**	**5.0**	**4.5**	**5.4**	**4.1**	**5.0**	**3.9**
SD of litter size	**3.2**	**0.0**	**2.2**	**2.5**	**2.5**	**2.1**	**2.1**	**2.0**
% Died in 1st three days of life	**5.1%**	**5.6%**	**15.8%**	**13.6%**	**42.4%**	**36.0%**	**16.8%**	**36%**
% of total that died by weaning ~4 weeks	**5.9%**	**11.1%**	**23.0%**	**32.2%**	**59.3%**	**44.0%**	**20.0%**	**42%**
Avg Length of Mating till 1st Litter:	**29**	**22**	**34**	**25**	**35**	**28**	**26**	**34**
Total number of unique mating males:	**7**	**1**	**12**	**5**	**6**	**7**	**13**	**16**
Total number of mating pairs set up:	**8**	**1**	**>16**	**14**	**10**	**11**	**22**	**17**
Total number of mating pairs with progeny	**7**	**1**	**N/A**	**7**	**4**	**11**	**21**	**15**
% females who became pregnant and gave birth at least once:	**87.5%**	**100.0%**	**N/A**	**50.0%**	**40.0%**	**100.0%**	**95.5%**	**88.2%**

1360

1361

Supplement Table 5 N-termini detected in MEFs, (excel sheet)

Supplement Table 6. Genotypes of offspring from *Naa12*$^{+/-}$ female mice crossed to the *Naa12*$^{+/-}$ male mice.

Genotype (Expected Mendelian %)	Naa12$^{+/+}$ (25%)	Naa12$^{+/-}$ (50%)	Naa12$^{-/-}$ (25%)
Adults (n=117)	26 (22%)	62 (53%)	29 (25%)

Expected and observed Mendelian ratio of genotypes in offspring from crosses.

Supplement Table 7. Genotypes of offspring from *Naa10*$^{+/-}$ *Naa12*$^{+/+}$ female mice crossed to the *Naa10*$^{+/y}$ *Naa12*$^{+/-}$ male mice.

Genotype (Expected Mendelian %)	*Naa10*$^{(+/y)}$ *Naa12*$^{(+/-)}$ males (12.5%)	*Naa10*$^{(-/y)}$ *Naa12*$^{(+/-)}$ males (12.5%)	*Naa10*$^{(+/y)}$ *Naa12*$^{(+/+)}$ males (12.5%)	*Naa10*$^{(-/y)}$ *Naa12*$^{(+/+)}$ males (12.5%)
Newborn pups (n=214)	27 (12.6%)	0 (0%)	33 (15.4%)	21 (9.8%)
Genotype (Expected Mendelian %)	*Naa10*$^{(+/-)}$ *Naa12*$^{(+/+)}$ females (12.5%)	*Naa10*$^{(+/+)}$ *Naa12*$^{(+/+)}$ females (12.5%)	*Naa10*$^{(+/-)}$ *Naa12*$^{(+/-)}$ females (12.5%)	*Naa10*$^{(+/+)}$ *Naa12*$^{(+/-)}$ females (12.5%)
	31 (14.5%)	33 (15.4%)	9 (4.2%)	41 (19.2%)
Early neonatal death, unable to genotype = 19 (8.9%)				

Expected and observed Mendelian ratio of genotypes in offspring from crosses.

Supplement Table 8. Genotypes of offspring from *Naa10*$^{+/-}$ *Naa12*$^{+/+}$ female mice crossed to the *Naa10*$^{+/y}$ *Naa12*$^{-/-}$ male mice.

Genotype (Expected Mendelian %)	NAA10$^{+/Y}$ NAA12$^{+/-}$ male (25%)	NAA10$^{-/Y}$ NAA12$^{+/-}$ male (25%)	NAA10$^{+/+}$ NAA12$^{+/-}$ female (25%)	NAA10$^{+/-}$ NAA12$^{+/-}$ female (25%)
Newborn pups (n=252*)	78 (31%)	0 (0%)	83 (33%)	36 (14%)
***Early neonatal death, unable to genotype = 55 (22%)**				

Expected and observed Mendelian ratio of genotypes in offspring from crosses.

Supplement Table 9. Mendelian and Observed Offspring Distributions from Naa10(+/Y); Naa12(+/-) Male and Naa10(+/-); Naa12(+/-) Female Breeding

		Mendelian Genotype Distribution (%)			Observed Number (% Genotyped)		
#*	Offspring Genotypes	F	M	Total	E10.5	E18.5	Postnatal
1	Naa10 (+/+), Naa12 (+/+)	6.25		6.25	2 (6.9)	5 (15.2)	16 (10.2)
2	Naa10 (+/+), Naa12 (+/-)	12.50		12.50	4 (13.8)	7 (21.2)	28 (17.8)
3	Naa10 (+/+), Naa12 (-/-)	6.25		6.25	3 (10.3)	1 (3.0)	16 (10.2)
4	Naa10 (+/-), Naa12 (+/+)	6.25		6.25	3 (10.3)	1 (3.0)	14 (8.9)
5	Naa10 (+/-), Naa12 (+/-)	12.50		12.50	6 (20.7)	5 (15.2)	5 (3.2)
6	Naa10 (+/-), Naa12 (-/-)	6.25		6.25	2 (6.9)	0 (0.0)	0 (0.0)
7	Naa10 (+/Y), Naa12 (+/+)		6.25	6.25	1 (3.4)	4 (12.1)	17 (10.8)
8	Naa10 (+/Y), Naa12 (+/-)		12.50	12.50	1 (3.4)	5 (15.2)	31 (19.7)
9	Naa10 (+/Y), Naa12 (-/-)		6.25	6.25	3 (10.3)	3 (9.1)	17 (10.8)
10	Naa10 (-/Y), Naa12 (+/+)		6.25	6.25	0 (0.0)	1 (3.0)	17 (8.3)
11	Naa10 (-/Y), Naa12 (+/-)		12.50	12.50	4 (13.8)	1 (3.0)	0 (0.0)
12	Naa10 (-/Y), Naa12 (-/-)		6.25	6.25	0 (0.0)	0 (0.0)	0 (0.0)
	TOTAL (% Genotyped)	**50.0**	**50.0**	**100.0**	**29 (99.8)**	**33 (100.0)**	**157 (99.9)**
	Not Genotyped (% Total)				**3 (9.4)**	**23 (41.1)**	**0 (0.0)**
	TOTAL	**50.0**	**50.0**	**100.0**	**32**	**56**	**157**

F = Female; M = Male

*Genotypes in subsequent tables are numbered according to this table, which includes all possible genotypes from all crosses considered.

Supplement Table 10. Mendelian and Observed Offspring Distributions from Naa10(+/Y); Naa12(-/-) Male and Naa10(+/-); Naa12(+/-) Female Breeding

		Mendelian Genotype Distribution (%)			Observed Number (% Genotyped)				
#*	Offspring Genotypes	F	M	Total	E8.5	E10.5	E12.5	E18.5	Postnatal
2	Naa10 (+/+), Naa12 (+/-)	12.5		12.5	4 (19.0)	3 (10.7)	4 (16.0)	2 (18.2)	45 (25.1)
3	Naa10 (+/+), Naa12 (-/-)	12.5		12.5	6 (28.6)	8 (28.6)	1 (4.0)	2 (18.2)	35 (19.6)
5	Naa10 (+/-), Naa12 (+/-)	12.5		12.5	2 (9.5)	8 (28.6)	7 (28.0)	3 (27.3)	12 (6.7)
6	Naa10 (+/-), Naa12 (-/-)	12.5		12.5	1 (4.8)	1 (3.6)	0 (0.0)	0 (0.0)	0 (0.0)
8	Naa10 (+/Y), Naa12 (+/-)		12.5	12.5	1 (4.8)	3 (10.7)	7 (28.0)	0 (0.0)	40 (22.3)
9	Naa10 (+/Y), Naa12 (-/-)		12.5	12.5	7 (33.3)	4 (14.3)	6 (24.0)	4 (36.4)	47 (26.3)
11	Naa10 (-/Y), Naa12 (+/-)		12.5	12.5	0 (0.0)	1 (3.6)	0 (0.0)	0 (0.0)	0 (0.0)
12	Naa10 (-/Y), Naa12 (-/-)		12.5	12.5	0 (0.0)	0 (0.0)	0 (0.0)	0 (0.0)	0 (0.0)
TOTAL (% Genotyped)		**50.0**	**50.0**	**100.0**	**21 (100.0)**	**28 (100.1)**	**25 (100.0)**	**11 (100.1)**	**179 (100.0)**
Not Genotyped (% Total)					**4 (16.0)**	**12 (30.0)**	**19 (43.2)**	**7 (38.9)**	**2 (1.1)**
TOTAL		**50.0**	**50.0**	**100.0**	**25**	**40**	**44**	**18**	**181**

F = Female; M = Male

*Genotypes in this table are numbered according to **Supplement Table 9**, which includes all possible genotypes from all crosses considered.

Supplement Table 11. Mendelian and Observed Postnatal Offspring Distributions from Naa10(+/Y); Naa12(+/-) Male and Naa10(+/-); Naa12(+/+) Female Breeding

		Mendelian Genotype Distribution (%)			Observed Number (% Genotyped)	
#*	Offspring Genotypes	F	M	Total	Postnatal	
1	Naa10 (+/+), Naa12 (+/+)	12.5		12.5	33	(16.9)
2	Naa10 (+/+), Naa12 (+/-)	12.5		12.5	41	(21.0)
4	Naa10 (+/-), Naa12 (+/+)	12.5		12.5	31	(15.9)
5	Naa10 (+/-), Naa12 (+/-)	12.5		12.5	9	(4.6)
7	Naa10 (+/Y), Naa12 (+/+)		12.5	12.5	33	(16.9)
8	Naa10 (+/Y), Naa12 (+/-)		12.5	12.5	27	(13.8)
10	Naa10 (-/Y), Naa12 (+/+)		12.5	12.5	21	(10.8)
11	Naa10 (-/Y), Naa12 (+/-)		12.5	12.5	0	(0.0)
Total (% Genotyped)					**195**	**(99.9)**
Not Genotyped (% Total)					**19**	**(8.9)**
TOTAL		**50.0**	**50.0**	**100.0**	**214**	

F = Female; M = Male

*Genotypes in this table are numbered according to **Supplement Table 9**, which includes all possible genotypes from all crosses considered.

Supplement Table 12. Mendelian and Observed Postnatal Offspring Distributions from Naa10(+/Y); Naa12(-/-) Male and Naa10(+/-); Naa12(+/+) Female Breeding

		Mendelian Genotype Distribution (%)			Observed Number (% Genotyped)	
#*	Offspring Genotypes	F	M	Total	Postnatal	
2	Naa10 (+/+), Naa12 (+/-)	25.0		25.0	83	(42.1)
5	Naa10 (+/-), Naa12 (+/-)	25.0		25.0	36	(18.3)
8	Naa10 (+/Y), Naa12 (+/-)		25.0	25.0	78	(39.6)
11	Naa10 (-/Y), Naa12 (+/-)		25.0	25.0	0	(0.0)
Total (% Genotyped)					**197**	**(100.0)**
Not Genotyped (% Total)					**55**	**(21.8)**
TOTAL		**50.0**	**50.0**	**100.0**	**252**	

F = Female; M = Male

*Genotypes in this table are numbered according to **Supplement Table 9**, which includes all possible genotypes from all crosses considered.

Supplement Table 13. Mendelian and Observed Age-Specific Offspring Distributions from Four Crosses

		Observed Number at Age (% Genotyped)									
#*	Offspring Genotypes	E8.5		E10.5		E12.5		E18.5		Postnatal	
1	Naa10 (+/+), Naa12 (+/+)			2	(3.5)			5	(11.4)	16	(4.8)
2	Naa10 (+/+), Naa12 (+/-)	4	(19.0)	7	(12.3)	4	(16.0)	9	(20.5)	73	(21.7)
3	Naa10 (+/+), Naa12 (-/-)	6	(28.6)	11	(19.3)	1	(4.0)	3	(6.8)	51	(15.2)
4	Naa10 (+/-), Naa12 (+/+)			3	(5.3)			1	(2.3)	14	(4.2)
5	Naa10 (+/-), Naa12 (+/-)	2	(9.5)	14	(24.6)	7	(28.0)	8	(18.2)	17	(5.1)
6	Naa10 (+/-), Naa12 (-/-)	1	(4.8)	3	(5.3)	0	(0.0)	0	(0.0)	0	(0.0)
7	Naa10 (+/Y), Naa12 (+/+)			1	(1.8)			4	(9.1)	17	(5.1)
8	Naa10 (+/Y), Naa12 (+/-)	1	(4.8)	4	(7.0)	7	(28.0)	5	(11.4)	71	(21.1)
9	Naa10 (+/Y), Naa12 (-/-)	7	(33.3)	7	(12.3)	6	(24.0)	7	(15.9)	64	(19.0)
10	Naa10 (-/Y), Naa12 (+/+)			0	(0.0)			1	(2.3)	13	(3.9)
11	Naa10 (-/Y), Naa12 (+/-)	0	(0.0)	5	(8.8)	0	(0.0)	1	(2.3)	0	(0.0)
12	Naa10 (-/Y), Naa12 (-/-)	0	(0.0)	0	(0.0)	0	(0.0)	0	(0.0)	0	(0.0)
TOTAL (% Genotyped)		**21**	**(100.0)**	**57**	**(100.2)**	**25**	**(100.0)**	**44**	**(100.2)**	**336**	**(100.0)**

F = Female; M = Male

*Genotypes in this table are numbered according to **Supplement Table 9**, which includes all possible genotypes from all crosses considered.

Supplement Table 14. Mendelian and Observed Cumulative Offspring Distributions from All Four Crosses

		Cumulative Observed Number (% Genotyped)									
#*	Offspring Genotypes	E8.5		E10.5		E12.5		E18.5		Postnatal	
1	Naa10 (+/+), Naa12 (+/+)			2	(2.6)	2	(1.9)	7	(4.8)	23	(4.8)
2	Naa10 (+/+), Naa12 (+/-)	4	(19.0)	11	(14.1)	15	(14.6)	24	(16.3)	97	(20.1)
3	Naa10 (+/+), Naa12 (-/-)	6	(28.6)	17	(21.8)	18	(17.5)	21	(14.3)	72	(14.9)
4	Naa10 (+/-), Naa12 (+/+)			3	(3.8)	3	(2.9)	4	(2.7)	18	(3.7)
5	Naa10 (+/-), Naa12 (+/-)	2	(9.5)	16	(20.5)	23	(22.3)	31	(21.1)	48	(9.9)
6	Naa10 (+/-), Naa12 (-/-)	1	(4.8)	4	(5.1)	4	(3.9)	4	(2.7)	4	(0.8)
7	Naa10 (+/Y), Naa12 (+/+)			1	(1.3)	1	(1.0)	5	(3.4)	22	(4.6)
8	Naa10 (+/Y), Naa12 (+/-)	1	(4.8)	5	(6.4)	12	(11.7)	17	(11.6)	88	(18.2)
9	Naa10 (+/Y), Naa12 (-/-)	7	(33.3)	14	(17.9)	20	(19.4)	21	(18.4)	91	(18.8)
10	Naa10 (-/Y), Naa12 (+/+)			0	(0.0)	0	(0.0)	1	(0.7)	14	(2.9)
11	Naa10 (-/Y), Naa12 (+/-)	0	(0.0)	5	(6.4)	5	(4.9)	6	(4.1)	6	(1.2)
12	Naa10 (-/Y), Naa12 (-/-)	0	(0.0)	0	(0.0)	0	(0.0)	0	(0.0)	0	(0.0)
TOTAL (% Genotyped)		**21**	**(100.0)**	**78**	**(99.9)**	**103**	**(100.0)**	**147**	**(100.2)**	**483**	**(99.9)**

F = Female; M = Male

*Genotypes in this table are numbered according to **Supplement Table 9**, which includes all possible genotypes from all crosses considered.

1405 **Supplement Table 15. Mice analyzed by weighing, according to genotype.**

Females						
			Naa12 status			
			WT/WT	WT/KO	KO/KO	Total
Naa10 status	Pure C57BL/6J background Naa10 mice	WT/WT	67	N/A	N/A	67
		WT/KO	125	N/A	N/A	125
		KO/KO	15	N/A	N/A	15
		Subtotal	207	N/A	N/A	207
	mixed genetic background Naa10 and Naa12 mice	WT/WT	32	82	10	124
		WT/KO	35	23	0	58
		KO/KO	0	0	0	0
		Subtotal	67	105	10	182
	Total		274	105	10	389

1406

Males						
			Naa12 status			
			WT/WT	WT/KO	KO/KO	Total
Naa10 status	Pure C57BL/6J background Naa10 mice	WT	97	N/A	N/A	97
		KO	70	N/A	N/A	70
		Subtotal	167	N/A	N/A	167
	mixed genetic background Naa10 and Naa12 mice	WT	44	63	11	118
		KO	14	0	0	14
		Subtotal	58	63	11	132
	Total		225	63	11	299

1407

1408

Supplement Table 16. Effects of *Naa10* KO on growth rate of *Naa10* mice on pure genetic background.

	C57BL/6J inbred females (N = 207)															
	Effect of age and age^2				Effect of Naa10 KO				Effect of age and Naa10 KO				Effect of age, Naa10 KO, and interaction			
	Coeff.	SE	z	p > |z|	Coeff.	SE	z	p > |z|	Coeff.	SE	z	p > |z|	Coeff.	SE	z	p > |z|
Age in days	0.349	0.006	59.49	< 0.001					0.349	0.006	59.38	< 0.001	0.344	0.010	34.59	< 0.001
Age^2	- 0.001	0.00003	- 40.59	< 0.001					- 0.001	0.00003	- 40.56	< 0.001	- 0.001	0.00005	- 24.53	< 0.001
Naa10 KO					- 2.92	0.847	- 3.45	0.001	- 0.252	0.248	- 1.01	ns	- 0.219	0.451	- 0.49	ns
Age x KO													0.009	0.012	0.75	ns
Age^2 x KO													- 0.00009	0.00007	-1.27	ns
(constant)	2.518	0.204	12.35	< 0.001	17.23	0.690	24.96	< 0.001	2.697	0.272	9.93	< 0.001	2.633	0.382	6.90	< 0.001
Wald X^2 [a]	6547.29, p < 0.0001				11.93, p = 0.0006				6552.24, p < .0001				6611.63, p < 0.0001			

	C57BL/6J inbred males (N = 167)															
	Effect of age and age^2				Effect of Naa10 KO				Effect of age and Naa10 KO				Effect of age, Naa10 KO, and interaction			
	Coeff.	SE	z	p > |z|	Coeff.	SE	z	p > |z|	Coeff.	SE	z	p > |z|	Coeff.	SE	z	p > |z|
Age in days	0.454	0.008	60.16	< 0.001					0.454	0.007	62.20	< 0.001	0.467	0.009	51.68	< 0.001
Age^2	- 0.002	0.00005	- 39.76	< 0.001					-0.002	0.00004	- 41.16	< 0.001	- 0.002	0.00005	- 34.53	< 0.001
Naa10 KO					- 4.721	1.040	- 4.54	< 0.001	-2.578	0.304	- 8.47	< 0.001	- 1.351	0.504	- 2.68	0.007
Age x KO													- 0.035	0.015	- 2.32	0.020
Age^2 x KO													0.0001	0.00009	1.46	ns
(constant)	1.303	0.271	4.81	< 0.001	19.56	0.668	29.28	< 0.001	2.430	0.283	8.58	< 0.001	1.931	0.321	6.01	< 0.001
Wald X^2 [a]	7220.56, p < 0.0001				20.60, p < 0.0001				8007.09, p < 0.0001				8185.75, p < 0.0001			

[a] The Wald X^2 is a measure of the overall goodness of fit of the complete model.

1414 **Supplement Table 17. Effects of *Naa10* and *Naa12* Kos on growth rate on mixed genetic**
1415 **background**

	females (N = 182): effects of age and knockouts on weight																			
	Effect of age and age^2				Effects of age and Naa10 KO				Effects of age and Naa12 KO				Effects of age, Naa10 & Naa12 Kos				Effects: age, Naa10, Naa12, both Kos			
	Coeff	SE	z	p > |z|	Coeff	SE	z	p > |z|	Coeff	SE	z	p > |z|	Coeff	SE	z	p > |z|	Coeff	SE	z	p > |z|
Age	.	0.011	43.10	< 0.001	0.489	0.011	45.02	< 0.001	0.489	0.011	43.25	< 0.001	0.491	0.011	46.16	< 0.001	0.492	0.011	46.49	< 0.001
Age^2	-0.003	0.0001	-24.47	< 0.001	-0.003	0.0001	-25.58	< 0.001	-0.003	0.0001	-24.55	< 0.001	-0.003	0.0001	-26.21	< 0.001	-0.003	0.0001	-26.45	< 0.001
Naa10					-1.117	0.254	-4.40	< 0.001					-1.424	0.267	-5.33	< 0.001	-0.368	0.335	-1.10	ns
Naa12-Het									-0.377	0.247	-1.53	ns	-0.789	0.255	-3.09	0.002	0.039	0.287	0.14	ns
Naa12-Ho									-0.659	0.625	-1.05	ns	-1.376	0.621	-2.21	0.027				
Naa10-Naa12-Het																	-2.143	0.510	-4.20	< 0.001
(constant)	0.616	0.264	2.33	0.020	0.966	0.267	3.61	< 0.001	0.825	0.291	2.83	0.005	1.508	0.307	4.91	< 0.001	0.879	0.307	2.86	0.004
Wald X^2 [a]	4692.14, p < 0.0001				5116.03, p < 0.0001				4752.14, p < 0.0001				5396.11, p < 0.0001				5461.46, p < 0.0001			

1416

	females (N = 182): effects of age and knockouts on growth rate															
	Effects of age, Naa10 KO, interaction with age				Effects of age, Naa12 KO, interaction with age				Effects of age, both Kos & interaction with age				Effects: age, Kos & interaction with ea. Other			
	Coeff	SE	z	p > |z|	Coeff	SE	z	p > |z|	Coeff	SE	z	p > |z|	Coeff	SE	z	p > |z|
Age	0.508	0.013	39.24	< 0.001	0.491	0.015	32.64	< 0.001	0.523	0.018	29.09	< 0.001	0.496	0.011	46.35	< 0.001
Age^2	-0.003	0.0001	-22.76	< 0.001	-0.003	0.0002	-17.97	< 0.001	-0.003	0.0002	-16.71	< 0.001	-0.003	0.0001	-26.24	< 0.001
Naa10	0.109	0.547	0.20	ns					0.030	0.582	0.05	ns	-0.364	0.336	-1.08	ns
Age x Naa10	-0.059	0.023	-2.51	0.012					-0.068	0.025	-2.76	0.006				
Age^2 x Naa10	0.0006	0.0002	2.25	0.024					0.0006	0.0003	2.46	0.014				
Naa12-Het					-0.175	0.547	-0.32	ns	-0.099	0.557	-0.18	ns	0.036	0.288	0.13	ns
Age x Naa12-Het					-0.005	0.023	-0.23	ns	-0.029	0.023	-1.23	ns				
Age^2 x Naa12-Het					0.000004	0.0002	0.02	ns	0.0002	0.0002	0.97	ns				
Naa12-Ho					-0.882	1.584	-0.56	ns	-0.916	1.551	-0.59	ns				
Age x Naa12-Ho					0.003	0.073	0.04	ns	-0.029	0.071	-0.41	ns				
Age^2 x Naa12-Ho					0.00003	0.0007	0.04	ns	0.0003	0.001	0.47	ns				
Naa10-Naa12-Het													0.784	1.303	0.60	ns
Age x Naa10-Naa12-Het													-0.113	0.052	-2.15	0.031
Age^2 x Naa10-Naa12-Het													0.0009	0.0005	1.73	ns
(constant)	0.588	0.305	1.93	ns	0.756	0.348	2.17	0.030	0.790	0.426	1.85	ns	0.774	0.309	2.50	0.012
Wald X^2 [a]	5224.04, p < 0.0001				4758.89, p < 0.0001				5526.71, p < 0.0001				5586.86, p < 0.0001			

1417 Het : heterozygous
1418 Ho : homozygous
1419 [a] The Wald X^2 is a measure of the overall goodness of fit of the complete model.

1420

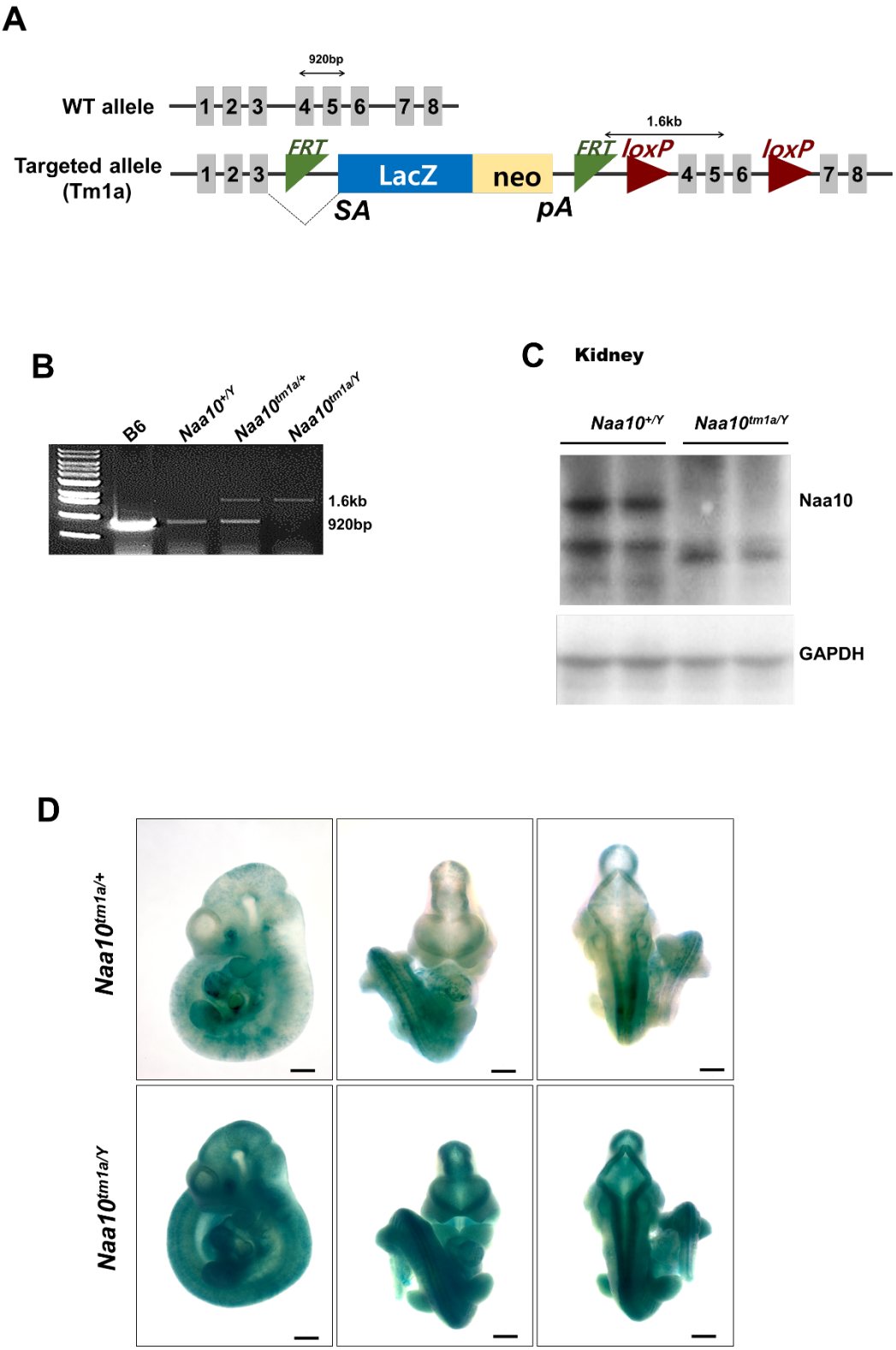

Supplement Fig. 1. Generation and confirmation of Naa10tm1a mice. (A) Schematic illustration of the Naa10tm1a mice. (B) PCR confirmation of Naa10 deficiency. (C) Confirmation of Naa10 protein in kidney tissue by Western blot. Naa10 protein is not detected in *Naa10*$^{-/Y}$ mouse. (D) Expression pattern of Naa10 in the embryo. β-gal staining represents Naa10 localization.

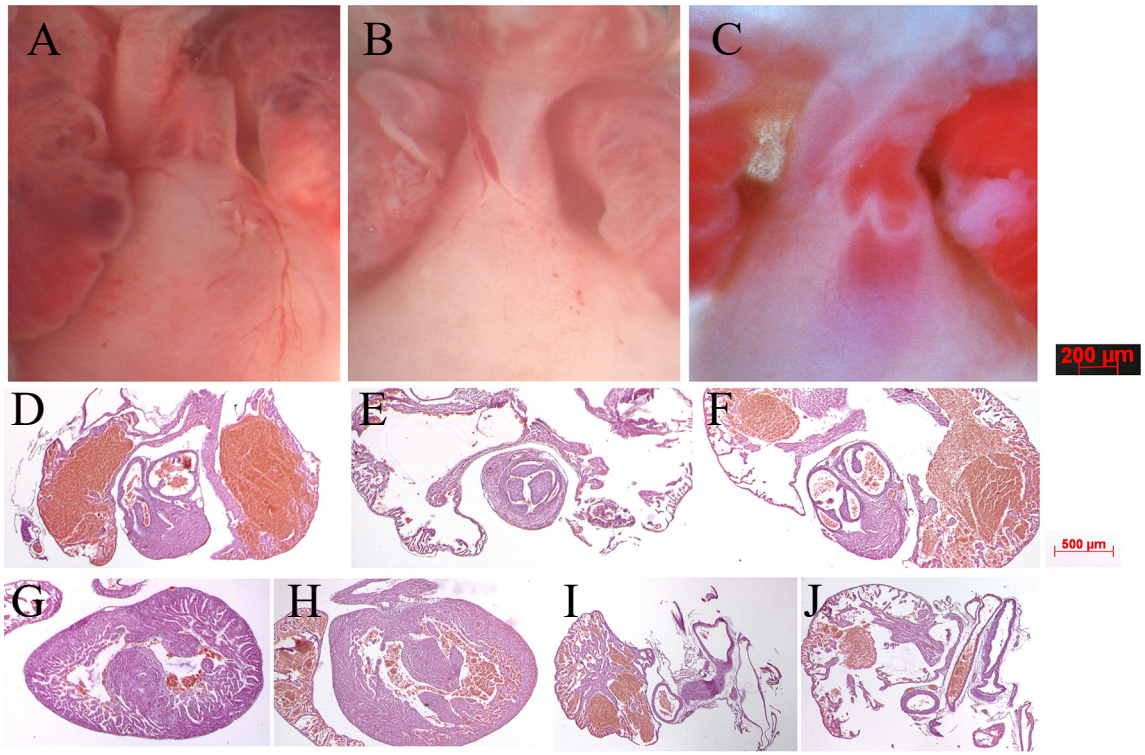

Supplement Fig. 2. Gross anatomy and histology of neonatal mouse hearts. (A) Wildtype male heart outflow tract region indicating separate aorta and pulmonary trunks nestled between left and right atria. (B) Naa10$^{-/-}$ female heart from dying P0 pup only has a single outflow tract emerging from the right ventricle, resulting in persistent truncus arteriosus. (C) Naa10$^{-/y}$ male heart from dying P0 pup has separate outflow tracts but both emerge from the right ventricle, resulting in double outlet right ventricle. (D) normal histology from wildtype male heart of pulmonary artery exiting the right ventricle. (E) histology from Naa10$^{-/-}$ heart of single outflow tract exiting the right ventricle with tricuspid valve leaflets. (F) histology from Naa10$^{-/y}$ heart of both pulmonary and aortic arteries emerging from right ventricle within the same plane. (G) Naa10$^{-/-}$ histology showing membranous VSD, (H) Naa10$^{-/y}$ histology showing muscular VSD. (I) normal heart revealing closed ductus arterious, (J) Naa10$^{-/-}$ histology showing open ductus arterious leading to pulmonary overload and likely lethality.

1421

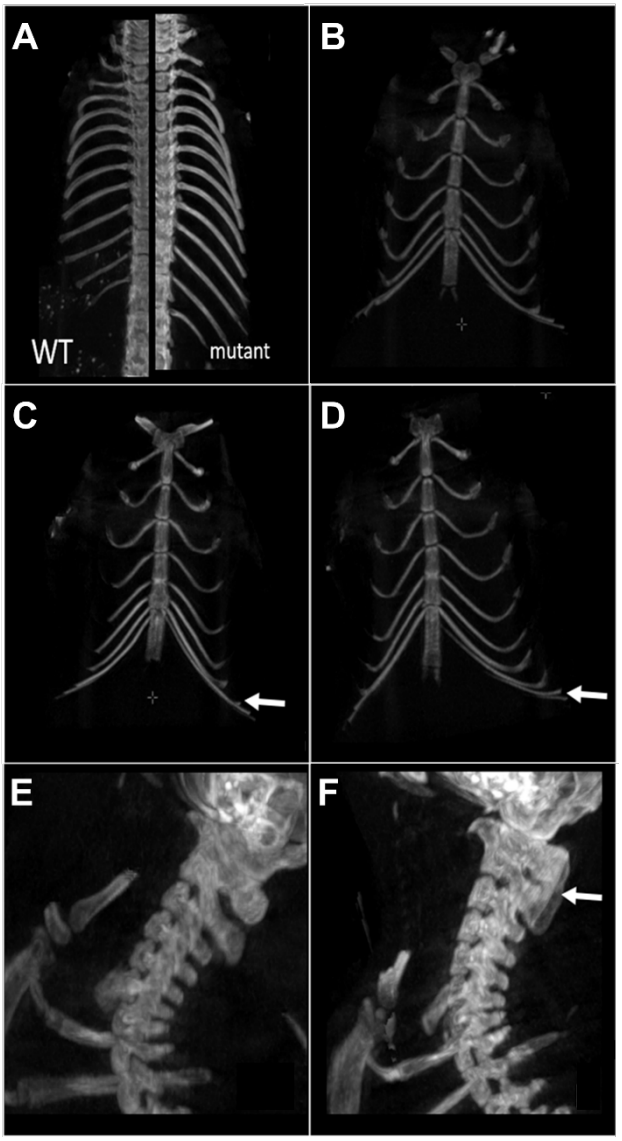

Supplement Fig. 3. Skeletal phenotype by CT scanning. (A) In WT mice 13 thoracic vertebrae and ribs are numbered whereas 14 thoracic vertebrae and ribs are counted in mutants (*Naa10*$^{-/Y}$) (WT on the left, mutant on the right). n=11 CT scans for *Naa10*$^{-/Y}$ compared to n=18 *Naa10*$^{+/Y}$. (B-D) Different number of ribs are linking the sternum between in *Naa10*$^{-/Y}$, *Naa10*$^{-/-}$ and WT. (B) 7 ribs linking the sternum in WT. (C) 8 ribs linking the sternum (the white arrow shows the 8th rib) in Naa10$^{-/Y}$. (D) 7 on one side + 7 and one almost linking on the other side. In 2 mice, an asymmetrical link was observed. White arrow shows the eighth asymmetrical rib. (E and F) Abnormalities in the cervical phenotype. (E) Cervical WT/ morphology. (F) Partial fusion of C1 and C2 dorsal arch in one mutant mouse.

1422

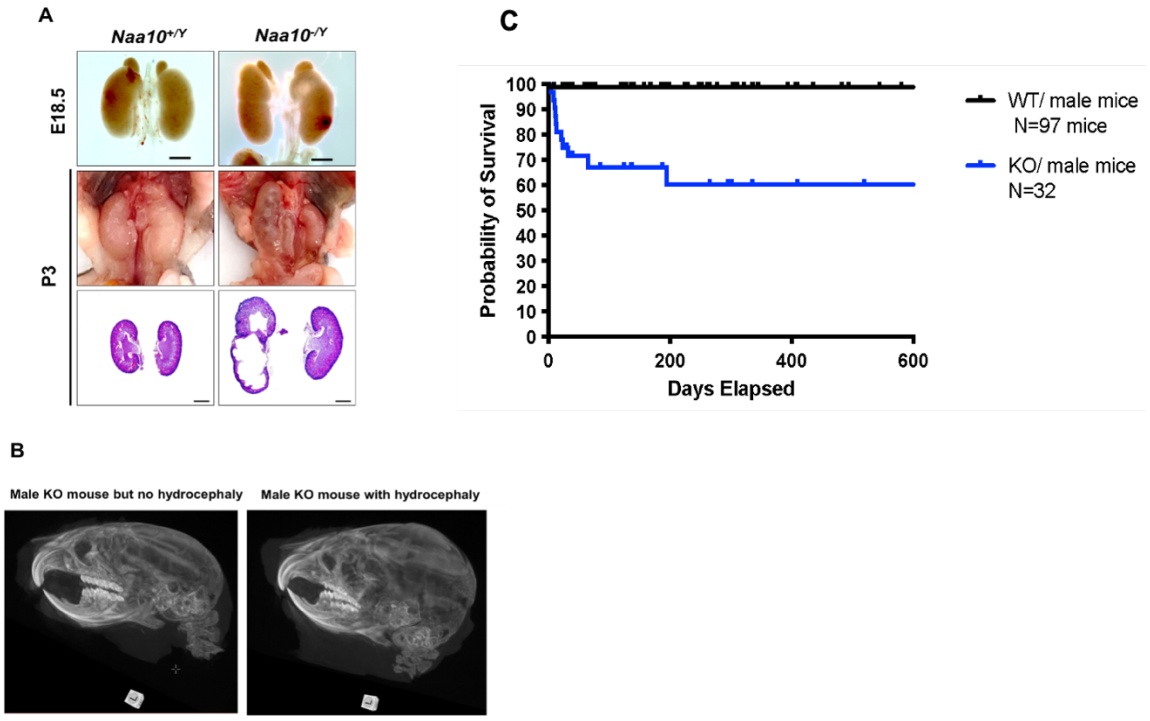

Supplement Fig. 4. Hydronephrosis and Hydrocephaly in Naa10 KO mice. (A) Representative images and histology of renal defects at E18.5 (n=6 out of 39 examined) and P3 (n= 4 out of 11 examined). (B) Hydrocephaly (n=3 CT scans for *Naa10*$^{-/Y}$ mice with hydrocephaly compared to n=3 *Naa10*$^{-/Y}$ mice without hydrocephaly). (C) Kaplan-Meier survival curve of the *Naa10*$^{+/Y}$ and *Naa10*$^{-/Y}$ male mice starting at 4 days of life, thus not including any mice that died in the first 3 days of life.

1423

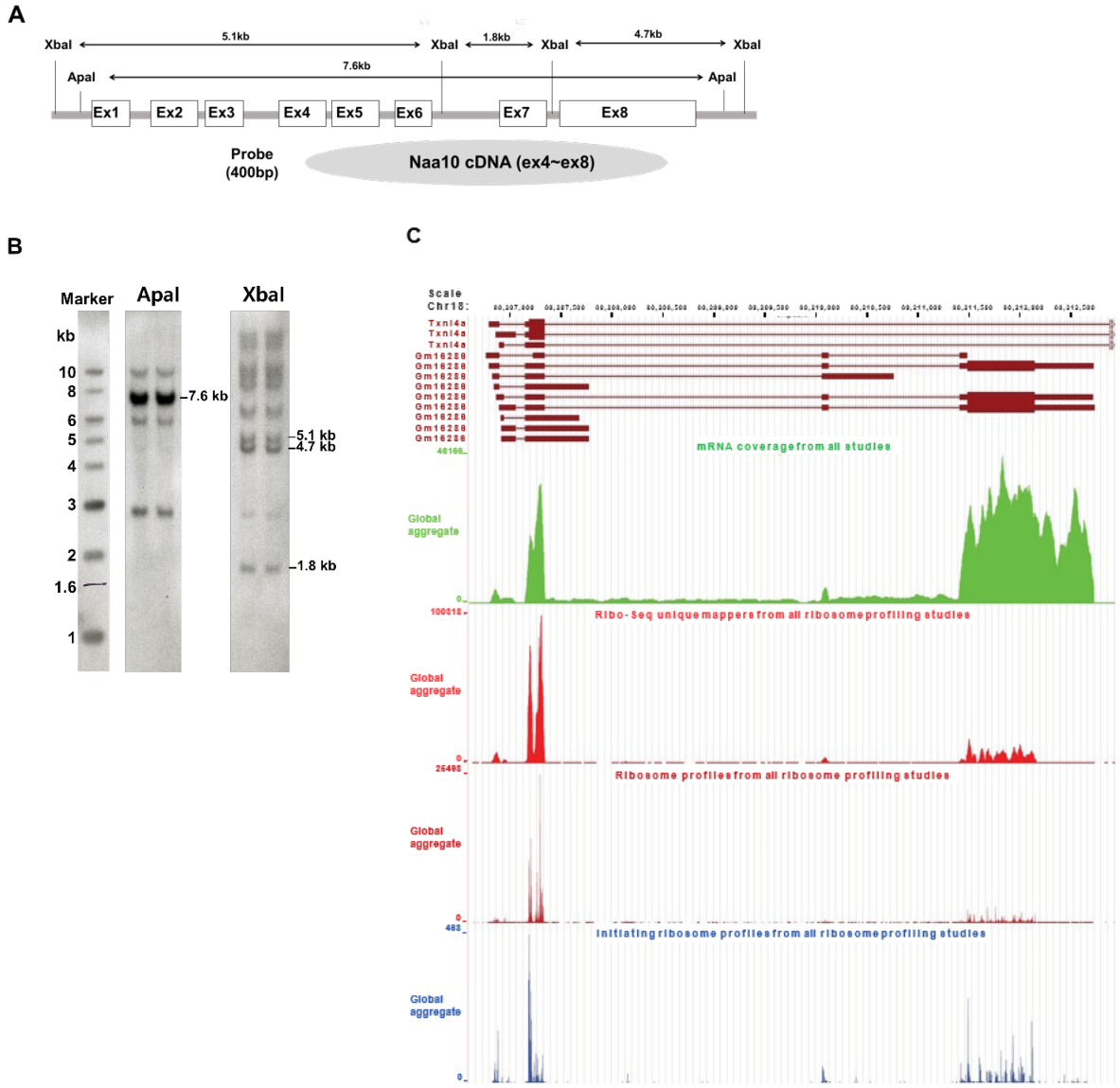

Supplement Fig. 5. Identification of a potential Naa10 homolog. (A) Construction of *Naa10* Southern blot probe. (B) Southern blot membrane after hybridization with a *Naa10* probe. Expected size band, restricted with Apa I and Xba I, were showed. (C) Ribosome profiling traces for the potential *Naa10* paralog (Gm16286, UniProt: Q9CQX6). Picture was modified from GWIPS genome browser, Chr 18, 80206601-80212942.

1424

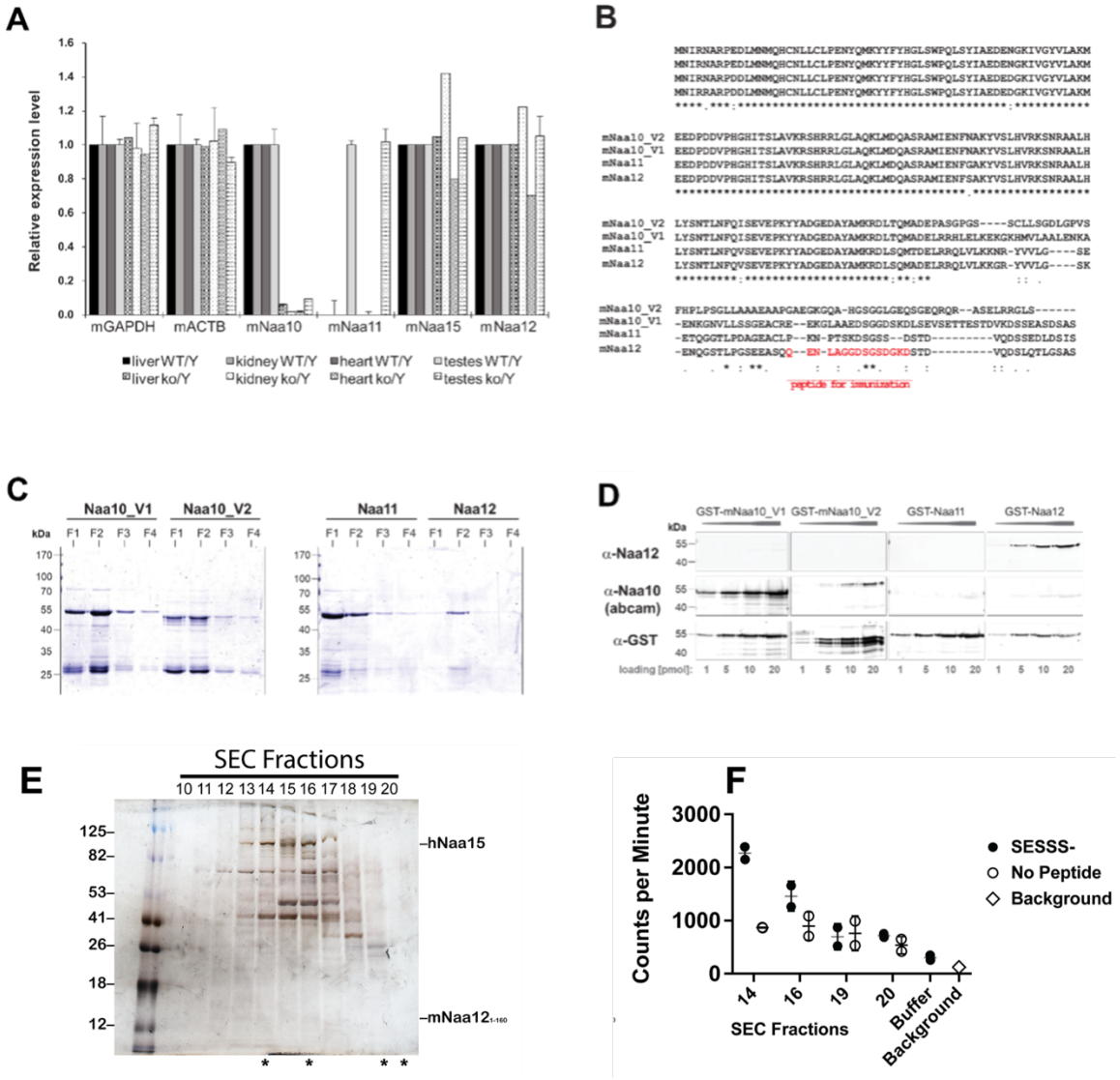

Supplement Fig. 6. Characterization of a potential Naa10 homolog. (A) qPCR analyses of mouse NATs (mNATs) in *Naa10* WT and KO adult mouse tissue. (B) Sequence alignment of mNaa10 isoforms and paralogs, including the potential Naa10 paralog mNaa12 (Gm16286, UniProt: Q9CQX6) using Clustal Omega (EMBL-EBI). The peptide used for immunization of rabbits to generate a specific antibody is indicated in red. (C) Full length mNAT cDNA from mouse was amplified and cloned into pGEX-4T1. Proteins were expressed in E. coli BL21 (DE3) and purified via GSH-Sepharose. Shown is a Coomassie stain of fraction 1-4. (D) Cross-reactivity and sensitivity of the used NAT antibodies. 1-20 pmol of GST-mNAT proteins were separated on SDS-PAGE followed by western blot, probed with the indicated antibodies. (E) Recombinant mouse Naa12/human Naa15 chimera complex. Silver-stained denaturing SDS-PAGE (left) containing fractions (#10-20) eluted from an S200 size-exclusion (SEC) chromatography column with fractions evaluated for NatA-type activity indicated (asterisks, below gel) with (F) corresponding radioactive acetyltransferase activity assay comparing the activity of indicated fractions and buffer control (chemical acetylation) towards the SESSS- peptide (filled circles), in the absence of peptide (open circles), and assay background (x). Error bars represent SD of two technical replicates.

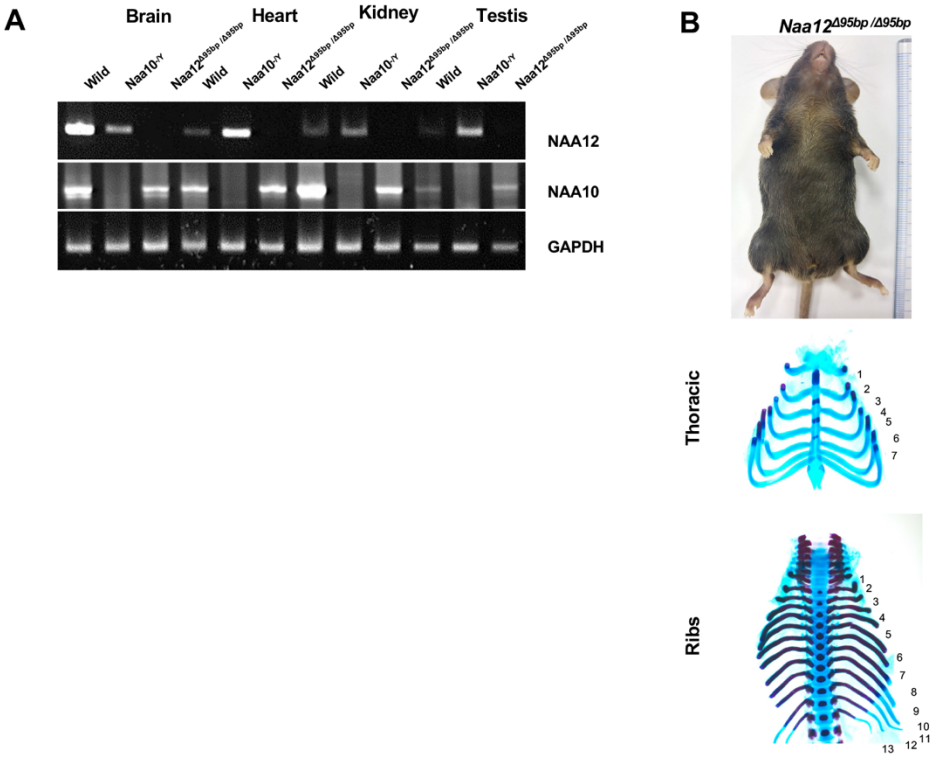

Supplement Fig. 7. Confirmation and characterization of Naa12 KO mice. (A) Expression of *Naa10* and *Naa12* in WT, *Naa10* KO and *Naa12* KO tissues, adult mice 13 weeks of age, (brain, heart, kidney and testis) by RT-PCR. Expression of GAPDH was analyzed as an endogenous control. (B) Phenotypes in *Naa12* KO mice. Lack of hypopigmentation (upper; N=29) and lack of supernumerary ribs (middle and bottom; E18.5; N=7) in *Naa12* KO mouse.

1425

1426

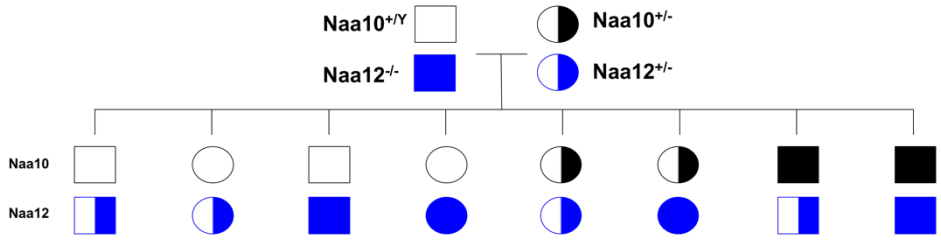

Genotype	Naa10$^{+/Y}$ Naa12$^{+/-}$	Naa10$^{+/+}$ Naa12$^{+/-}$	Naa10$^{+/Y}$ Naa12$^{-/-}$	Naa10$^{+/+}$ Naa12$^{-/-}$	Naa10$^{+/-}$ Naa12$^{+/-}$	Naa10$^{+/-}$ Naa12$^{-/-}$	Naa10$^{-/Y}$ Naa12$^{+/-}$	Naa10$^{-/Y}$ Naa12$^{-/-}$	Unable to genotype
E8.5 (n=21)	1	4	7	6	2	1	0	0	4
E10.5 (n=28)	3	3	4	8	8	1*	1*	0	12
E12.5 (n=25)	7	4	6	1	7	0	0	0	19
E18.5 (n=11)	0	2	4	2	3	0	0	0	7
Postnatal (n=179)	40	45	47	35	12	0	0	0	2

* lysed embryo

Supplement Fig. 8. Genotypes of offspring from *Naa10*$^{+/-}$ *Naa12*$^{+/-}$ female mice crossed to the *Naa10*$^{+/Y}$ *Naa12*$^{-/-}$ male mice. *Naa10 Naa12* DKO exhibit embryonic lethality. Pedigree of mating and genotypes of pups and embryos at E8.5, E10.5, E12.5 and E18.5.

1427

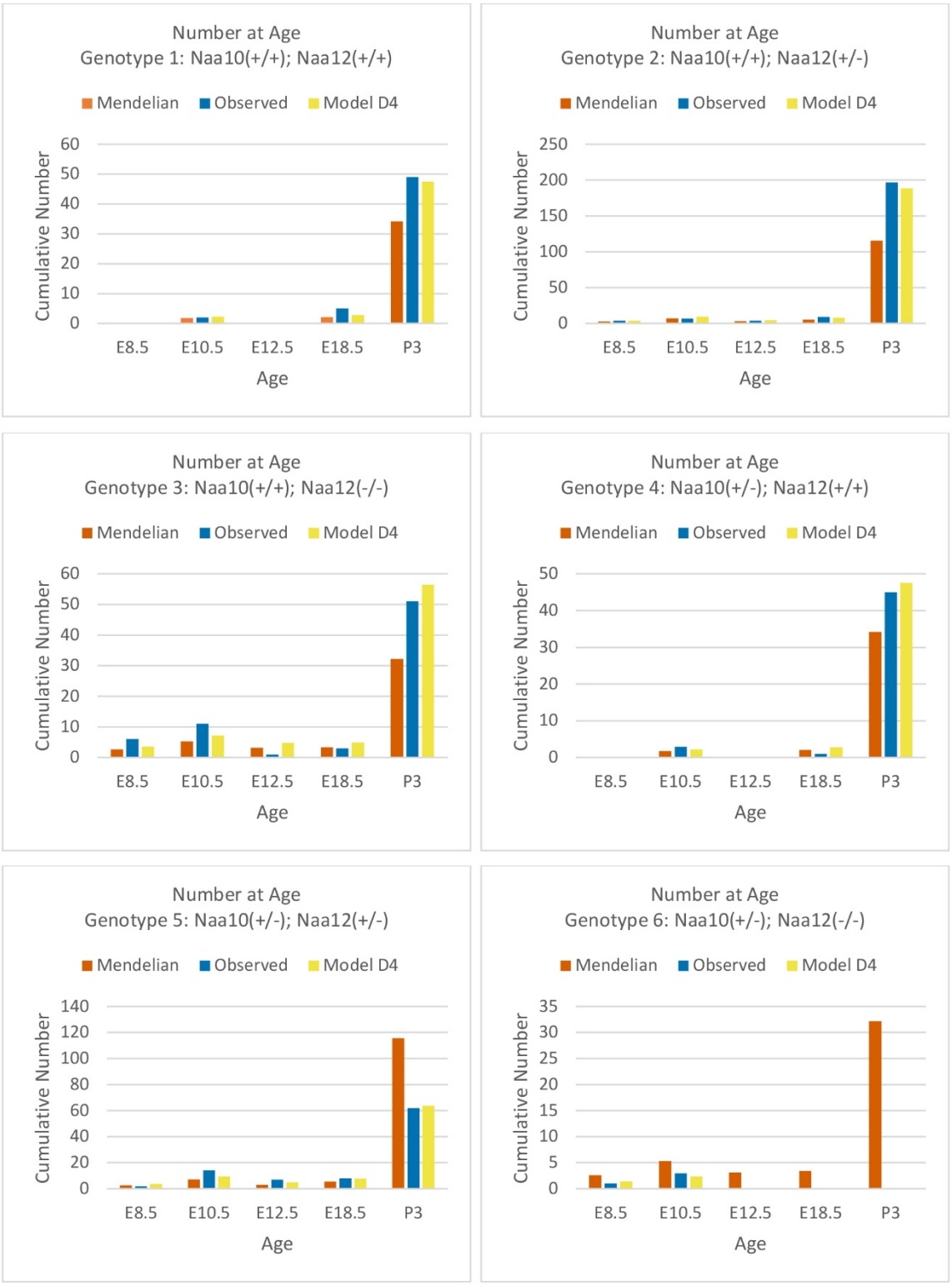

Supplement Fig. 9. Comparisons of Mendelian predicted, observed and model D_4 predicted offspring numbers for female genotypes (#1 - #6) at each age.

1428

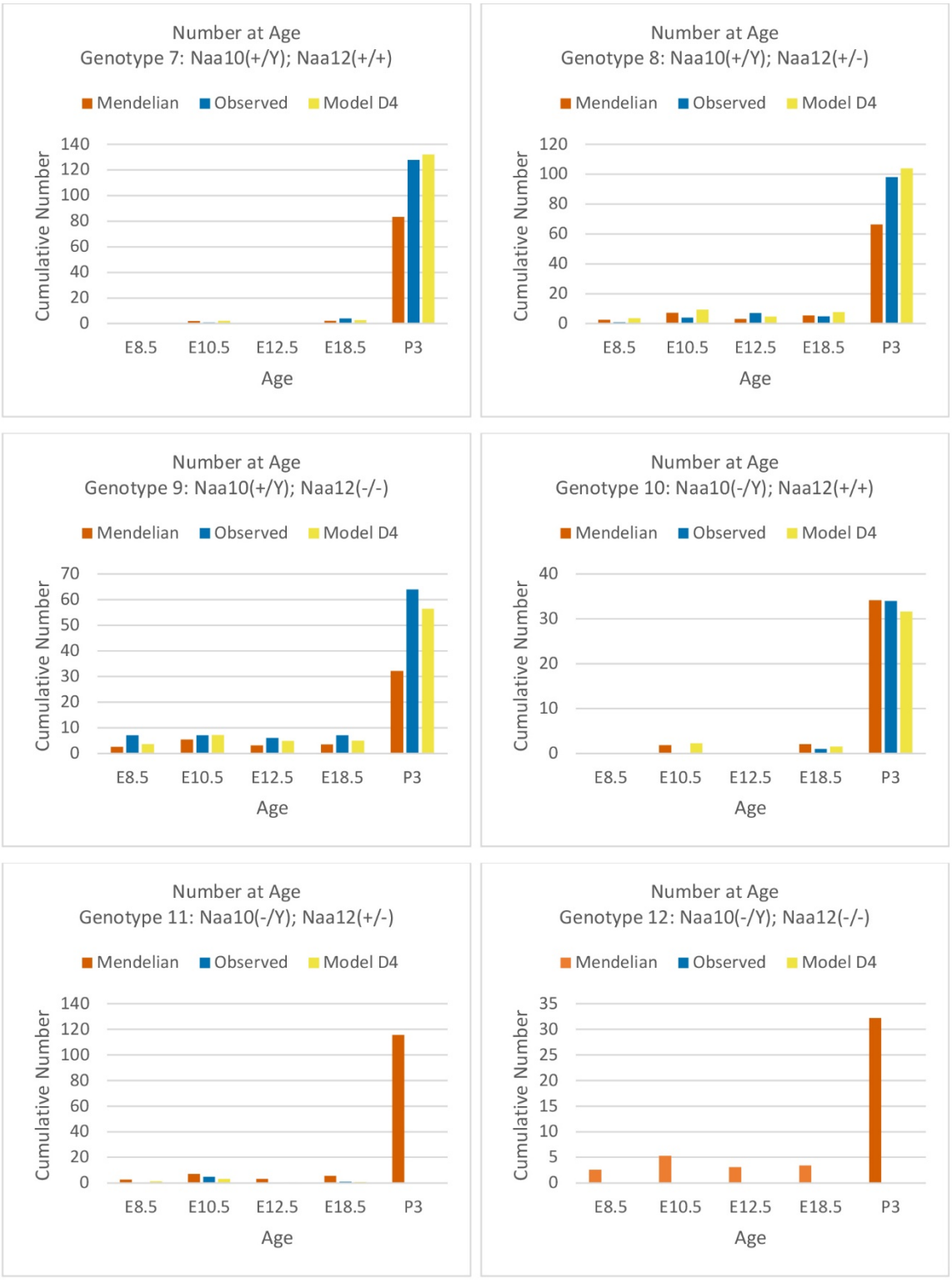

Supplement Fig. 10. Comparisons of Mendelian predicted, observed and model D_4 predicted offspring numbers for male genotypes (#7 - #12) at each age.

1429

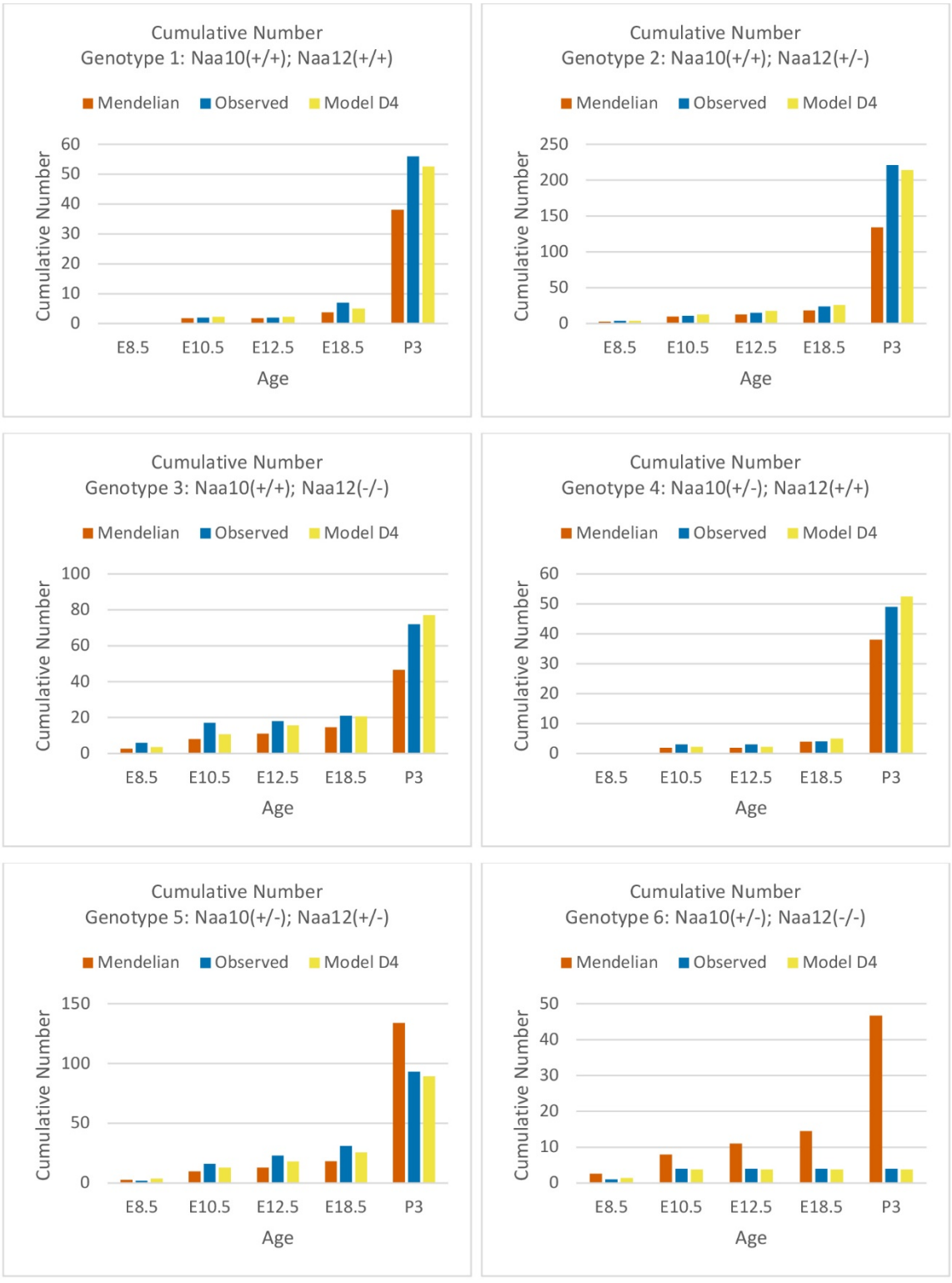

Supplement Fig. 11. Comparisons of cumulative Mendelian predicted, observed and model D_4 predicted offspring numbers for female genotypes (#1 - #6) at each age.

1430

Supplement Fig. 12. Comparisons of cumulative Mendelian predicted, observed and model D_4 predicted offspring numbers for male genotypes (#7 - #12) at each age.

1431